Dissertation

Submitted to the

Combined Faculties for the Natural Sciences and for Mathematics

of the Ruperto-Carola University of Heidelberg, Germany

for the degree of

Doctor of Natural Sciences

Presented by

M.Sc. Viktor Fleming

Born in Mitschurino, Kazakhstan

Oral examination: 13.12.2018

Immunosuppression in malignant melanoma induced by tumor-derived extracellular vesicles

Referees:

Prof. Dr. Viktor Umansky

Prof. Dr. Rienk Offringa

Declaration according to § 8 (3) b) and c) of the doctoral degree regulations:

b) I hereby declare that I have written the submitted dissertation myself and in this process have used no other sources or materials than those expressly indicated,

c) I hereby declare that I have not applied to be examined at any other institution, nor have I used the dissertation in this or any other form at any other institution as an examination paper, nor submitted it to any other faculty as a dissertation.

Heidelberg,

Name (Viktor Fleming)

The work described in this thesis was started in December 2015 and completed in November 2018 under the supervision of Prof. Dr. Viktor Umansky at the Research Group “Clinical Cooperation Unit Dermato-Oncology“ of the German Cancer Research Center (DKFZ), Heidelberg and the University Medical Center Mannheim.

This work is dedicated to my family. Their support and motivation in testing times was crucial for the success of this Ph.D. thesis.

Furthermore, a special thanks goes to Sarah Kolleth who embellished my time as a doctoral student.

Thank you!

Publications

Publications:

Fleming V, Hu X, Weller C, Weber R, , Riester Z, Hüser L, Sun Q, Nagibin V, Kirschning C, Bronte V, Utikal J, Altevogt P, Umansky V. Melanoma extracellular vesicles induce immunosuppressive myeloid cells by PD-L1 upregulation via TLR4 signaling (submitted)

Christopher Groth, Xiaoying Hu, Rebekka Weber, **Viktor Fleming**, Peter Altevogt, Jochen Utikal, Viktor Umansky. Immunosuppression mediated by myeloid-derived suppressor cells (MDSCs) during tumour progression. **Br J Cancer** (accepted)

Huber V, Vallacchi V, **Fleming V**, Hu X, Cova A, Dugo M, Shahaj M, Sulsenti R, Vergani E et al. miRNAs delivered by tumor extracellular vesicles induce myeloid suppressor cells in melanoma patients and predict resistance to immunotherapy ***J of Clin Invest*** 2018 Sep

Weber R, **Fleming V**, Hu X, Nagibin V, Groth C, Altevogt P, Utikal J, Umansky V. Myeloid-derived suppressor cells hinder the anti-cancer activity of immune checkpoint inhibitors. ***Front. Immunol.*** 2018 June

Fleming V, Hu X, Weber R, Nagibin V, Groth C, Altevogt P, Utikal J, Umansky V. Review: Targeting myeloid-derived suppressor cells to bypass tumor-induced immunosuppression. ***Front. Immunol.*** 2018 Mar

Blattner C*, **Fleming V***, Weber R, Himmelhan B, Altevogt P, Gebhardt C, Schulze TJ, Razon et al. CCR5+ myeloid-derived suppressor cells are enriched and activated in melanoma lesions. ***Cancer Res*****.** 2018 Jan **(*equally contributed)**

Fleming V & Umansky V**.** Editorial: Two MDSC faces in obesity: correcting metabolic dysfunctions but promoting tumor development. ***J of Leukocyte Biology.*** 2017 Dec

Sammar M, Siwetz M, Meiri H, **Fleming V**, Altevogt P, Huppertz B. Expression of CD24 and Siglec-10 in first trimester placenta: implications for immune tolerance at the fetal-maternal interface. ***Histochem Cell Biol*****.** 2017 May

Umansky V, Blattner C, **Fleming V**, Hu X, Gebhardt C, Altevogt P, Utikal J. Myeloid-derived suppressor cells and tumor escape from immune surveillance. ***Semin Immunopathol***. 2017 Apr

Mairhofer DG, Ortner D, Tripp CH, Schaffenrath S, **Fleming V**, Heger L, Komenda K, Reider D, et al. Impaired gp100-specific CD8(+) T-Cell responses in the presence of myeloid-derived suppressor cells in a spontaneous mouse melanoma model. **J Invest Dermatol**. 2015 Nov

Conference presentations:

Selected talks:

06/2018 Keystone Symposia: Exosomes/Microvesicles: Heterogeneity, Biogenesis, Function and Therapeutic Developments in **Breckenridge, USA**

04/2018 Mye-EUNITER: Myeloid Derived Suppressor Cells: Identification and implications in Human Diseases in **Crete, Greece**

Poster presentations:

07/2018 Curious 2018 at Merck KGaA in **Darmstadt, Germany**

05/2018 CIMT – The association for cancer immunotherapy in **Mainz, Germany**

11/2017 Hallmarks of skin cancer in Heidelberg, **Germany**

05/2017 ISEV - International society for extracellular research in **Toronto, Canada**

04/2017 CITIM – Cancer immunotherapy & immuno-monitoring in **Prague, Czech Republic**

05/2016 CIMT – The association for cancer immunotherapy in **Mainz, Germany**

Table of Content

Summary

The aim of this project was to investigate the role of tumor-derived extracellular vesicles (EV) in the induction of immunosuppression in malignant melanoma. Here, we focused on the effect of tumor-derived EV isolated from the *Ret* murine melanoma model (Ret) on bone marrow (BM)-derived immature myeloid cells (IMC). We demonstrated that IMC efficiently took up Ret-EV that resulted in the secretion of inflammatory molecules and upregulation of miRNA resembling an immunosuppressive phenotype. Furthermore, we found that Ret-EV upregulated the expression of PD-L1 on IMC. This PD-L1 expression was induced due the TLR signaling pathway, where TLR4 played a dominant role followed by TLR2 and TLR7. The TLR signaling led to the activation of NF-κB, thereby inducing the transcription of PD-L1. Blocking the NF-κB pathway diminished the Ret-EV-mediated PD-L1 upregulation on IMC. To test whether IMC becomes immunosuppressive upon the treatment with Ret-EV, we performed inhibition of T cell proliferation and IFN-γ secretion assays. Here, we demonstrated that IMC became immunosuppressive and converted into MDSC. The immunosuppressive activity of Ret-EV-treated IMC was mainly due to the induction of PD-L1. By blocking PD-L1 with neutralizing antibodies, we could almost completely abrogate the immunosuppressive properties of Ret-EV-treated IMC. Investigating the ligands for this TLR-dependent upregulation of PD-L1, we found that the inducible heat shock protein (HSP) 86 was the dominant ligand on Ret-EV, inducing TLR4 signaling in IMC upon Ret-EV treatment. Inhibition of all inducible HSP on EV by KNK-437 resulted in the reduction of the Ret-EV mediated conversion of IMC into MDSC. Furthermore, we stably knocked-down HSP86 on Ret cells. By co-culturing HSP86-deficient Ret cells with IMC, we could not observe a PD-L1 upregulation, whereas the scramble control showed a strong increase in PD-L1 expression. When using DMA to block EV secretion, the EV-mediated PD-L1 upregulation was strongly diminished. Finally, we observed an impaired tumor growth of HSP86-deficient Ret cells compared to wild type cells *in vivo* that was accompanied by reduced levels of MDSC expressing PD-L1 in the tumor microenvironment (TME).

Taken together, our findings demonstrate a critical role in converting IMC into MDSC for HSP86 on EV that could be a promising target for immunotherapy.

Zusammenfassung

Das Ziel dieser Arbeit war es den Effekt von extrazellulären Vesikeln des Tumors (EV) auf die Induktion der Immunsuppression im Malignen Melanom zu untersuchen. Hierbei isolierten wir die EV vom *Ret* melanoma model. Im Fokus stand der Effekt der EV auf myeloide Vorläuferzellen aus dem Knochenmark (IMC). Wir konnten demonstrieren, dass IMC die EV internalisierten, was wiederrum zur Ausschüttung von inflammatorischen Zytokinen und zur Expression von miRNAs führte, welche mit einem immunsuppressiven Phänotyp assoziiert wurden. Des Weiteren konnten wir deutlich darstellen, dass IMC nach der Behandlung mit EV PD-L1 hochregulierten. Die PD-L1 Induktion war abhängig vom TLR Signalweg, wobei insbesondere TLR4 eine dominante Rolle gespielt hat, gefolgt von TLR2 und TLR7. Die TLR vermittelte Signalkaskade aktivierte NF-κB, was letztendlich zur PD-L1 Expression führte. Die Blockierung von NF-κB unterdrückte die EV-vermittelte Hochregulation von PD-L1 auf IMC. Um zu testen, ob die EV-behandelte IMC immunsuppressiv wurden, führten wir T Zell Proliferationsexperimente und IFN-γ Sekretion-Analysen durch. Hierbei konnten wir beweisen, dass die IMC immunsuppressiv geworden sind und dadurch zu MDSC konvertierten. Die Immunsuppression wurde hauptsächlich PD-L1 zugeordnet, da durch die Verwendung von PD-L1 neutralisierenden Antikörpern der immunsuppressive Effekt verschwand. Auf der Suche nach dem entsprechenden Auslöser der TLR-abhängigen Signalkaskade in IMC, fanden wir das induzierbare HSP86 als Liganden auf der Oberfläche der EV. Durch die biochemische Inhibierung von HSP86 mit KNK-437, konnten wir die TLR-vermittelte Signalkaskade ausschalten und daher auch die Konvertierung der IMC zu MDSC unterdrücken. Zusätzlich haben wir die Expression von HSP86 permanent mittels shRNA blockiert. Die Ko-Kultivierung von HSP86-Defizienten Ret Zellen mit IMC führte zu keiner Hochregulation von PD-L1 auf IMC, wobei hingegen die entsprechenden Kontrol-Ret-Zellen eine starke Hochregulation von PD-L1 auf IMC induzierten. Die PD-L1 Induktion war EV-vermittelt, da durch die Blockade der EV Sekretion mittels DMA die PD-L1 Hochregulierung ausblieb. Letztendlich beobachteten wir ein

verlangsamtes Wachstum *in vivo* von HSP86 defizienten Tumoren, welche mit einer Reduktion von PD-L1 auf MDSC im Tumormikromillieu einherging.

Zusammengefasst demonstrieren wir in dieser Arbeit eine kritische Rolle von HSP86 auf Tumor Vesikeln in der Konvertierung von IMC zu MDSC. Somit ist HSP86 ein vielversprechender Angriffspunkt für die Immuntherapie.

1 Introduction

1.1 Malignant Melanoma

Malignant melanoma (MM) is a fast progressing, aggressive and therapy-resistant form of skin cancer [1-3]. It arise from melanin-producing melanocytes, which are present at the basal layer of the epidermis, inner ear, eyes and leptomeninges [4]. The most frequent type of MM is the cutaneous form [3]. The main reason for the malignant transformation of melanocytes into neoplastic cells is the accumulation of mutations mainly due to UV exposure [5]. Some gene mutations are commonly occurring in MM. The most predominant mutation is occurred in the B-rapidly accelerated fibrosarcoma $(B\text{-}RAF)^{V600E}$ gene [5]. More than 50% of all melanoma patients are bearing this mutation, which leads to the hyper activation of this serine/threonine kinase, leading to the constant activation of the mitogen-activated protein kinase (MAPK) signaling cascade and Rat sarcoma (RAS)-RAF pathway, promoting an excessive proliferation of melanocytes [6]. Furthermore, N-RAS mutations are found in 15 – 20 % of all melanomas. This type of mutation is associated with an aggressive behavior and poor clinical outcome [7].

During last 50 years, the morbidity of MM increased dramatically [8]. In 1960, the lifetime risk to get MM was about 1:600, whereas nowadays it increased up to 1:100 [9]. One explanation is the changed lifestyle during the last centuries, whereas people tend to be more outside and being scantily dressed. Although, MM accounts only for 1 % of all types of skin cancers, it causes about 90 % of all skin cancer-related death [1]. This is due to the resistance to radio –and chemotherapies and the aggressive nature of melanoma cells. They rapidly leave the dermis and most frequently metastasize into lung, liver, bones and brain [1]. The type of skin, amounts of naevi and genetic factors are further important factors for developing MM [5]. Although it is widely accepted that moles on the skin can transform into MM, only 25 % of all MM are formed by pre-exiting naevi. Interestingly, men and women show a gender-specific pattern in developing MM. Men show a higher risk in developing MM and they mainly tend to get MM on the back, whereas woman mostly develop MM in areas close to joints [9]. Besides

the gender-dependent differences, MM is also an area-dependent phenomenon. It occurs more frequently in Northern Europe and North America as compared to Asia, Africa, and Latin America [3].

1.1.1 Treatment of MM

In recent years, the treating opportunities for MM become much more versatile and successful. The approval of immune-checkpoint inhibitors, especially ipilimumab in 2011, nivolumumab and pembrolizumab in 2014 achieved unprecedented success in treating melanoma patients [2, 4].

Ipilimumab is an antibody towards cytotoxic T lymphocyte-associated antigen 4 (CTLA-4) on T cells. CTLA-4 is an immune-checkpoint molecule, which binds to B-7 proteins mainly on dendritic cells [10]. The activation of CTLA-4 inhibits T cells by reducing their proliferation and cytokine production. The use of ipilimumab prevents the exhaustion of T cells and restores their pro-inflammatory phenotype, as well their clonal expansion and infiltration [11]. Administration of ipilimumab in clinical trials increased the overall-survival by 10.1 months. A further phase-III study showed that combinational therapy with the conventional chemotherapeutic drug dacarbazine prolonged overall survival up to 11.2 months, whereas the dacarbazine monotherapy increased it to 9.1 months [12].

Nivolumumab and pembrolizumab are blocking antibodies against programmed cell death protein I (PD-1) [13]. Similar to CTLA-4, PD-1 is an inhibitory checkpoint molecule on activated T cells. Binding to its ligand PD-ligand 1 (PD-L1) or PD-ligand 2 (PD-L2) leads to the inactivation of effector T cells. Both PD-1 antibodies replaced ipilimumab as the first-line treatment [13]. Nivolumumab showed in clinical trials superior benefits compared to ipilimumab. Monotherapy of nivolumumab achieved a progression-free survival (PFS) of 6.9 months and in combination with ipilimumab a median PFS of 11.5 months [14]. Nivolumumab monotherapy showed an overall response rate of 40 % compared to 13.9 % by dacarbazine treatment [15].

The second anti-PD-1 antibody pembrolizumab achieved in clinical trials a median PFS of more than 24 months and the overall response rate was about 33 %, whereas ipilimumab showed a response rate of 12 % in this study [16].

Combinatorial studies of ipilimumab and nivolumumab showed a response rate of 58 %. The PFS increased up to 11.5 months by using both monoclonal antibodies versus 6.9 months by nivolumumab monotherapy. Since May 2016, the combinatorial treatment was approved as the most efficient therapy for MM in Germany [17].

Targeting PD-L1 is also a promising method to treat MM patients. Clinical trials with PD-L1 blocking antibodies like durvalumab, atezolizumab and avelumumab are ongoing.

Besides immune-checkpoint Inhibitors, also targeted therapy improved the treatment of MM. About 60 % of all MM patients harbor the B-RAF^{V600E} mutation [5]. In the recent years, vemurafenib and dabrafenib were approved as selective mutant B-RAF-inhibitors. Clinical studies reported an overall response rate of 50 % of B-RAF inhibitors in advanced unresectable melanoma, and the median PFS ranged from 5.3 – 7.3 months [18]. However, the long-term treatment is limited due to the fast acquisition of resistance mechanisms to those drugs [6]. One possibility to bypass the acquired resistance is to target downstream signaling enzymes of B-RAF. Hereby, targeting MEK is an efficient way. Trametinib and cobimetinib are approved MEK-inhibitors for treating MM [19]. Combined therapies with BRAF –and MEK-inhibitors showed improved clinical responses compared to monotherapy. Overall response-rates of 67 % were achieved with a median PFS of 12.3 months [20].

In 2015, the FDA approved talimogen laherparepvec (T-VEC), a genetically modified herpes simplex virus, to treat MM [21]. This oncolytical virus infects normal and melanoma cells but replicates only in melanoma cells that result in their lysis. Furthermore, during virus replication, melanoma cells are forced to produce and secrete granulocyte-macrophage colony-stimulating factor (GM-CSF), which stimulates the host immune system [22]. In clinical trials, T-VEC showed an overall response rate of 28 %, and median PFS was

increased to 19.6 months. T-VEC was described to be a very safe treatment with minor adverse effects [21, 23].

Therefore, the unprecedented success of immunotherapy highlighted the crucial role of our immune system in controlling tumor development. Understanding the tumor microenvironment (TME) and its interaction with the immune system will help to create new effective treatment strategies.

1.2 Role of the immune system in cancer

The unprecedented success of immunotherapy demonstrated undoubtedly the importance of the immune system in cancer development. This led to the addition of inflammation to the hallmarks of cancer [24-26]. However, the idea that our immune system controls the tumor growth was set already in 1909. Paul Ehrlich reported that the immune system developed mechanisms to suppress tumor formation [27]. Later on, Mac Farlane Burnet and Lewis Thomas postulated in 1957: “In large long lived animals....inheritable genetic changes must be common in somatic cells and a proportion of these changes will represent steps toward malignancy. It is an evolutionary necessity that there should be some mechanism for elimination or inactivity of such potentially dangerous mutant cells and it is postulated that this mechanism is of immunological character" [28]. This hypothesis was the start of the immunosurveillance concept. However, the lack of experimental designs and technologies made it impossible to prove the concept. In 1990, new mouse models, genetic engineering and monoclonal antibodies provided the opportunity to prove the immunosurveillance hypothesis [29]. Robert Schreiber and colleagues proposed a revised version of the immunosurveillance concept, which was termed immunoediting and comprises of three different phases: elimination, equilibrium and escape [29]

1.2.1 Elimination

Immune cells are able to recognize the malignant transformation of tumor cells. This is due to inflammatory signals, which are caused by tumor cells when they proliferate and damage the nascent tissue. Innate immune cells, like natural killer (NK) cells, dendritic cells (DC) and macrophages are recruited and clear the tumor cells [30]. The inflammatory environment is strengthened by the aberrant death of tumor cells that in turn further activate innate and adaptive immune cells. If in this phase, the tumors will be fully eliminated, the immunoediting concept ends at this point [31, 32].

1.2.2 Equilibrium

The equilibrium phase is following the elimination phase when the immune cells fail to clear the tumor cells. The tumor is not dormant, as believed before, but rather continues to proliferate [33]. Hereby, the tumor cells acquire mutations due to the genetic instability of malignant cells. Because of the immunological pressure during this phase, a selection will favor tumor cells, which are less antigenic [29].

1.2.3 Escape

Tumor cells acquired enough properties in the equilibrium phase to avoid the immune system [33]. The loss of immune recognition could be achieved by three main reasons: I) Loss or down regulation of the major histocompatibility complex (MHC) on tumor cells. II) Impaired ability of antigen processing. III) lacking of antigens recognized by immune cells [34]. Furthermore, the tumor cells established in the equilibrium phase an immunosuppressive microenvironment. Hereby, different stroma and immune cells helps the tumor growing. Many factors were found in an immunosuppressive microenvironment that promote tumor growth [35, 36]. However, one major factor that protect tumor cells from the anti-tumorigenic immune cells are myeloid-derived suppressor cells [37].

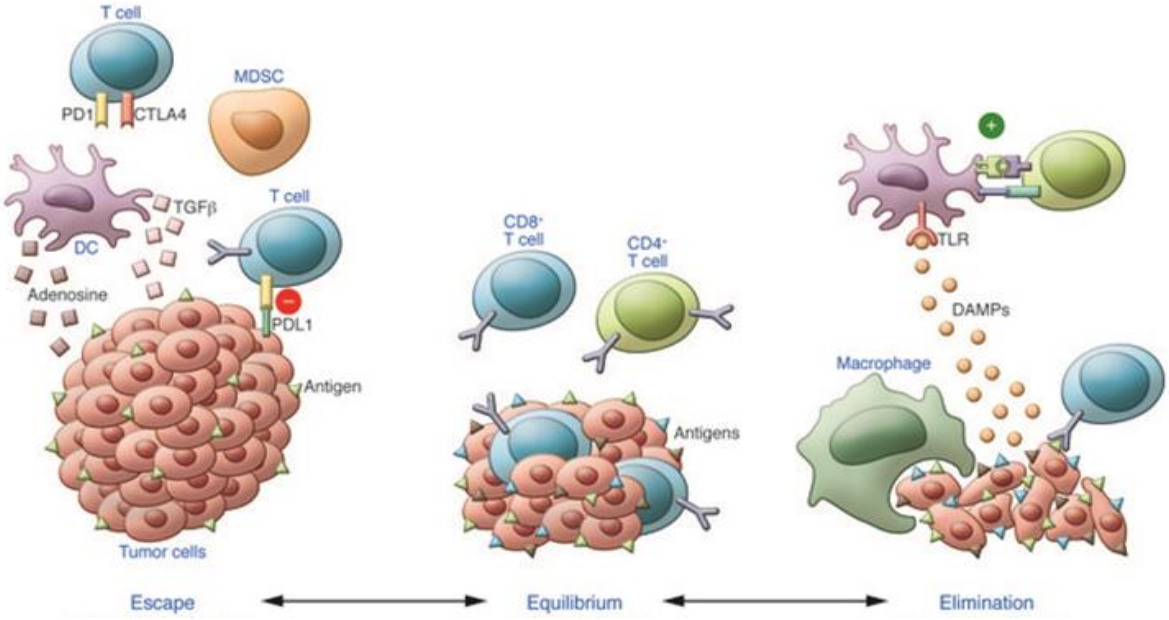

Figure 1: The concept of Immunoediting. Tumor cells and immune cells are in constant interaction that is divided in three phases. In the “Elimination” phase, immune cells attack and kill the tumor cells. A high immunological pressure on tumor cells characterizes the “Equilibrium” phase. However, in this phase some tumor cells survive due to favoring mutations. In the “Escape” phase, tumor cells acquired properties that hide them from our immune system. Figure was adopted from Kalbasi et al., 2013 [38]

1.3 Myeloid-derived suppressor cells (MDSC)

MDSC represent a heterogeneous population of cells that show an immature and immunosuppressive phenotype [37, 39]. During the last decades, it was proven that MDSC play a major role in inducing an immunosuppressive TME and promote tumor progression [40]. Their frequency and activity was negatively correlated with tumor progression, metastasis, recurrence and resistance to therapy [41-43]. Especially, the response to immunotherapy seems to be dependent on MDSC frequency and function [44, 45]. Because of these aforementioned data, MDSC are considered to be a target for future therapies [46].

1.3.1 Biology and function of MDSC

MDSC are generated within the bone marrow (BM) by the alternative activation of immature myeloid cells (IMC) [39, 47]. Usually, IMC differentiate into mature macrophages, DC or granulocytes under steady-state conditions. During acute infections IMC rapidly differentiate into monocytes or neutrophils, which form the first line of defense against invading pathogens [37]. This differentiation is promoted by a short-term production of several soluble factors like granulocyte macrophage colony-stimulating factor (GM-CSF), tumor necrosis factor (TNF)-α, and interleukin (IL)-1β and IL-6 [46, 47]. However, during chronic infections, obesity or cancer, this differentiation is altered due to a persistent secretion of those soluble factors. The fully differentiation of IMC is blocked, and they acquire an immunosuppressive phenotype, which results in the generation of MDSC [37]. They migrate to peripheral lymph nodes and to the site of tumor by following distinct gradients of chemokine (C-C motif) ligands (CCL) and C-X-C motif chemokine (CXCL) that are secreted by the TME [48, 49].

Within the TME, MDSC inhibit effector T cells [37]. Furthermore, MDSC promote tumor progression by non-immunological ways. For example, they produce large amounts of matrix metalloproteinases (MMP), especially MMP9 [50]. Those MMP hydrolyze the extracellular matrix and basal membrane. This remodeling process enables tumor cells to leave the TME, enter into the blood stream and form metastasis [51]. It is known that tumor cells prepare the pre-metastatic niche before entering into the blood stream [52]. This process is still poorly understood but first studies indicate that MDSC play a major role in this process [53]. Moreover, MDSC produce large amounts of vascular endothelial growth factor (VEGF) and basic fibroblast growth factor (bFGF) [46], key factors to induce angiogenesis. The latter is a further hallmark of tumor progression, as it enables nutrition, vasculature and dissemination of the tumor [25].

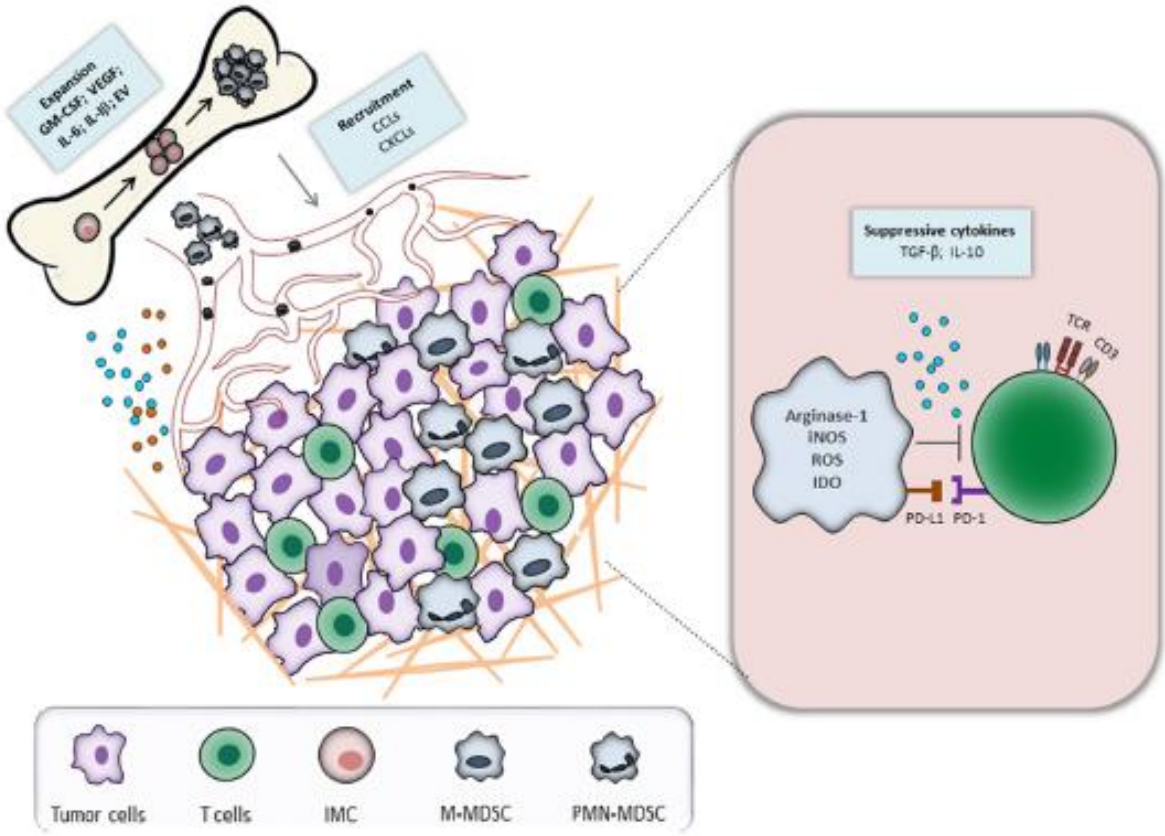

Figure 2: Biology of MDSC. MDSC arise from IMC in the bone marrow due to constant but weak activation by cytokines. MDSC leave the BM and migrate to the TME following the CCL and CXCL gradient released by tumor and immune cells. Within the TME, MDSC support tumor growth especially by suppressing T cells. Here fore, they use various mechanisms. Figure was adopted from Fleming *et al*., 2018 [46]

1.3.2 Immunosuppressive activity of MDSC

As mentioned before, the hallmark of MDSC biology is their capability to inhibit the function of effector T cells and consequently turning off the major player of anti-tumor immunity. Thereby, MDSC use various different inhibitory mechanisms. One mechanism is the production of arginase-I (Arg-1) [54], an intracellular enzyme, which is crucial for the urea cycle. It converts L-arginine into L-ornithine and urea. The catabolism of arginine leads to its depletion. Although T cells are dependent on arginine for their metabolism, they cannot produce arginine by themselves [55]. Therefore, the lack of arginine results in the

translational blockade in effector T cells, resulting in cell cycle arrest G_0-G_1 [56]. Furthermore, T cells becomes insensitive for T cell receptor (TCR) signaling because the expression of ζ-chain, which is essential for the signaling, is decreasing upon translational blockade [57].

Next to Arg-1, MDSC produce inducible nitric oxide synthase (iNOS), which catabolize L-arginine as well [58]. The product of the iNOS reaction is nitric oxide (NO), which can modify the T cell receptor by nitrosylation, resulting in less affine T cell receptors [46]. Moreover, NO nitrosylate important pathway mediators of the IL-2 pathway that is crucial for T cell function and proliferation [54, 58].

Besides depleting L-arginine, MDSC also catabolize L-tryptophan, a further essential amino acid for effector T cells [59]. By the expression of indoleamine 2,3-dioxygenase (IDO), MDSC convert L-tryptophan into kynurenine and 3-hydroxykynurenine [46]. This catabolic conversion has several negative effects on T cells. First, the starvation of L-tryptophan results in the differentiation of $CD4^+$ T cells into immunosuppressive regulatory T cells. Second, kynurenine and 3-hydroxykynurenine directly suppress effector T cells by impairing their function and proliferation. Third, kynurenine induces apoptosis in thymocytes [60, 61]. In addition, studies reported that kynurenine inhibit the anti-tumorigenic function of NK cells [60].

Reactive oxygen species (ROS) is another important immunosuppressive mediator utilized by MDSC [37, 62]. High concentrations of ROS initiate the apoptosis of T cells. Similar to Arg-1, ROS can also dampen the expression of the TCR ζ-chain. ROS interacts with NO that results in peroxynitrite production [41]. Like NO, peroxynitrite nitrosylate the TCR, which results in impaired antigen recognition and T cell signaling [46].

1.4 Programmed death-1 receptor/Programmed death-ligand 1

MDSC also express high levels of PD-L1 [37]. The PD-1/PD-L1 axis becomes incredibly important during the last years due to the approval of anti-PD1 blocking antibodies for treating several cancer types [13, 63]. Originally, PD-1 was first described in 1992 when scientists studied novel receptors in T cells that undergo apoptosis [63]. PD-1 is up regulated upon activation of effector T cells and consists of a single extracellular immunoglobulin-like variable domain. It contains an immunoreceptor tyrosine based inhibitory motif (ITIM) and immunoreceptor tyrosine based switch motif (ITSM) [64]. PD-L1 and PD-L2 were discovered 9 years later as ligands for PD-1 [63]. Both ligands consist of extracellular IgV and IgC domains and lack an intracellular signaling domain [64]. PD-L1, but not PD-L2, can also bind to CD80 (B7.1). PD-L1 and PD-L2 are widely expressed on hematopoietic cells, epithelial cells and endothelial cells [13].

1.4.1 PD-1 signaling cascade in T cells

The binding of PD-L1 to PD-1 results in inhibitory signals in T cells [65]. Upon ligation, the ITIM and ITSM motifs on the intracellular domain of PD-1 becomes phosphorylated. Src homology region 2 domain-containing phosphatase (SHP)-1 and SHP2 are recruited to the phosphorylated cytoplasmic tail of the PD-1 receptor [65]. The activation of SHP-1 and SHP-2 impairs T cell receptor signaling as SHP-1 and SHP-2 dephosphorylates important downstream adaptor molecules including ζ-chain-associated protein kinase 70 (ZAP70) and CD3 ζ-chain. Inhibiting these pathways leads to decreased production of interferon (IFN)-γ and IL-2, which are important cytokines to sustain effector T cell activity [65]. Moreover, SHP-1 and SHP-2 were shown to inhibit the PI3K/AKT pathway. Impaired AKT activity in $CD4^+$ T cells generates regulatory T cells [65].

1.4.2 Regulation of PD-L1 expression

Inflammatory signals were shown to be strong inducers of PD-L1 [66]. IFN-γ produced by activated T cells was described to be one of the strongest regulators [67]. Interestingly, the IFN-γ induced PD-L1 expression seems to be context dependent. IFN-γ neutralizing antibodies were shown to inhibit PD-L1 expression on tumor cells in a sarcoma mouse model, whereas PD-L1 expression on immunosuppressive macrophages was unchanged [68]. Besides IFN-γ, also type-I interferons induce PD-L1 expression on tumor and myeloid cells [69].

Ligands for toll-like receptors (TLR) were verified to induce PD-L1 upregulation on melanoma cells, endothelial cells and dendritic cells [69]. Especially, ligands for TLR3, TLR4 and TLR7/8 were described to induce PD-L1 expression [69, 70]. Furthermore, IL-17 and TNF-α were shown to stimulate PD-L1 expression on monocytes and prostate cancer cells [69]. For DC, IL-1β, IL-6, IL-10 and IL-27 were demonstrated to up regulate PD-L1 [69]. In addition to inflammatory cytokines, also oncogenic signaling was proved to be a major driver for PD-L1 upregulation [66, 71]. MYC oncogene overexpression was associated with high levels of tumorigenic PD-L1. Targeting MYC resulted in decreased levels of PD-L1 on tumor cells [72]. Most tumor cells show a hyper-activated MEK-ERK signaling mainly due to mutated tyrosine kinases like B-RAF. Activated MER-ERK pathway was confirmed to induce PD-L1 upregulation on many cancer cell lines, which was abrogated upon MEK inhibition [66]. Activation of epidermal growth factor receptor (EGFR) and downstream effector molecules were proved to induce PD-L1 expression in multiple tumor models. A further hallmark of tumor progression is a hypoxic microenvironment. Hypoxia induces the transcription factor hypoxia-inducible factor (HIF)-1α that directly binds hypoxia response element (HRE) on the PD-L1 promoter and initiates the synthesis of PD-L1 on tumor and myeloid cells [73]. Recently, many micro RNA (miRNA) were associated with the regulation of PD-L1 [74]. Especially, miRNA-513 and miRNA-155 were shown to be important suppressors of PD-L1 expression at the post-transcriptional level [74].

1.5 Extracellular Vesicles

Cells use various mechanisms to communicate. Besides direct cell to cell interaction and secretion of soluble factors, extracellular vesicles (EV) are important mediators of long range communication [75].

EV consist of three subsets, which differ in their size distribution and their biogenesis [76]. The apoptotic bodies are 1 to 5 µm in size and are formed by cells undergoing apoptosis. To the second type of EV belong microvesicles (sometimes also called as ectosomes or microparticles). They are 100 nm – 1000 nm and are produced by the outward budding of the limiting plasma membrane. Exosomes form the smallest type of EV. They are described to be 30 nm – 150 nm in diameter and are generated within multivesicular bodies (MVB) by inward budding of the limiting membrane. By fusion of the multivesicular bodies with the plasma membrane, exosomes are released into the extracellular space and can act as a mediator of communication. As exosomes and microvesicles overlap in size, and most used isolation methods do not specifically isolate a distinct type of EV, it is recommended to use the general term EV [75].

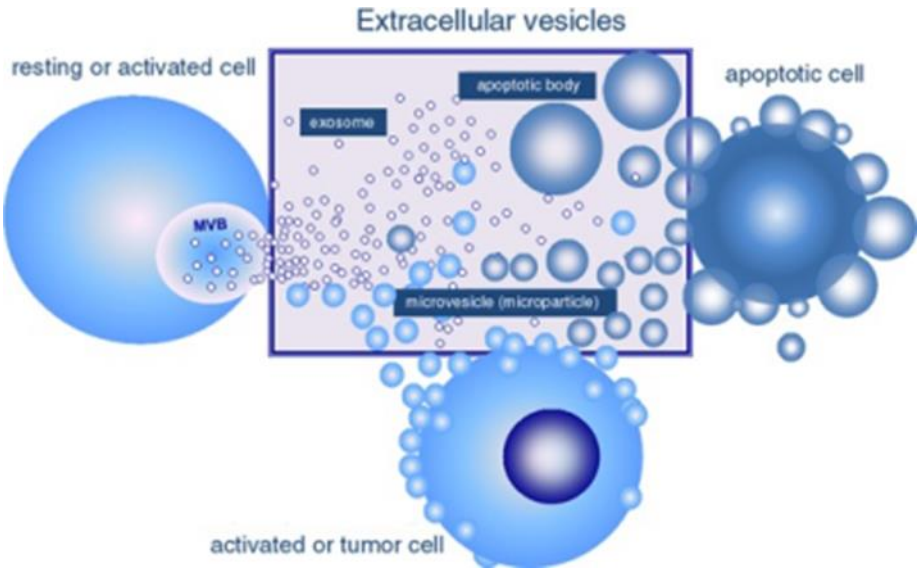

Figure 3: Subsets of EV. EV consists of three different subsets. The smallest subsets are the exosomes, which are generated within MVB. By the fusion of the MVB with the plasma membrane, exosomes gets released into the extracellular space. The second subsets are the microvesicles. The outward budding of the plasma membrane creates them. The biggest subset is called apoptotic bodies. They are produced by cells undergoing apoptosis. Figure was adopted from György *et al*., 2011 [77].

1.5.1 EV in cancer progression

During the last decades, the interest on EV in cancer research gained an enormous level. This was especially due to the following findings: I) EV carry functional miRNA and oncogenes to recipient cells [78], II) EV derived from immune cells were able to present antigens on MHC molecules and induced T cell activation [79], and III) EV were shown to be crucial for organotropic metastasis formation [80].

Since then, the understanding of the role of EV in cancer progression immensely increased. It was revealed that EV encourage tumor progression by promoting angiogenesis. Studies reported that EV-derived miRNA-17-92 regulates integrin-α5, which stimulates tube formation and proliferation of endothelial cells [81]. Furthermore, miRNA-9 in EV was found

to be internalized by endothelial cells and to exhibit pro-angiogenic properties by the activation of JAK-STAT signaling [82]. In addition, tumor-derived EV contain high amounts of pro-angiogenic molecules such as VEGF, IL-8, PDGF and FGF, which augment angiogenesis by recipient endothelial cells. EV support directly the proliferation of tumor cells. Tumor-derived EV contain high amounts of miRNA-222 [83]. In an autocrine manner, tumor cells take up miRNA-222 containing EV that directly results in enhanced PI3K/AKT activity and therefore higher proliferation of tumors cells [84]. Distinct tumor-derived EV were reported to transport CD97 [85]. Recipient tumor cells incorporated functionally CD97 on their surface, which leads to enhanced activity of MAPK-signaling pathway and results in tumor cell proliferation. Mutated forms of epidermal growth factor receptor variant III (EGFRVIII) were found on the surface of EV [86]. The uptake and integration of this mutant EGFRVIII resulted as well in higher proliferation rates of tumor cells due to the promotion of anti-apoptotic pathways [87]. It was found that EV promote the formation of metastasis in multiply ways. Tumor-derived EV are found to express high amounts of MMP on their surface. These MMP remodel the extracellular-matrix and create a leaky environment that favors the spread of cancer cells [88]. Moreover, studies reported the potential of EV to promote epithelial to mesenchymal transition (EMT) [89].

1.6 Pathogen Recognition Receptors (PRR)

The innate immune system evolved mechanisms to recognize invading pathogens and damaged cells using pathogen recognition receptors (PRR) that recognize pathogen-associated molecular patterns (PAMP) or damage-associated molecular patterns (DAMP) [90]. During last decades, many families of PRR were discovered and studied. In addition to immune cells also epithelial and endothelial cells express PRR on their cell surface or with in the cytosol [90]. By recognizing the respective PAMP or DAMP, cells starts to induce their defense mechanisms to counteract the pathogens. They produce a distinct set of cytokines to upregulate their antigen-presenting activity of immune cells and to block the proliferation and metabolism of intracellular pathogens [91].

PRR are classified into four major groups: Toll-like Receptors (TLR), c-type lectine receptors (CLR), nucleotide-binding oligomerization domain (NOD)-like receptors and retinoic-acid-inducible gene I (RIG-I)-like receptors (RLR) [92, 93].

CLR are membrane bound receptors, which are internalized upon PAMP binding. They mainly recognize carbohydrate structures expressed on pathogens. Two types of CLR are described based on the structure of recognized carbohydrates. DEC205 and macrophage-mannose receptor belongs to the type-I CLR, whereas DCIR, DC-sign and Dectin-I are members of the type-II family [94].

Only few members of the RLR are found by now. They are expressed exclusively in the cytoplasm and recognize viral DNA, resulting in the production of high amounts of type-I IFN and, in some cases, in the initiation of apoptosis [95].

Nod-like receptors are also intracellular sensors. They recognize peptidoglycans especially on intracellular bacteria. The recognition of PAMP induces the activation of the nuclear factor 'κ-light-chain-enhancer' of activated B-cells (NF-κB) pathway, leading to the induction of immune responses [96]. Furthermore, the cells undergo apoptosis [97].

1.6.1 Diversity of Toll-like Receptors (TLR)

In 1995, Christiane Nüsslein-Volhard and Eric Wieschaus were honored with the Nobel Prize for the discovery of the *toll* gene in *Drosophila melanogaster* in 1985. Mutants of the *toll* gene in Drosophila were shown to be sensitive to fungal infections and showed impaired immunity. Later on, TLR were also found in mammalians and their role in innate immunity was intensively studied [91]. TLR are type-I transmembrane proteins, belonging to the IL-1 receptor (IL-1R) superfamily due to their structural homology in the cytoplasmic region (TIR domain) [98]. However, the extracellular domain of IL-1R contains three conserved immunoglobulin-like motifs, whereas the extracellular domain of TLR consists of leucine-rich repeats that are important in the recognition of PAMP and DAMP [98]. 13 different TLR were described so far [91]. TLR1, TLR2, TLR4, TLR6 and TLR10 are membrane-bound receptors

on the plasma membrane and TLR3, TLR7, TLR8 and TLR9 are expressed intracellularly on the endosomal membrane. TLR11, TLR12 and TLR 13 were only identified in mice [91].

1.6.2 TLR ligands

TLR recognize a broad spectrum of different PAMP. Lipoproteins and peptidoglycans from different gram-positive bacteria are recognized by TLR1, TLR2 and TLR6. TLR4 recognizes lipopolysaccharides (LPS) on the surface of gram-negative bacteria. Flagelin, a major protein of the bacterial Flagella, is recognized by TLR5. TLR7 and TLR8 sense intracellular single-stranded viral RNA, whereas TLR9 recognize bacterial and viral DNA upon CpG motifs [91, 99]. Ligands of TLR10 are still under discussion [100]. TLR11 and TLR12 which are only found in mice recognize profiling, a component of the protozoa *Toxoplasma gondii*. TLR13 were described to differentiate between bacterial and host ribosomes due to sequence-specific motifs [99]. Recently, more non-pathogenic TLR ligands were found. In particular, ligands that are associated with damaged cells like oxidized lipoproteins, HMGB1 and S100 proteins were described to induce TLR signaling [101-104]. Table 1 shows an overview of all TLR with their respective ligands.

Toll-like receptor	Ligand	Source
TLR1	triacyl lipopeptides	Gram positive/ negative bacteria
TLR2	Glycolipids	Gram positive/ negative bacteria
	Lipopeptides	Gram positive/ negative bacteria
	Lipoproteins	Gram positive/ negative bacteria
	lipoteichoic acid	Gram positive bacteria
	HSP70	Host
	zymosan	Fungi
TLR3	double-stranded RNA	viruses
TLR4	LPS	Gram negative bacteria
	Several HSP	Host
	Fibrinogen	Host
	Heparan sulfate	Host
	Hyaluronic acid	Host
	nickel	Surfaces
TLR5	Flagellin	Gram positive/ negative bacteria
	Profilin	Toxoplasma gondii
TLR6	diacyl lipopeptides	Mycoplasma
TLR7	single-stranded RNA	RNA viruses
TLR8	single-stranded Viral RNA	RNA viruses
	bacterial RNA	Gram positive/ negative bacteria
TLR9	unmethylated CpG DNA	Gram positive/ negative bacteria & viruses
TLR10	triacylated lipopeptides	Gram positive/ negative bacteria
TLR11 (mouse)	Profilin	Toxoplasma gondii
TLR12 (mouse)	Profilin	Toxoplasma gondii
TLR13 (mouse)	bacterial ribosomal RNA sequence "CGGAAAGACC"	Gram positive/ negative bacteria Viruses

Table 1: TLR ligands and their source. Modified from Wikipedia.org

1.6.3 TLR signaling

The activation of TLR signaling induces inflammatory cytokine production, leading to the stimulation of adaptive immune responses [91]. Binding of the respective ligand to the TLR activates the TIR domain, which was found in many IL-1R and TLR molecules. It contains three boxes, which are important for protein-protein interaction (box1 and box2) and cellular localization (box3) [105]. The TIR domain of TLR can bind five distinct adaptor molecules. Myeloid differentiation primary response 88 (MyD88) and TIR-domain-containing adapter-inducing interferon-β (TRIF) are the best studied for TLR signaling [98, 99]. MyD88 binds to all TLR except TLR3, whereas TRIF is found on TLR4 and TLR3 [91]. Depending on the recruited adaptor molecule, various kinases, especially IL-1R associated kinase (IRAK) 4 or ubiquitin ligases (especially TNF receptor associated factor (TRAF) 6 becomes activated. IRAK4 and TRAF6 phosphorylate further downstream molecules/kinases that activate further proteins dependent on the adaptor molecule that was recruited to the TLR [91, 98, 99]. The TLR signaling results in the activation of NF-κB that induces the production of various inflammatory cytokines and chemokines. Furthermore, the TLR signaling induces the activation of p38 MAP kinase (MAPK) and JNK MAPK pathways [105]. Type-I IFN will be also produced due to the activation of interferon response factor (IRF) 3 and 7 [91, 99].

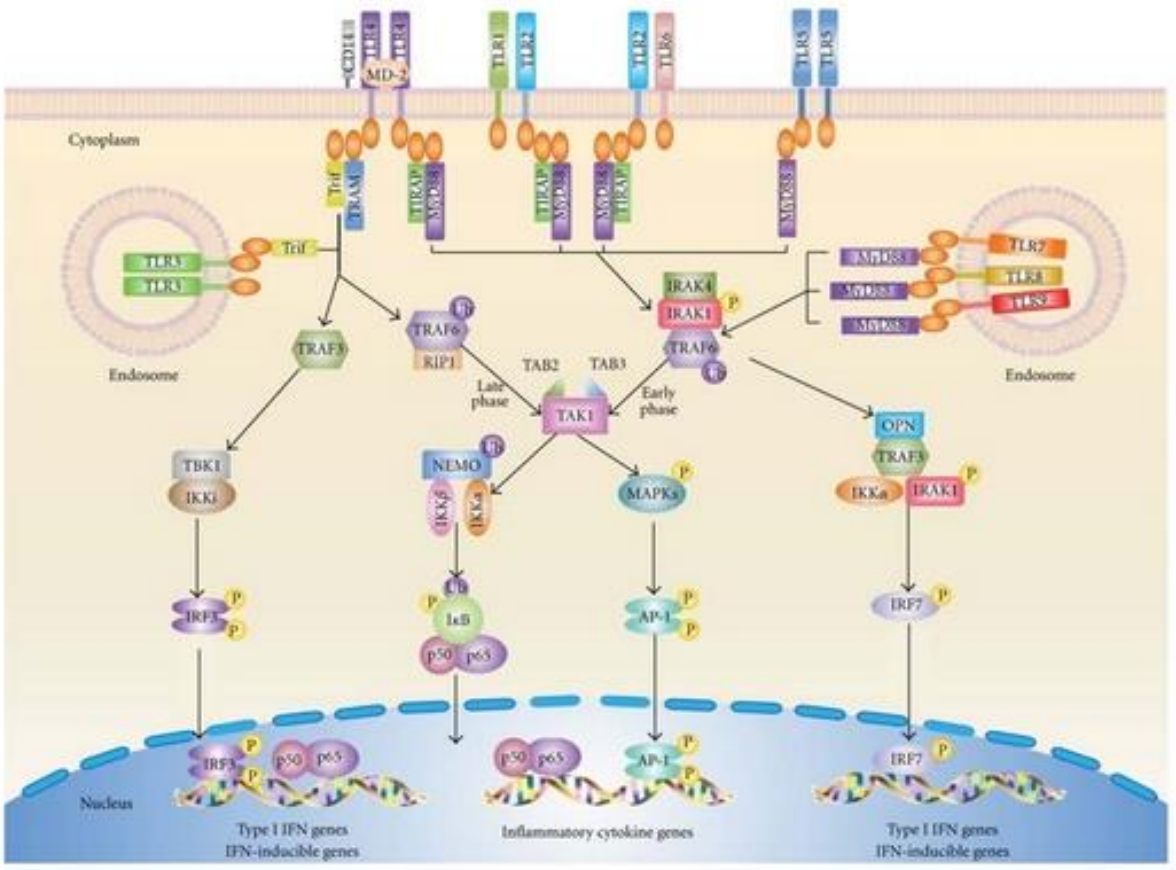

Figure 4: Signaling pathway in TLR. TLR recognizes specific PAMP and DAMP from pathogens or Host cell. TLR3, TLR7, TLR8 and TLR9 are found on endosomal/lysosomal membrane, whereas the others are localized on the plasma membrane. Upon binding to its respective ligand, TLR recruit adaptor protein MyD88 or TRIF. MyD88 recruits IRAK4. Through the interaction of IRAK4 and TLR, IRAK1 becomes phosphorylated and binds TRAF6. TRAF6 activates NF-κB through phosphorylation of its inhibitor. Furthermore, TRAF6 activates MAPK signaling that result in activated JNK and p38 pathways. These transcription factors foster the transcription of inflammatory genes and cytokines. In addition, adaptor molecule TRIF recruits RIP1, which in turn activates TRAF3 that promotes the recruiting of IκB kinase (IKK) ε/ Tank-binding kinase 1 (TBK1), leading to the phosphorylation of IRF3. IRF transmigrate to the nucleus and activates Type-I IFN and IFN-induced genes [106].

1.7 Heat-shock proteins

Cells developed mechanisms to counteract stress conditions. Hereby, they evolved a class of highly conserved proteins that are called chaperons. They sense damaged or miss-folded proteins. and refold them or mark for lysosomal degradation [107].

Heat-shock proteins (HSP) belong to the biggest class of chaperones. They were discovered in 1962 in *Drosophila melanogaster,* as a family of genes that are induced upon heat-shock and refold heat-damaged proteins [108]. HSP have multiple acting as a molecular chaperone and being involved in many cellular responses, development and differentiation [109].

In mice and humans, five classes of HSP were defined. They are classified based on their molecular mass and sequence homology: Hsp27, Hsp60, Hsp70, Hsp90, and Hsp110 [110]. Each HSP family has members that are expressed constitutively and those that are induced under stress conditions. Every singly HSP has its own specific role and are expressed in specific organelles. Furthermore, due to their specific binding groove, they have a distinct and specific group of proteins that they bind and modulate[109].

1.7.1 Hsp90 family

Members of the Hsp90 family are one of the most abundant proteins in the cell [111, 112]. They account for 1 – 2 % of all cellular proteins. Hsp90 members are found in the endoplasmatic reticulum, mitochondria and cytosol. Two main members are expressed in the cytoplasma: constitutively expressed Hsp84 (Hsp90β) Hsp86 (Hsp90α) induced upon stressed conditions like oxidative stress or heat-shock [112].

Under steady-state, Hsp90 regulates the maturation of proteins, intracellular trafficking, lysosomal degradation and signaling pathways [111]. In stressed cells, Hsp90 is mainly responsible for preventing aggregation of proteins and refolding damaged proteins [113]. For their chaperone activity, Hsp90 homodimers use ATP to undergo conformational changes.

For most of the proteins, Hsp90 needs the support of Hsp70 and Hsp40, which act downstream of Hsp90. Compared to Hsp70 and other HSP, Hsp90 is more specific to targets. The Hsp90 chaperone complex activity is described in detail in figure 5 [111] [109].

HSP90 is considered as a major driver of cancer progression [114, 115]. Cancer cells utilize the activity of HSP90 that interacts with many oncogenes, like B-Raf, mutated p53, c-MET and prevents their degradation. Furthermore, cancer cells produce enormous amounts of proteins. To survive this proteotoxic stress, cancer cells are dependent on the proper function of HSP90 [109].

Recent studies showed a beneficial effect of targeting the HSP90 family proteins. The main anti-HSP90 drug used in clinical trials is 17-DMAG, the natural occurring geldanamycin found in *Streptomyces hygrocopicus* [116]. It mainly binds competitively to the ATP-binding side and inhibits the chaperone activity of HSP90. Pre-clinical trials with 17-DMAG showed antiangiogenic and antitumor activity in mouse melanoma models. In human epidermal growth factor receptor 2 (Her-2) -positive breast cancer, 17-DMAG also showed beneficial effects [117]. Her-2 interacts with HSP90. Due to the lack of HSP90 activity, Her-2 showed higher degradation. Besides anti-tumor effects, 17-DMAG was described to inhibit inflammation, mainly by blocking the NF-κB pathway. There are many phase I and II clinical trials ongoing in different cancer entities with 17-DMAG used alone or in combination with other agents [116].

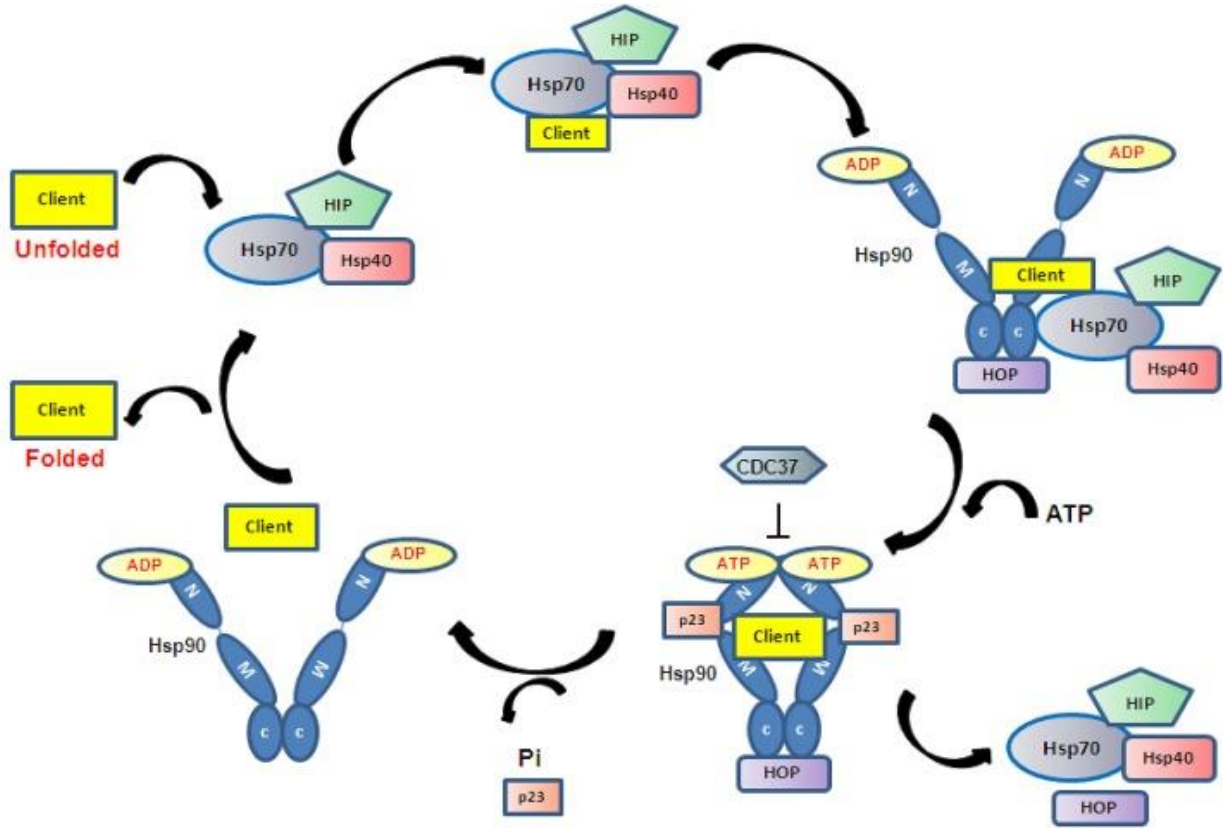

Figure 5: The Hsp90 chaperone complex. Freshly translated peptides are linked to the HSP70/HSP40 complex by hydrophobic residues. The Hsp70/Hsp40 complex carries the client to HSP90 dimers. HOP supports the binding of Hsp70/Hsp40 to Hsp90. HOP also facilitates the transfer of the client to Hsp90. Exchange of ADP to ATP leads to the dissociation of the Hsp70/Hsp40 complex and close the Hsp90 complex with the client. P23 stabilize the complex. Upon ATP hydrolysis p23 and the client dissociates from the Hsp90 complex as fully maturated and folded protein[109].

2 Aim of the project

The aim of this study was to investigate the role of tumor-derived EV in the induction of immunosuppression in malignant melanoma. Here, we focused on the interaction between cells from a myeloid origin and melanoma-derived EV. In particular, we studied the effect of EV isolated from the *Ret* melanoma cell line on immature myeloid cells (IMC) from the bone marrow of C57BL/6 mice. In order to test if Ret-EV are able to convert IMC into immunosuppressive MDSC, we analyzed immunosuppressive mediators upon Ret-EV treatment and performed T cell proliferation studies to evaluate the immunosuppressive potential. Furthermore, we investigated the signaling pathways involved in the reprogramming of IMC into MDSC and search for key targets inducing those signaling pathways. Finally, we performed tumor growth studies with Ret cells deficient in essential genes for the reprogramming of IMC into MDSC to test if we can block the EV-mediated induction of immunosuppression in malignant melanoma.

3 Material and Methods

3.1 Materials

3.1.1 Mouse strains

Wild type C57BL/6 mice were purchased from Charles River laboratories (Sulzfeld, Germany). Those mice were crossed and kept under pathogen-free conditions in the animal facility of the German Cancer Research Center (Heidelberg, Germany). *Tlr2*$^{-/-}$ *and Tlr7*$^{-/-}$ mice with C57BL/6 background were obtained from Beatrix Schumak, University of Bonn. *Tlr4*$^{-/-}$*; MyD88*$^{-/-}$ and *MyD88*$^{-/-}$*/Trif*$^{-/-}$ mice with C57BL/6 background were obtained from Carsten Kirschning, University of Essen-Duisburg. Experiments were performed in accordance with government and institutional guidelines and regulations.

3.1.2 Cell lines

The Ret cell line (Ret) was isolated from cutaneous melanoma developed in *Ret* transgenic mice [118] and cultured in RPMI-1640 supplemented with 10 % FBS and 1% Penicillin-Streptomycin [119].

MSC-1 and MSC-2 cells were established by isolating splenic cells from BALB/c mice followed by virus-induced immortalization [120]. They reflect a cell line to study myeloid suppressive cells. MSC-1 cells are permanently suppressive, whereas MSC-2 are suppressive upon treatment with IL-4. (MSC-1 and MSC-2 cells were kindly provided by Dr. Stefano Ugel, University of Verona)

3.1.3 Laboratory equipment

Device	Name	Provider
Balance	BP 3100P	Sartorius
Cell culture incubator	Hera cell	Heraeus
Centrifuges	BiofugeprimoR MEGAFUGE 40R Labofuge 400R	Heraeus Heraeus Heraeus
Confocal microscope	TCS SP2	Leica
Flow cytometer	FACS Canto II	BD Biosciences
Flow cytometer	FACS Lyric	BD Biosciences
Heating block	Digital Block Heater HX-2	Peqlab
Imaging system	Fusion SL	VilberLourmat
Laminar flow hood	Hera safe	Thermo Electron Cooperation
Magnetic stirrer	RCT basic	IKA Werke
Microplate Reader	Tecan infinite M200	Tecan
Microscope	DMIL	Leica
N2 tank		
Nanoparticle tracking system	NanoSight NS300	NanoSight
Pipettes	Transferpette ® S	Brand
Power supply	PowerPacTM HC High Current	BioRad
Real-Time PCR machine	MX3005 qPCR Systrm	Stratagene
Shaker	Logic shaker	NeoLab
Thermal Cycler	DNA Engine Peltier Thermal Cycler	Biorad
Transfer device	iBlotTM Gel Transfer Device	Thermo Scientific
Ultracentrifugation rotor	Surespin 630	Sorvall
Ultracentrifuge	SorvallDiscovery 90SE	Hitachi
Vortexer	REAX top Vortex Genie 2	Heidolph Scientific Industries
Water bath	DC3	HAAKE, GFL

3.1.4 Cell culture products

Product	Company	Catalog No.
100 µm cell strainer	BD	CLS431751-50EA
12-well flat bottom with lid	BD	353043
15 mL conical tubes	Falcon	352096
24-well flat bottom with lid	Greiner bio-one	622160
40 µm cell strainer	BD	
5 mL round-bottom polypropylene tubes with cell strainer	BD	352235
5 mL round-bottom polypropylene tubes	BD	352008
50 mL conical tubes	Falcon	352070
6-well flat bottom with lid	Thermo Fisher Scientific	140675
96-well flat bottom with lid	TPP®	92096
96-well U-bottom with lid	Sigma Aldrich	M9436-100EA
Amicon® Ultra Centrifugal tube	Merck Millipore	UFC905024
Cell culture flasks T75	Sigma Aldrich	C7231-120EA
Cryovial, 2 mL sterile	Sigma Aldrich	V5760-500EA
Filter tips: 20, 200, 1000 µL	Steinbrenner	L1000
Safe lock tubes: 0.5, 1.5 and 2 mL	Eppendorf	SL-GPS-L10, L250,
serological pipettes: 5, 10 and 25 mL, sterile	Greiner bio-one	606180; 607180
Syringe 1 mL	BD	
Cellstar Cell culture flask 25 cm2	Greiner	658170
iBlotTMGel Transfer Stacks	Thermo Fisher Scientific	IB24002
Neubauer chamber	Brand	
Needles Sterican® Ø 0.40 x 20 mm	B. Braun	4657705
PVDF membrane	Thermo Fisher Scientific	88520
Stericup&Steritop 0.22 µm Millipore Express PLUS membrane	Merck Millipore	SCGPU02RE
TC dish, 150 Standard	Sarstedt	3903
ThickBlot Filter Paper	BioRad	1703

3.1.5 Cell culture media

Product	Company	Catalog No.
0.4 % Trypan blue solution	Sigma Aldrich	T8154
2-β-Mercaptoethanol (50 mM)	Gibco	31350
Bovin serum albumin	Sigma	7030-50G
Dimethylsulfoxid (DMSO)	Merck	109678
Dimethylsulphoxide Hybrid Max (DMSO)	Sigma Aldrich	472301-100ML
DPBS (1x)	Gibco	14190-094
Fetal Bovine Serum	PAN Biotech GmbH	3702-P260718
HEPES Buffer (1M)	Sigma Aldrich	H0887
Hygromycin B	Carl Roth	1287.1
Kanamycinsulfate	Sigma Aldrich	60615
MACS BSA Stock Solution (10 %)	Miltenyi Biotec	130-091-376
MEM NEAA (100x)	Gibco	11140-035
OptiMEMTM	Gibco	31985070
Penicillin/ Streptomycin	PAA	P11-010
RPMI Medium 1640 (1x) + GlutaMAX™	Gibco	61870-010
sodium pyruvate (100 mM)	Gibco	11360-039
UltraPure™ EDTA (0.5M, pH 8.0)	Gibco	15575

3.1.6 Chemicals

Product	Company	Catalog No.
10 % Tween® 20 Solution	Biorad	161-0781
10 x Permeabilization Buffer	eBioscience	00-8333-56
7-AAD	BD	51-68981E
ACK lysis buffer	Gibco	A10492-01
Acrylamide solution	Carl Roth	2267.2
Albumin IgG free	Carl Roth	3737.4
Amiloride,5'-(N,N-Dimethyl)-hydrochloride	Enzo	ALX-550-261-M005
Ammonium-persulfate (APS)	Sigma-Aldrich	A-3678

ATX Ponceau S red staining solution	Sigma-Aldrich	09189-IL-F
Carboxyfluorescein succinimidyl ester (CFSE)	Biolegend	423801
Clear PAGE LDS sample buffer (4x)	Invitrogen	MP0007
Fluoromount-G	Southern Biotech	0100-01
Glycine	Carl Roth	3908.1
KNK-437	Sigma Aldrich	SML0964-5MG
LB-Agar	Carl Roth	X965.1
LB-Media	Carl Roth	X968.1
Lipofectamine 3000 Transfection Reagent	Invitrogen	L3000001
Methanol	Carl Roth	8388
MISSION® shRNA Bacterial stock	Sigma Aldrich	SHCLNG
MISSION® TRC2 pLKO.5-puro Non-mammalian Control Plasmid DNA	Sigma Aldrich	SHC202
PageRuler Protein ladder prestained	Thermo Fisher Scientific	26616
Pierce® ECL Western Blotting Substrate	Thermo Fisher Scientific	#32106
Pierce® RIPA Buffer 100 ml	Sigma Aldrich	89900
Powdered milk	Carl Roth	T145.3
Roti-Phenol/ Chloroform/Isoamylalkohol	Carl Roth	A156.1
Rotiphorese Gel 30 (37,5:1)	Carl Roth	3029.1
SDS	Carl Roth	0183.3
SIG10 5α Chemically Competent cells	Sigma Aldrich	CMC
Temed	Biorad	#1610800
TRIS	Carl Roth	0188.3
Trizol ® Reagent	Life Technologies	15596018
Trypan Blue Solution	Sigma Aldrich	T8154
Trypsin	ThermoFisher Scientific	15400054

3.1.7 Kits

Product	Company	Catalog No.
Arginase Activity Assay Kit	Sigma Aldrich	MAK112-1KT
$CD8^+$ T cell isolation kit	Miltenyi Biotec	130-104-075
CellROX® Reagents	Thermo Fisher Scientific	C10422
FoxP3/ Transcription Factor Fixation/ Permeabilisation Concentrate and Diluent	eBioscience	00-5521-00
Isolate II Biofluids RNA Kit	Bioline	BIO-52086
Mouse IFN-γ ELISA MAX™ Deluxe	Biolegend	430804
Myeloid-derived Suppressor cell isolation kit	Miltenyi Biotec	130-094-538
NOS Detection Kit	Cell technologies	NOS200-2
Pierce™ BCA Protein Assay Kit	Thermo Fisher Scientific	23227
Pierce™ LAL Chromogenic Endotoxin Quantitation Kit	Thermo Fisher Scientific	88282
SensiFAST™ SYBR® Lo-ROX Kit	Bioline	BIO-94020
Toxisensor™ Chromogenic LAL Endotoxin Assay	GeneScript	L00350
Venor ® GeM Classic Mycoplasma Detection Kit	Minerva	11-1050

3.1.8 Primers for mRNA

Primer	Orientation	Sequence
18S RNA	forward reverse	5'-CGCGGTTCTATTTTGTTGGT-3' 5'-AGTCGGCATCGTTTATGGTC-3'
IL-1β	forward reverse	5'-TGTGAAATGCCACCTTTTGA-3' 5'-GGTCAAAGGTTTGGAAGCAG-3'
IL-6	forward reverse	5'-TGATGCACTTGCAGAAAACA-3' 5'-ACCAGAGGAAATTTTCAATAGGC-3'
Il-10	forward reverse	5'-GACGTGGAAGTGGCAGAAGAG-3' 5'-TGCCACAAGCAGGAATGAGA-3'
IL-17	forward reverse	5'-CAGCAGCGATCATCCCTCAAAG-3' 5'-TGAGGTTGACCTTCACATTCTGGA-3'
TNF-α	forward reverse	5'-GACGTGGAAGTGGCAGAAGAG-3' 5'-TGCCACAAGCAGGAATGAGA-3'
COX2	forward reverse	5'-TCTGGAACATTGTGAACAACATC-3' 5'-AAGCTCCTTATTTCCCTTCACAC
PD-L1	forward reverse	5'-TGGACAAACAGTGACCACCAA-3' 5'-CCCCTCTGTCCGGGAAGT-3'

3.1.9 Antibodies

Product	Clone	Company	Catalog No.
Alix	1A12	Santa Cruz	Sc-53540
Anti-Mouse IgG from rabbit	Polyclonal	Sigma-Aldrich	A9044-2ML
Anti-Rabbit IgG from Goat	Polyclonal	Sigma-Aldrich	A0545-1ML
anti-Tubulin Beta 3-Alexa Fluor 594	AA13	Biolegend	TUBB3
ARG-1-APC	MAB58681	RnD Systems	IC5856A
Calreticulin	D3E6	Cell signaling	12238S
CD11b-APC-Cy7	M1/70	BD	557657
CD45-V500	HI30	BD	557657
CD81	D5O2Q	Cell signaling	10037S
CD8-eFluor 450	53-6.7	eBiosciences	48-0081-80
CD9	EM04	Thermo Fisher Scientific	MA1-10309
FcR Blocking Reagent	2.4G2	BD	553141
GAPDH	1D4	Biolegend	919501
Gr-1-PE-Cy7	RB6-8C5	BD	552985
HSP72	Polyclonal	GeneTex	GTX111088
HSP86	Polyclonal	Novus Biologicals	NB120-2928
Human Phospho-RelA/NF-κ B	S536	RnD Systems	MAB72261-SP
Human/Mouse RelA/ NF-κ B	D14E12	RnD Systems	MAB50781
PD-L1-BV421	MIH5	BD	564716

3.1.10 shRNA

TRC Number	Gene	Clone ID	Company
TRCN0000321086	HSP90AA1	NM_010480.5-589s21c1	Sigma-Aldrich
TRCN0000321084	HSP90AA1	NM_010480.5-2221s21c1	Sigma-Aldrich
TRCN0000321007	HSP90AA1	NM_010480.5-1282s21c1	Sigma-Aldrich
TRCN0000321085	HSP90AA1	NM_010480.5-440S21c1	Sigma-Aldrich
TRCN0000321083	HSP90AA1	NM_010480.5-2743s21c1	Sigma-Aldrich

3.1.11 Primers for miRNA

Primer	Sequence
hsa-21-5p	UAGCUUAUCAGACUGAUGUUGA
hsa-125a-5p	UCCCUGAGACCCUUUAACCUGUGA
hsa-125b-5p	UCCCUGAGACCCUAACUUGUGA
hsa-146a-5p	UGAGAACUGAAUUCCAUGGGUU
hsa-155-5p	UUAAUGCUAAUUGUGAUAGGGGU
mmu-690	AAAGGCUAGGCUCACAACCAAA
hsa-let7e-5p	UGAGGUAGGAGGUUGUAUAGUU
U6	GUGCUCGCUUCGGCAGCACAUAUACUAAAAUUGGAACGAU ACAGAGAAGAUUAGCAUGGCCCCUGCGCAAGGAUGACACG CAAAUUCGUGAAGCGUUCCAUAUUUUU

3.1.12 Cell culture media

Name	Composition
Freezing medium	75 % FBS 25 % DMSO
MDSC exosome-depleted medium	500 ml RPMI Medium 1640 (1x) + GlutaMAXTM 10 % FBS (Ultracentrifuged at 23000 rpm for 16h) 1 % Penicillin/ Streptomycin 10 mM HEPES 1 mM Sodium Pyruvate 50 µM β-Mercaptoethanol 1 mM MEM Non-essential amino acids
MDSC Medium	500 ml RPMI Medium 1640 (1x) + GlutaMAXTM 10 % FBS 1 % Penicillin/ Streptomycin 10 mM HEPES 1 mM Sodium Pyruvate 50 µM β-Mercaptoethanol 1 mM MEM Non-essential amino acids

MSC Medium	500 ml RPMI Medium 1640 (1x) + GlutaMAXTM 10 % FBS 1 % Penicillin/ Streptomycin 10 mM HEPES
Ret Medium	500 ml RPMI Medium 1640 (1x) + GlutaMAXTM 10 % FBS 1 % Penicillin/ Streptomycin

3.1.13 Buffers

Name	**Composition**
1 x TBS	5 ml 1 M Tris/HCl, pH 8 15 ml 1 M NaCl 470 ml ddH_2O
10 % Separating polyacrylamide gel	21.3 ml ddH_2O 13.3 ml 30 % Acrylamide solution 5.3 ml 3 M Tris/HCL, pH 8.8 400 µl 10 % SDS 133 µl 10 % APS TEMED
10 x Running buffer	30 g Tris base 144 g Glycine 10 g SDS 10 l ddH_2O
10 x Transfer buffer	121.2 g Tris base 576 g Glycine 4 l ddH_2O
Blocking buffer for western blot	DPBS 3 % BSA 0.05 % Tween-20 in TBS
Blocking buffer for immunofluorescence	DPBS 5 % FBS 0.3 % Triton X-100
FACS buffer	DPBS 2 % FBS 0.2 % NaN3
MACS buffer	DPBS 1% BSA 0.5 mM EDTA
NP-40 lysis buffer	50 mMTris HCl, pH 8.0 150 mM NaCl 5 mM EDTA 10 % NP40 1 x Protease Inhibitor
Stacking polyacrylamide gel	6 ml ddH2O 1.35 ml 30 % Acrylamide solution 2.5 ml 0.5 M Tris/HCl, pH 6.8 100 µl 10 % SDS 100 µl 10 % APS 10 µl TEMED

3.1.14 Software for data analysis

Product	Version	Company
Flow Jo	7.6.1	Tree Star Inc.
GraphPad PRISM	5	GraphPad Software Inc.
NanoSight NTA software	3.0 0064	NanoSight

3.2 Methods

3.2.1 Isolation of EV

To study the interaction between melanoma-derived EV and the immune system, we established a protocol for isolating EV from the murine *Ret* melanoma cell line (Ret). Here, we used a modified EV-isolation protocol described by Lobb and Möller [121]. First, Ret cells were expanded in 100 x 75 cm^2 cell culture dishes. When Ret cells reached a confluence of 80-90 %, the media was discarded and Ret cells were washed with 5 ml PBS. PBS was discarded and serum-free Ret culture media was added to Ret cells. We chose to take serum-free media to exclude any exogenous vesicles that are present in the commercial available serum. After 24 h supernatant was taken and replaced by complete media. After Ret cells recovered from starvation stress, the procedure was repeated up to three times. The collected EV conditioned supernatant was frozen at -20 °C. On the day of isolation, the EV-containing supernatant was thawed at 37°C. The supernatant was sterile filtered through 0.22 µm filters, followed by a 100 kDA size exclusion filtration at 3800 g for 30 min at RT using Amicon Ultra Centrifugal Filters. This allowed us to get rid of proteins smaller than 100 kDA. After the size exclusion filtration, the concentrate was filled up with PBS and ultra-centrifuged for 90 min at 100.000 g and 4 °C. Afterwards, the Pellet was re-suspended in 500 µl sterile PBS and stored at -20 °C. The EV isolation method is illustrated schematically in Figure 6.

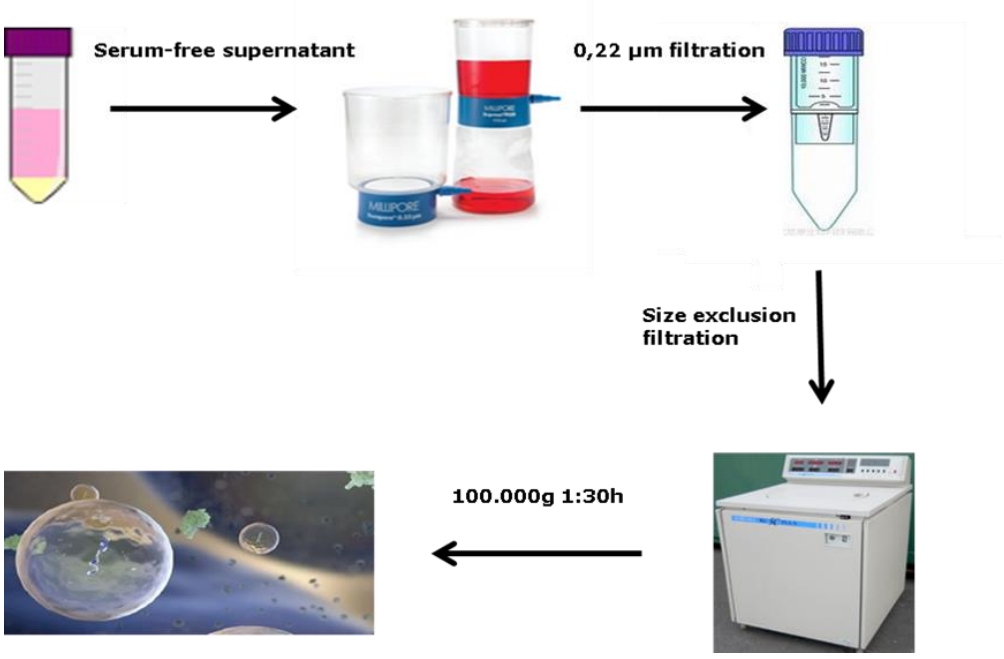

Figure 6: Isolation of Ret-EV. Ret-EV containing supernatant was sterile filtered with 0.22 µm filters. Afterwards, sterile supernatant was concentrated by 100 kDA size exclusion filtration. The concentrate was ultra-centrifuged by 100.000 g ultracentrifugation at 4°C for 90 min. EV-containing Pellet was re-suspended in sterile PBS.

3.2.2 Characterization of EV

3.2.3 Nanoparticle tracking analysis

To measure the concentration and size distribution of EV, we performed nanoparticle tracking analysis (NTA). This method calculates the size and concentration of EV according to the scattered laser light, which results due to the Brownian movement of particles. For this, EV were diluted 1:1000 in sterile filtered PBS and transferred via a 1 ml syringe into the detection chamber of the NanoSight NS300 microscope. Laser was switched on and focused via the NanoSight NTA software 3.0 0064. Camera level was set on seven and detection threshold on five. Capturing of EV was recorded for five times each 60 seconds. Temperature was monitored and updated after each run. After each batch of EV, detection chamber was washed with sterile filtered PBS.

3.2.4 Immunogold labeling of Ret-EV

To visualize EV and the EV-marker CD81 on EV, electron microscopy was done. Here, Immunogold labeling and detection via electron microscope was performed by the DKFZ core facility. Briefly, EV were labelled with 1:50 diluted rabbit anti-CD81 antibody followed by the detection of CD81-Antibody with 10 nm protein-A-Gold (Au10). Images were taken with an EM910 (Carl Zeiss, Oberkochen, Germany) at 80 kV and images were registered with a CCD-Camera (TRS-system, Tröndle, Moorenweis, Germany) using the proprietary software ImageSP.

3.2.5 MicroRNA microarray

For the isolation of miRNA from Ret-EV, we used the ISOLATE II Biofluids RNA Kit from Bioline (Germany). Here, we loaded 50 µg Ret-EV onto the column and followed the manufactures protocol. After isolation of whole RNA, concentration was determined via Nanodrop device and quality check was investigated by using Bioanalyzer. MicroRNA microarray was kindly performed by the DKFZ genomics and proteomics core facility using Mouse miRNA Microarray from Agilent.

3.2.6 Confocal microscopy

To test weather Ret-EV are taken up by myeloid cells, we performed uptake studies using confocal microscopy. First, 50 µg Ret-EV or PBS as a control were stained with 5 µM CFSE for 5 min at 37 °C. Labeled Ret-EV and PBS were transferred into ultracentrifugation tubes and filled up with PBS. Ret-EV and control was then ultra-centrifuged for 90 min at 100.000 g and 4 °C to wash out CFSE and afterwards re-suspended in sterile PBS. MSC-1 cells that were seeded onto cover slips in 6-well plates before were treated with labeled Ret-EV and control for 24 h. Next day, supernatant was aspirated and MSC-1 cells were fixed using 2 ml 4 % paraformaldehyde for 15 min at RT. Paraformaldehyde was removed afterwards and fixed MSC-1 cells were rinsed three times with PBS for 5 min each. Afterwards, MSC-1 cells

were blocked for 60 min at RT using blocking buffer followed by three times rinsing with PBS for 5 min. The blocked MSC-I cells were then stained for their cytoskeleton using 1:400 in blocking buffer diluted anti-Tubulin Beta 3 Antibody for 60 min at RT. After the staining, the cells were washed three times with PBS and mounted using Fluoromount-G overnight at RT. Images were taken by Diego (Medical University Mannheim) using Leica TCS SP2 confocal microscope.

3.2.7 Coupling of EV on latex beads

The size of EV are under the size threshold of the BD Canto and BD Lyric flow cytometers. To increase the size of EV and therefore, to allow flow cytometry analysis of EV, we had to couple them on latex beads. For this purpose, we diluted 1 µl of 4 µm latex beads with 1000 µl PBS. 50 µg of EV were added to the latex beads and incubated for 60 min at RT on a shaking platform (900rpm). Afterwards, we added 100 µl of 1M Glycin/PBS and 100 µl of 10 % BSA in PBS to block the latex beads. Blocking was done for 30 min at RT on a shaking platform. The beads were washed with 1 ml FACS buffer at 13.000 g for 2 min two times. After washing, 1 µl primary antibody in 100 µl FACS buffer was added to the EV-coupled latex beads and stained for 60 min at 4 °C in the dark. After the staining, EV-coupled latex beads were washed twice at 13.000 g for 2 min with 1 ml FACS buffer. Subsequently, 1 µl of secondary antibody in 100 µl FACS buffer was added and incubated for 60 min at 4°C in the dark, followed by two times washing at 13.000 g for 2 min with 1 ml FACS buffer. After washing EV-coupled latex beads were ready for flow cytometry.

3.2.8 Gating of latex beads

In order to analyze EV-coupled on latex beads, we needed an appropriate gating strategy. The gating strategy is shown in Figure 7. First, Forwardscatter (FSC) area (A) was set against Sidewardscatter (SSC) area (A) to gate on latex beads, based on their morphology.

Afterwards, the PE intensity was compared against the secondary PE-conjugated antibody as a negative control (shown in red) and CD9-PE staining (in blue) as a positive control.

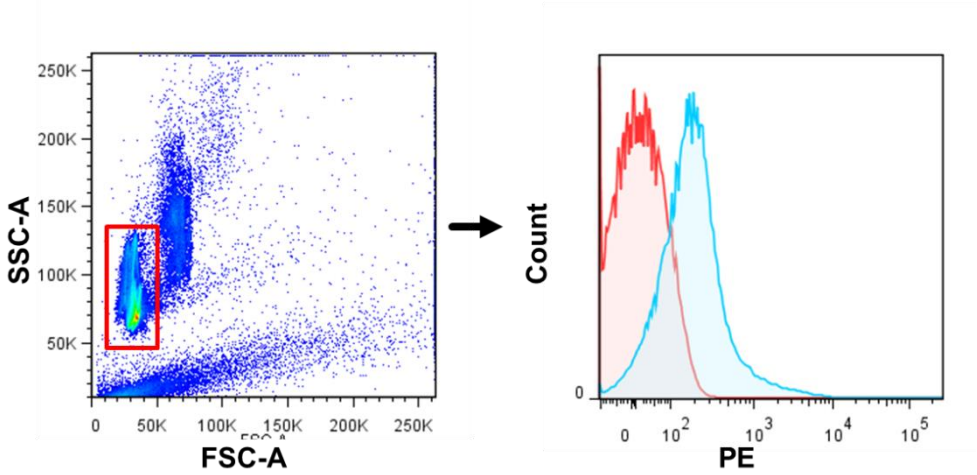

Figure 7: Gating strategy of EV-coupled on latex beads.

3.3 Biochemical methods

3.3.1 Protein isolation

Cells: For the protein isolation, we used 1 x 10^6 cells of the respective cell line. Cells were transferred to an Eppendorf tube and washed with PBS at 300 g for 5 min at 4 °C. Afterwards, cells were re-suspended in 300 µl NP-40 lysis buffer. The cells were lysed for 30 min at 4 °C on a shaking platform. After cell lysis, the cell debris was removed by centrifugation at 13.000 g for 10 min at 4 °C. The supernatant was transferred to a new Eppendorf tube and stored at -20 °C. If protein was needed for Western blot analysis, lysate was mixed with LDL-buffer supplemented with 5 % β-mercaptoethanol in a ratio of one to four prior storage.

EV: For the protein isolation we used 20 - 30 µg of respective EV. We add 1 x LDL-sample buffer supplemented with 5 % β-mercaptoethanol to the EV. Then, EV were boiled at 95 °C for 5 min and stored at -20 °C.

3.3.2 Bicinchoninic-acid assay

To determine the protein concentration of cell lysate or EV, we performed the Bicinchoninic-acid assay (BCA) by using the Pierce™ BCA Protein Assay Kit. First, we prepared the working reagent by diluting 4.9 ml of BCA Reagent A with 0.1 ml of BCA Reagent B. Then, 0.2 ml of the working reagent was transferred to wells of a 96-well microplate containing either 25 µl of the premixed protein standard or the unknown protein sample. The mixture was incubated for 30 min at 37 °C. After incubation, plate was cooled down to RT followed by the measuring of the absorbance at 562 nm using the microplate reader.

3.3.3 SDS-polyacrylamide gel electrophoreses (SDS-PAGE)

SDS-Page represents a gel electrophorese-based method to separate protein mixtures according to their molecular weight. For this purpose, premade SDS-gels were inserted into electrophoresis chambers and the device was filled up with 1 x running buffer. 10 – 20 µg of proteins were loaded into the wells of the SDS gel, as well 7 µl of the protein ladder. Proteins were separated at 80 V until the leading front runs out of the SDS gel.

3.3.4 Western blot analysis

After the SDS-PAGE was finished, the separated proteins on the SDS-gel were transferred onto a Polyvinylidenfluorid (PVDF) membrane. For this, we used the semi-dry botting technique. First, three Whatman papers were soaked with 1 x transfer buffer and put onto the anode of the blotting device. Then, the PVDF was activated in methanol and washed in ddH_2O, followed by soaking in 1 x transfer buffer. The activated PVDF membrane was placed on the Whatman papers. The SDS-gel was equilibrated in 1 x transfer buffer and placed above the PVDF membrane, followed by three stacks of Whatman papers. The proteins were then transferred onto three PVDF membrane at 0.6 mA/per blotting stack for 90 min.

3.3.5 Immunoblotting

To detect the immobilized proteins on the PVDF membrane, we had to label them with the appropriate antibody and mark the antibody for chemiluminescence. First, the PVDF membrane was blocked with 3 % BSA in TBS for 30 min at RT to prevent non-specific binding of antibodies. After the blocking, primary antibody in TBS-T supplemented with 3 % BSA was added to the membrane and incubated on a shaking platform for 60 min at RT. Afterwards, the membrane was washed three times with TBS-T for 5 min at RT. Then the horseradish-peroxidase conjugated secondary antibody (in TBS-T supplemented with 3 % BSA) was added and incubated on a shaking platform either for 60 min at RT or 24 h at 4 °C. Subsequently, the PVDF membrane was again washed three times with TBS-T for 5 min at RT. In order to detect the respective antibody, the PVDF membrane was incubated with 5 ml with Pierce® ECL Western Blotting Substrate for 1 min. This solution contains luminol that becomes oxidized by the horseradish peroxidase and therefore starts emitting light. This light was detected by the Fusion SL detection device.

3.3.6 RNA isolaton

For RNA Isolation from cells and EV, the ISOLATE II Biofluids RNA Kit was used and whole RNA was isolated according manufactures protocol. Isolated RNA was stored at -80 °C until further downstream applications.

3.3.7 cDNA synthesis

The RNA was thawed up on ice and concentration was measured using the NanoDrop device. For the cDNA synthesis we used the Sensi FAST™ cDNA Synthesis Kit from Bioline. 1 µg of RNA was used and the DNA synthesis was performed according to the manufacturer's protocol. For the miRNA experiments a different kit was used. Here, the miRCURY LNA™ Universal RT microRNA PCR Kit by EXIQON was chosen and the

preparations were done according to the manufacturer´s protocol. The cDNA samples were finally stored at -20°C for further use.

3.3.8 RT-PCR of mRNA

To evaluate the expression of selected mRNA, we performed RT-PCR using the Sybr green technology. Therefore, a master mix was prepared containing 1 µg of cDNA (diluted in ddH_2O), 1 mM of respective forward and reserve primer and 17,5 µl Sybr green (Sensi FAST™ SYBR Low-ROX Kit from Bioline). 10 µl of the master mix was transferred as triplicates to a 96-well microplate. For the amplification of mRNA the MX3005P qPCR System from Stratagene was used. Amplification program is shown in table 2.

Step	Temperature	Duration	Cycles
1	50 °C	2 min	1
2	95 °C	10 s	42
3	59 – 63 °C	1 min	42
4	95 °C	1 min	1
5	65 °C	30 s	1
6	95 °C	30 s	1

Table 2: Program for mRNA amplification

3.3.9 RT-PCR of mRNA

To evaluate the expression of selected miRNA, we performed RT-PCR using the Sybr green technology. For specific primer binding, we used locked nucleic acid (LNA) primers from Exiqon. For this purpose, a master mix was prepared containing 1 µg of cDNA (diluted in ddH_2O), 3 µl of respective LNA primer and 17,5 µl Sybr green (Sensi FAST™ SYBR Low-ROX Kit from Bioline). 10 µl of the master mix was transferred as triplicates to a 96-well microplate. For the amplification of mRNA the MX3005P qPCR System from Stratagene was. Amplification program is shown in table 3.

Step	Temperature	Duration	Cycles
1	50 °C	2 min	1
2	95 °C	10 s	45
3	60 °C	1 min	45
4	4 °C	endless	1

Table 3: Program for miRNA amplification

3.4 Cell culture

3.4.1 Isolation of IMC

We used IMC from the BM to study myeloid cells because of their high amounts in the BM and the convenient isolation procedure. IMC were isolated from the tibia and femur of 8 – 12 weeks old C57Bl/6 mice. Therefore, mice were sacrificed by cervical dislocation and the femur and tibia were removed and kept in sterile PBS. Tibia and femur, as well whole cell culture procedure was done under the cell culture hood to allow sterile conditions. First, the endings of tibia and femur were chopped to have access to the BM. Subsequently, BM was flushed out with sterile PBS into a 50 ml conical tube by using a syringe. BM was then filtered through a 100 µm cell strainer to separate remaining fat tissue and hair. BM cells were washed with PBS at 300 g for 5 min and 4 °C. The supernatant was discarded and erythrocytes were lysed with 1 ml Ammonium-Chloride-Potassium (ACK) lysis Buffer for 3 min at RT. After lysis, BM cells were washed with PBS at 300 g for 5 min and 4 °C. To specifically isolate IMC from whole BM cells, we used the MDSC isolation Kit from Miltenyi Biotech. This kit specifically isolates Ly-6G and Gr-1 positive cells via magnetic separation. First, BM cells were re-suspended in 300 µl MACS buffer and 50 µl FC block reagent was added and incubated for 5 min on ice. Then, 100 µl anti-Ly6G-biotin antibodies were added an incubated for further 10 min on ice. After Incubation, cells were washed with PBS at 300 g for 5 min and 4 °C. Pellet was re-suspended in 800 µl MACS buffer and 200 µl anti-biotin MicroBeads and incubated for 15 min on ice. Cells were then washed with PBS at 300 g for 5

min and 4 °C and cell pellet was re-suspended with 500 µl MACS buffer. Cells were then transferred into a LS column on a magnetic rack that was prior equilibrated with 5 ml MACS buffer tubes. LS column were washed three times with 3 ml MACS buffer and flow through that contained Ly6G negative cells was collected in a 15 ml conical tube. The LS column was detached from magnetic rack and 5 ml MACS buffer was applied and flushed out with a plunger. Those cells were the Ly-6G positive cells and were kept on ice until further use. Next, Ly6G negative cells were taken and washed with PBS at 300 g for 5 min and 4 °C and cell pellet was re-suspended with 400 µl MACS buffer and 100 µl anti-Gr1-biotin antibody. Cells were stained for 10 min on ice and then washed with PBS at 300 g for 5 min and 4 °C. Cell pellet was re-suspended with 800 µl MACS buffer and 200 µl anti-streptavidin MicroBeads and incubated for 15 min on ice. Subsequently, cells were washed with PBS at 300 g for 5 min and 4 °C and cell pellet was re-suspended with 500 µl MACS buffer. Cells were then applied on a pre-equilibrated MS column on a magnetic rack, followed by three times washing with 500 µl MACS buffer. At the end, MS column was detached from magnetic rack and 1 ml MACS buffer was added to the column. Column was flushed out with a plunge into the conical which contains the Ly-6G positive cells. The isolated IMC were then stored on ice until further use.

3.4.2 Gating of IMC

In order to analyze IMC, we needed an appropriate gating strategy. The gating strategy is shown in Figure 8. First, forwardscatter (FSC) area (A) was set against sidewardscatter (SSC) area (A) to gate IMC, based on their morphology and living state. Afterwards, FSC-A against FSC-H was chosen to exclude duplets. Subsequently, CD11b and Gr-1 positive cells were gated and checked for their PD-L1 expression. Here, we used the fluorescence minus one (FMO) as the border for gating.

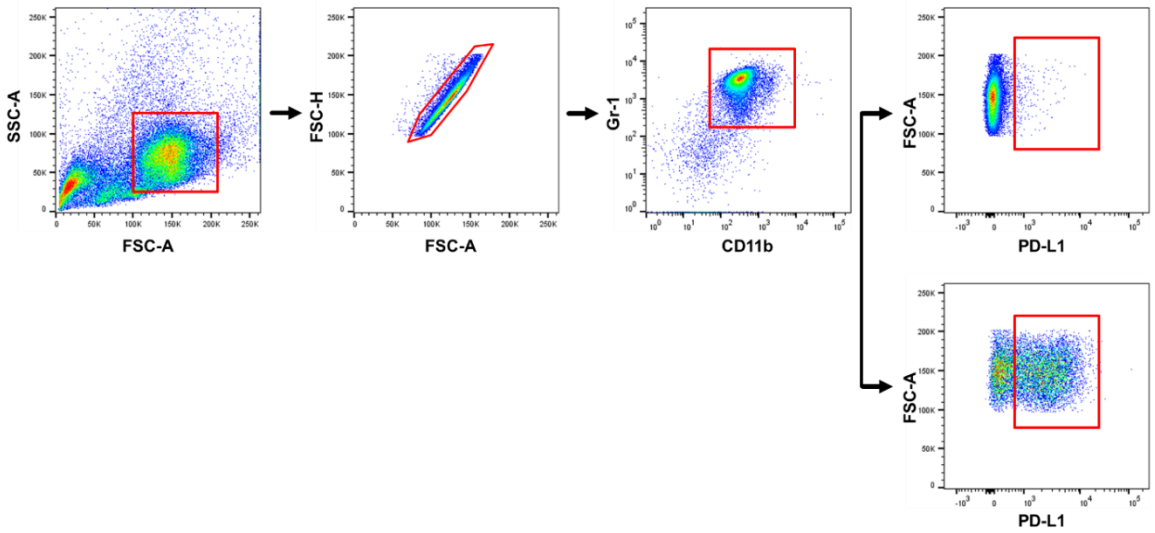

Figure 8: Gating strategy of isolated IMC

3.4.3 EV treatment of IMC

To investigate the effects of Ret-EV on IMC, we cultured the isolated IMC in EV-depleted MDSC media. 100.000 IMC in 100 µl media were added to wells of a 96-well plate (U-bottom) and treated with 50 ug/ml Ret-EV for either 3 h or 16 h. After incubation with Ret-EV, IMC were prepared for further analysis

3.4.4 Co-culture studies

To investigate Ret-EV mediated upregulation of PD-L1 on IMC, we performed in addition to EV treatment experiments, co-culture studies with Ret cells and IMC. The co-culture studies were moreover a control to exclude artificial effects of the harsh procedure of ultracentrifugation, as well endotoxins. For this purpose, we used a trans-well system. In a 24-well plate 2.5 x 10^5 ret cells or fibroblasts were seeded and cultured overnight to assure enough secreted EV in the media. To block EV secretion by ret cells, we added 15 µM 5-(N,N-Dimethyl)amiloride hydrochloride (DMA), an inhibitor of the Na2+/H+ antiporter that was shown to reduce EV secretion. Next day, 2.5 x 10^5 isolated IMC were added above the ret cells in a trans-well insert with a pore size of 0.4 µm. The co-culture was incubated overnight 37 °C and 5 % CO2 for 24 h and next day, IMC were taken and prepared for flow cytometric analysis.

3.5

3.6 Tissue preparation

3.6.1 Bone marrow

BM cells were isolated from the tibia and femur of C57Bl/6 mice. Therefore, mice were sacrificed by cervical dislocation and the femur and tibia were removed and kept in sterile PBS. Tibia and femur, as well whole cell culture procedure was done under the cell culture hood to allow sterile conditions. First, the endings of tibia and femur were chopped to have access to the BM. Subsequently, BM was flushed out with sterile PBS into a 50 ml conical tube by using a syringe. BM was then filtered through a 100 µm cell strainer to separate remaining fat tissue and hair. BM cells were washed with PBS at 300 g for 5 min and 4 °C. The supernatant was discarded and erythrocytes were lysed with 1 ml Ammonium-Chloride-Potassium (ACK) lysis Buffer for 3 min at RT. After lysis BM cells were washed with PBS at 300 g for 5 min and 4 °C and were ready for the staining for flow cytometry.

3.6.2 Gating of BM cells

To analyze whole BM, we first excluded duplets by using FSC-A against FSC-H. Afterwards, we gated based on the morphology by SSC-A and FSC-A. To exclude dead cells, we gated on 7-AAD negative cells. Finally, CD11b and Gr-1 positive cells were gated.

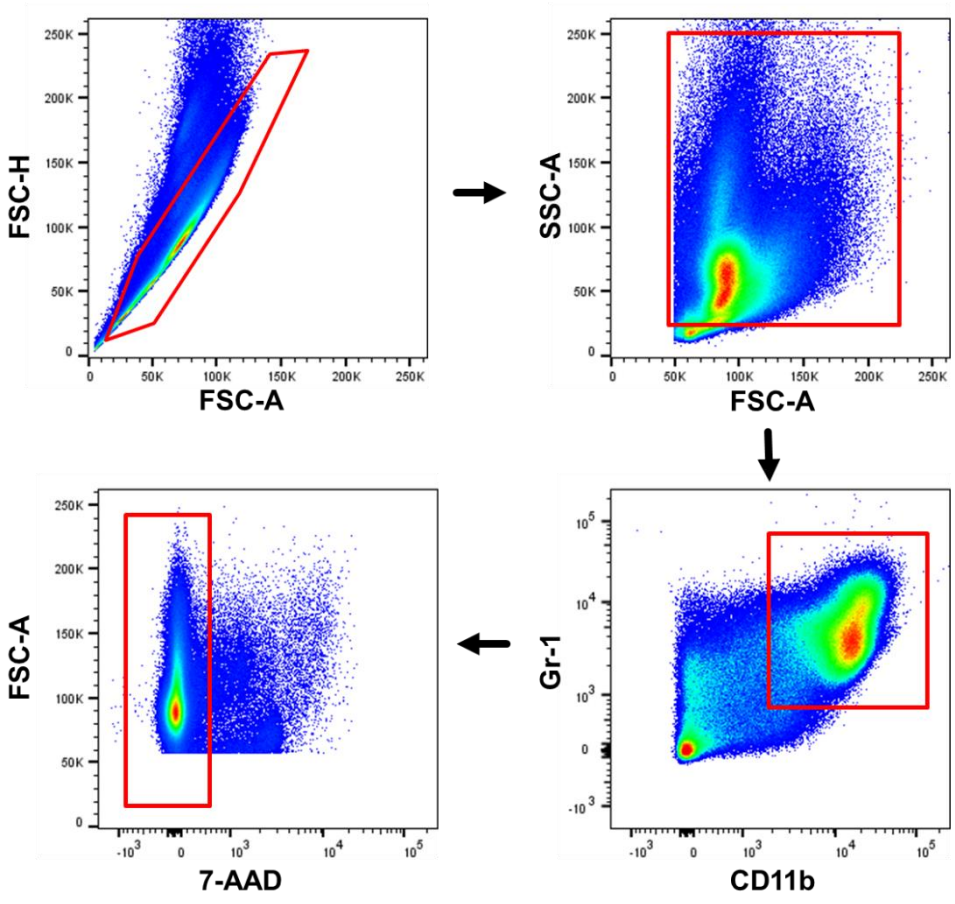

Figure 9: Gating strategy for BM cells

3.6.3 Tumor

As a source for the tumors, we used the transplantable *Ret* model. Here, we diluted 500.000 Ret cells in 100 µl sterile PBS. Ret cells were then injected subcutaneously into the right flank of mice. During tumor development, tumor growth was monitored and measured with a caliper. After 14 days or when tumor reached the size of 1.5 cm in diameter, tumor-bearing mice were sacrificed by cervical dislocation. Tumor was extracted and transferred into sterile PBS. Afterwards, single cell suspension was prepared by pushing through the tumor tissue through 100 µm cell strainer by using a plunge. Tumor cells were washed in PBS at 300 g for 5 min and 4 °C and again pushed through a 40 µm cell strainer. Subsequently, tumors were washed again at 300 g for 5 min and 4 °C and prepared for the staining for flow cytometry.

3.6.4 Gating of tumor

To analyze MDSC in the TME, we used following gating strategy: First duplets were excluded by using FSC-A against FSC-H. Next, we gated based on the morphology by using SSC-A and FSC-A. To exclude dead cells, we gated on 7-AAD negative cells. To select leukocytes in the TME, we gated on CD45 positive cells. Finally, we gated in CD11b and Gr-1 positive cells that are MDSC. The Gr-1 higher population represents PMN-MDSC and the population underneath represents the monocytic MDSC.

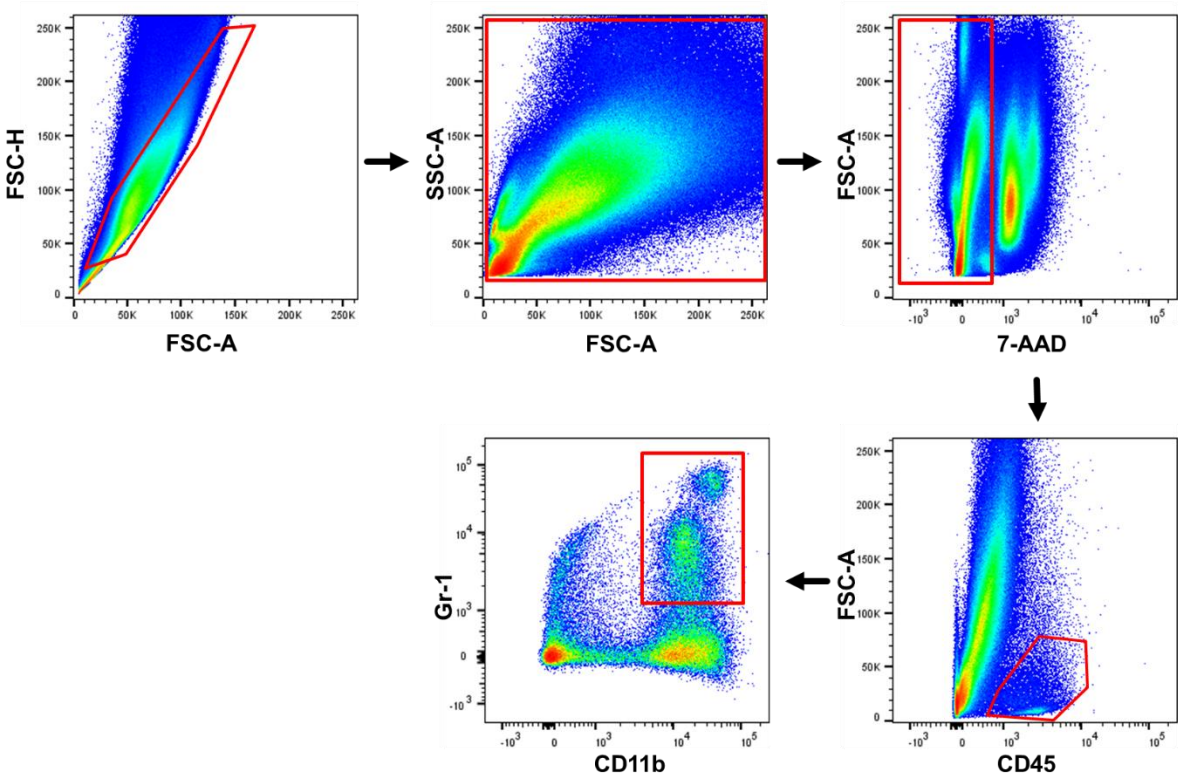

Figure 10: Gating strategy of tumor tissue

3.6.5 Spleen

Spleen was taken from C57Bl/6 mice. Mice were sacrificed by cervical dislocation, followed by the extraction of the spleen. The spleen was transferred into sterile PBS in a 6-well plate and mechanically dissociated using scissors and tweezers. Afterwards, spleen fragments

were pressed through a 100 µm cell strainer to get single cell suspensions. Subsequently, Cells were washed at 300 g for 5 min and 4 °C. Cell pellet was lysed for 3 min at RT by using 1 ml of ACK lysis buffer. After 3 min, 20 ml PBS was added and cells were washed at 300 g for 5 min and 4 °C. Cell pellet was re-suspended in 300 µl MACS buffer and stored at 4 °C until further need.

3.6.6 Adult mouse cardiac fibroblast isolation

As a control for Ret-EV, we used EV isolated from heart fibroblasts. Heart fibroblasts are easy and quick to isolate and produce abundant amounts of EV. For this purpose, adult mouse hearts from freshly euthanized mice were placed on Petri dish with sterile ice cold PBS, the blood was pumped out with forceps, and hearts were transferred in a clean Petri dish. Hearts were minced on ice with scissors, and per each 5 hearts 25ml of lysis buffer containing 100 U/ml of collagenase and 0.1 % of trypsin in HBSS were added. Tissue was digested in this buffer on constant shaking at 37^{o}C for 10 minutes. Supernatant was collected in a Falcon tube, and digestion was continued until tissue was dissolved (7-10 cycles of digestion). After centrifugation (300 x g at +4 ^{o}C for 5 min), cells were re-suspended (5 ml per 1 heart) in DMEM/F12 media, containing 10 % FBS and 100 U/ml of PenStrep, and plated into 100 mm cell culture dishes (10 ml of cell suspension per dish). After 2 h the media was changed, and only fibroblasts were adhered at this time point. Fibroblasts were cultivated upon 80- 90 % confluence and split in ratio1:5. After the confluence of 80-90 % was achieved again, the isolation of EVs was performed as usual.

3.6.7 Staining for flow cytometry

For visualizing the cells via flow cytometry, we had to prior stain them with fluorophore-conjugated antibodies or fluorescent chemical compounds. For this, 1x10^{6} cells (for tumor cells 3x10^{6} were used) were seeded into a 96-well U-bottom plate and centrifuged at 300 g for 5 min 4 °C. Supernatant was discarded and pellet was re-suspended with 100 µl

1:100 Fc-Block in FACS buffer and incubated for 10 min on ice. Next, 100 µl FACS buffer was added and cells were washed at 300 g for 5 min and 4 °C. Next, master mix containing conjugating antibodies and fluorescent chemical compounds were added to stain surface antigens, NO, ROS or dead cells. Cells were re-suspended in 50 µl master mix and incubated for 30 min on ice in the dark. After staining, cells were washed at 300 g for 5 min and 4 °C. Cells were then either re-suspended in 100 µl FACS buffer and ready for flow cytometry or if intracellular staining was needed, cells were re-suspended in 200 µL of fixation/permeabilization solution (1:4 dilution) (eBioscience) for 30 min at 4 °C in the dark. Afterwards, cells were washed twice with 200 µL permeabilization buffer. Subsequently, supernatant was discarded and cells were stained with conjugating antibodies targeting intracellular antigens for 30 min at 4 °C in the dark. After staining, cells were washed at 300 g for 5 min and 4 °C and pellets were re-suspended in 100 µL permeabilization buffer. Finally, cells were ready to be measured via flow cytometry.

3.6.8 Proliferation assay

To determine the immunosuppressive activity of IMC after EV treatment we performed T cell proliferation assays. Here, we treated IMC as mentioned before with Ret-EV and incubated them for 16 h. Next day, Ret-EV were washed out twice at 300 g for 5 min at 4 °C. If needed, IMC were incubated with neutralizing antibody against PD-L1 for 15 min on ice, followed by a washing step. In parallel splenic $CD8^+$ T cells were isolated and prepared for the assay by using the $CD8^+$ isolation kit from Miltenyi. As mentioned before, we prepared single cell suspensions from spleen and re-suspended splenic cells in 300 µl MACS buffer. 100 µl of $CD8^+$ antibody-biotin cocktail was added and incubated for 10 min on ice. Afterwards, 400 µl MACS buffer and 200 µl Streptadvidin-MicroBeads were added and incubated for 15 min on ice. After staining, 10 ml PBS was added and cells were washed at 300 g for 5 min and 4 °C. Supernatant was discarded and cell pellet was re-suspended with 500 µl MACS buffer. Cells were then applied on a pre-equilibrated MS column on a magnetic rack, followed by three times washing with 500 µl MACS buffer. The flow through was collected, which resembles

$CD8^+$ T cells. T cells were centrifuged at 300 g for 5 min and 4 °C and re-suspended in 2 ml PBS containing 5 uM Carboxyfluorescein diacetate succinimidyl ester (CFSE). Cells were stained at 37 °C for 5 min. Afterwards, 10 ml MACS buffer was added and labeled T cells were washed at 300 g for 5 min and 4 °C. T cells were re-suspended in MDSC buffer to a concentration of 1.000.000 cells/ml. T cells were then treated with 2 µl per 20.000 T cells with pre-washed CD3/CD28 Dynabeads. T cells were then added to IMC in indicated ratios and incubated for 72 h. After three days, cells were washed at 300 g for 5 min and FC-Block reagent (1:100 in FACS buffer), as well CD8-eFluor antibody (1:100 in FACS buffer) were added. After cells were stained for 15 min on ice in the dark, they were washed and re-suspended in 100 µl FACS buffer, followed by flow cytometry.

3.6.9 Gating of proliferating $CD8^+$ T cells

In order to investigate the proliferation of splenic $CD8^+$ T cells, we performed the following gating strategy. First, morphology was gated based on FSA-A and FSC-A. Subsequently, we gated on CD8 and checked its CFSE intensity. The un-proliferated gate was set according to CFSE-labeled $CD8^+$ T cells but without CD2/CD28 activation.

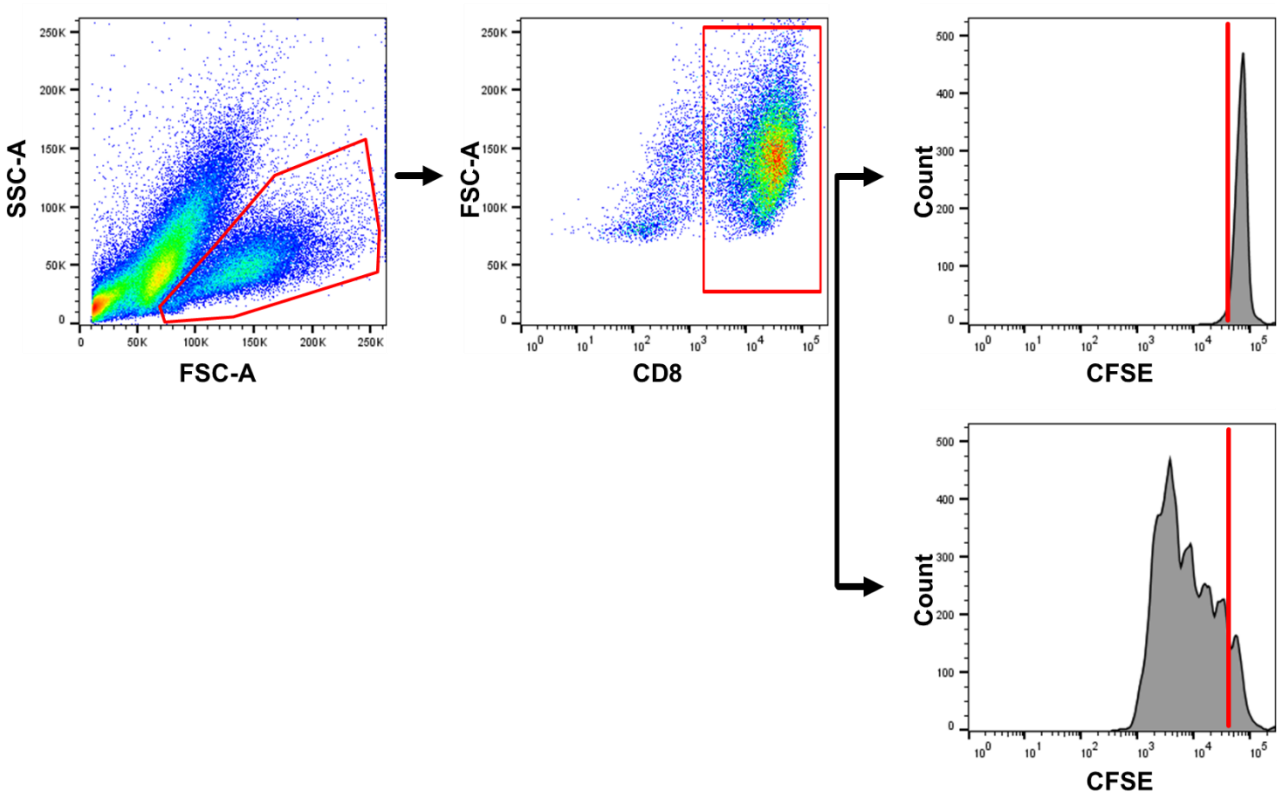

Figure 11: Gating strategy for proliferating T cells.

3.6.10 Interferon-γ secretion

Besides testing the suppressive activity of EV-treated IMC in proliferation assays, we performed additionally IFN-γ secretion assays. Here, we used 50 µl of the supernatant from the proliferation assay and transferred this supernatant in an IFN-γ pre-coated NUNC Maxisorp 96-well ELISA plate and followed the manufactures instruction. Briefly, the supernatant was incubated in the sealed plate for 2 h at RT on a shaking platform. Afterwards, plates were washed four times with PBS. Subsequently, 100 µl detection antibody was added and incubated for 1 h at RT on a shaking platform. Plate was washed four times and 100 µl Av-HRP was added and incubated for 30 min at RT on a shaking platform. After washing the plate four times, 100 µl of TMD-substrate was added and incubated for 30 min at RT on a shaking platform. Finally, the reaction was stopped by adding 100 µl 1 M H_2SO_4 and absorbance was measured 450 nm within 30 min.

3.6.11 Arginase Activity Assay

In order to measure Arginase 1 activity, we used the Arginase activity assay Kit from Sigma-Aldrich. Here, we seeded 500.000 IMC into a 24-well plate and treated them with 50µg/ml Ret-EV or PBS as a control for 16 h at 37 °C. Next day, cells were taken and lysed with 100 µl NP-40 lysis buffer for 30 min at 4 °C. Cell lysate was centrifuged for 15 min at 13.0000 g. Subsequently, 100 µl of supernatant was taken and used for the Arginase activity assay, which was performed according to the manufactures protocol. Arginase activity was measured at 430 nm and calculated according to manufactures equation.

3.6.12 Transduction with lentiviral particles

Lentiviral transduction was kindly performed by Dr. Hüser, DKFZ. Briefly, HEK293T cells were used for lentiviral particle production. For transfection, plasmid containing respective shRNA (11 µg) was incubated with the packaging plasmids VSV-G (5.5 µg) and pCMV-dR 8.91 (8.25 µg) in DMEM and X-treme GENE® (Roche) solution for 30 min and added to HEK293T producer cells. After incubation for 12, 24, 36 and 48 h, the supernatant was collected and virus particles were concentrated by ultracentrifugation. Then Ret cells were incubated with concentrated virus for 24 h. Upon the first infection, Ret cells were re-infected with the same virus in fresh medium, and after 48 h of transduction, the cells were washed twice with PBS and cultured. To select transduced cells, 2 µg/ml puromycin was added for 3 days.

3.6.13 Alamar blue assay

In order to test whether transduced cells were impaired in their proliferation, alamar blue assays were performed by Dr. Hüser, DKFZ. Briefly, Ret melanoma cells with stably knocked down HSP86 or treated with scrambled sequence shRNA construct were seeded in 96 well plates at a density of 2500 cells/well. Alamar blue (10% of the culture medium volume) was added after cell attachment for 4 h followed by the measurement of florescence at an

emission wavelength of 535 nm and an excitation wavelength of 590 nm using a SpectraMax M5 microplate reader (Tecan Infinite F200 PRO). Cells were incubated further for 24, 48 and 72 h; alamar blue was added for the 4 h before the end of each time point and the fluorescence was measured.

3.6.14 Statistics

Statistical analyses were performed using GraphPad Prism (GraphPad Software) on at least 3 independent experiments if not indicated differently. Data were analyzed with a one-way ANOVA test for multiple groups or an unpaired two-tailed Student´s t test for two groups. A value of $P < 0.05$ was considered as statistically significant.

4 Results

4.1 Characterization of Ret-EVs

To study the interaction between melanoma-derived EV and the immune system, we established a protocol for isolating EV from the murine *Ret* melanoma cell line (Ret). Therefore, we used a modified EV-isolation protocol described by Lobb and Möller [121].

To verify the quality of our isolated Ret-EV, we performed several quality checks, which are in accordance with the guidelines “Minimal experimental requirements for definition of extracellular vesicles” [122]. Each batch of Ret-EV was analyzed by nanoparticle tracking analysis (NTA). This method measures the concentration and size distribution of particles due to their Brownian movement. Figure 7A demonstrates a representative histogram after the NTA. Ret-EV are 99.1 nm ± 7.2 nm in diameter and the concentration is 1-5 x 10^{12} EV/ml. Furthermore, we performed Western blot analysis of Ret-EV and the respective Ret cell lysate to demonstrate the presence of EV markers. Figure 7B shows that the EV surface markers CD9 and CD81 and the intraluminal EV-marker ALIX are strongly enriched in the Ret-EV samples. Importantly, we could exclude calreticulin in the Ret-EV preparations. Since calreticulin is a protein located in the endoplasmatic reticulum, this result indicates that our Ret-EV preparations are free from other organelles and cell debris. As a last quality check, CD81-immunogold labeling of Ret-EV was performed in the DKFZ electron microscopy core facility. Figure 7C shows a representative snap-shot of Ret-EV. The result shows the presence of CD81 on the Ret-EV the size distribution, which is about 100 nm.

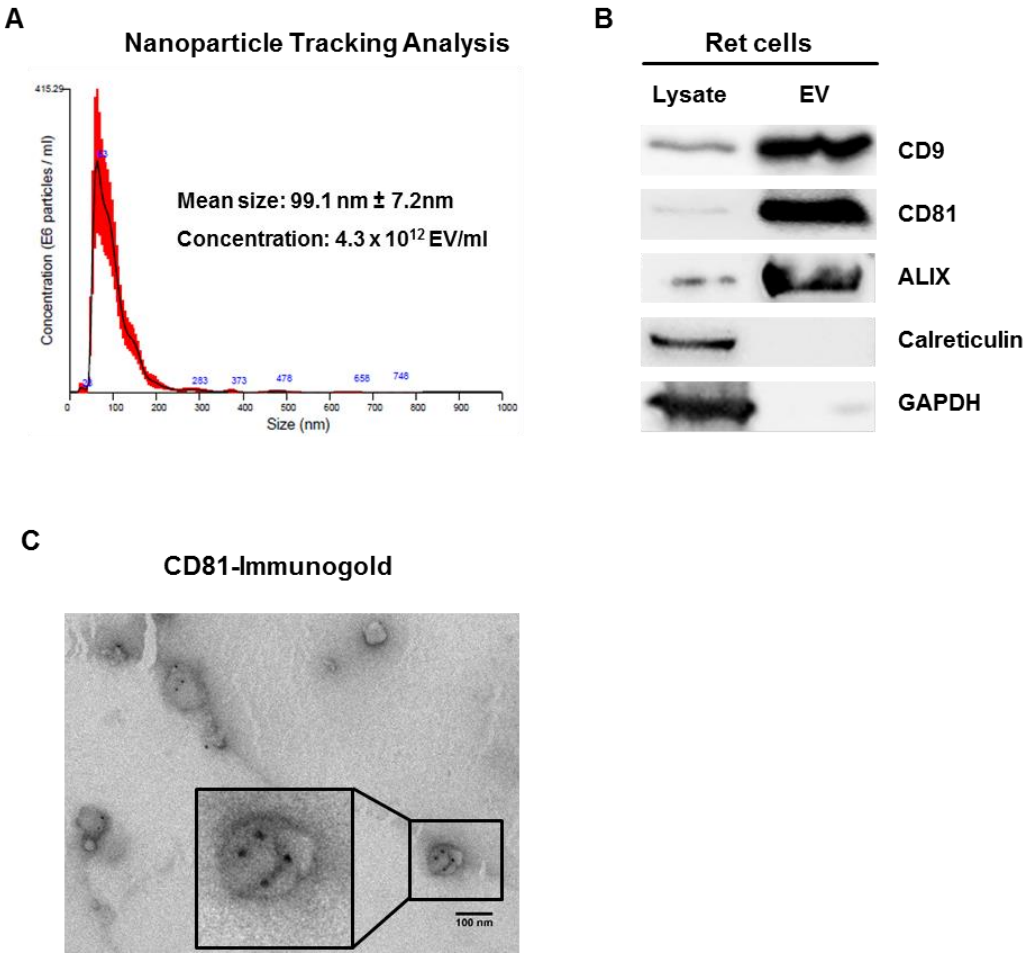

Figure 12: Characterization of Ret-EV. Ret-EV were isolated by filtration and ultracentrifugation. **A)** Nanoparticle tracking analysis of Ret-EV. **B)** Representative sample showing the expression of EV- markers (CD9, CD81 and ALIX) detected by Western blot analysis. The ER marker calreticulin was used as a negative control. **C)** EV marker CD81 detected by immunogold labeling and electron microscopy.

4.2 Ret-EV are taken up by myeloid cells

EV are known to trigger signaling pathways in cells. This could be achieved either by EV binding to surface receptors or their uptake by cells, where the transferred cargo can stimulate signaling pathways in the cytoplasm. To test whether our Ret-EV are taken up by myeloid cells, we treated the immortalized myeloid suppressor cell line (MSC)-1 or IMC with CFSE-labeled Ret-EV. Figure 8 demonstrates the uptake of CFSE-labeled RET-EV by MSC-1 cells visualized by confocal microscopy (Fig. 8A) and IMC analyzed by flow cytometry (Fig. 8B).

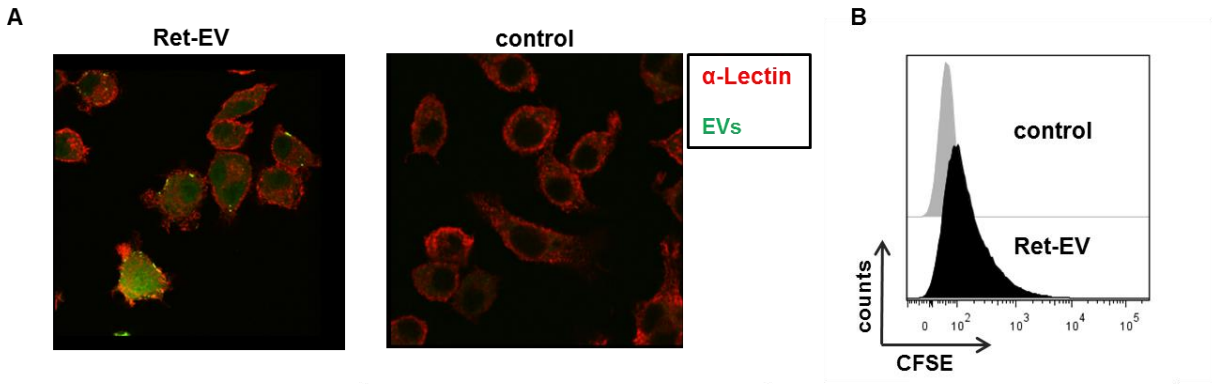

Figure 13: Uptake of Ret-EV by myeloid cells. Ret-EV were labeled with CFSE and incubated with murine MSC-1 cells or BM-derived IMC for 16 h. As a control, we incubated CFSE in PBS with the same concentration as Ret-EV. After CFSE labeling Ret-EV and control were ultra-centrifuged to wash out residual CFSE. **A)** The internalization of CFSE-Ret-EV by MSC-1 cells was measured by fluorescent confocal microscopy **B)** and by IMC via flow cytometry.

4.3 Ret-EV alters global miRNA expression in IMC

Recent publication highlighted the EV-mediated conversion of myeloid cells into immunosuppressive cells like MDSC or M2 macrophages [84, 123, 124]. Especially, miRNA seems to be important for this conversion mediated by tumor-derived EV [125]. To assess if RET-EV could induce an immunosuppressive phenotype of IMC by altering their miRNA expression pattern, we performed miRNA microarrays. The heat-map (Fig. 9A) and volcano plot (Fig. 9B) display a differential expression pattern of distinct miRNA in IMC after Ret-EV treatment. In total 119 miRNA are significantly down regulated, whereas 83 are upregulated.

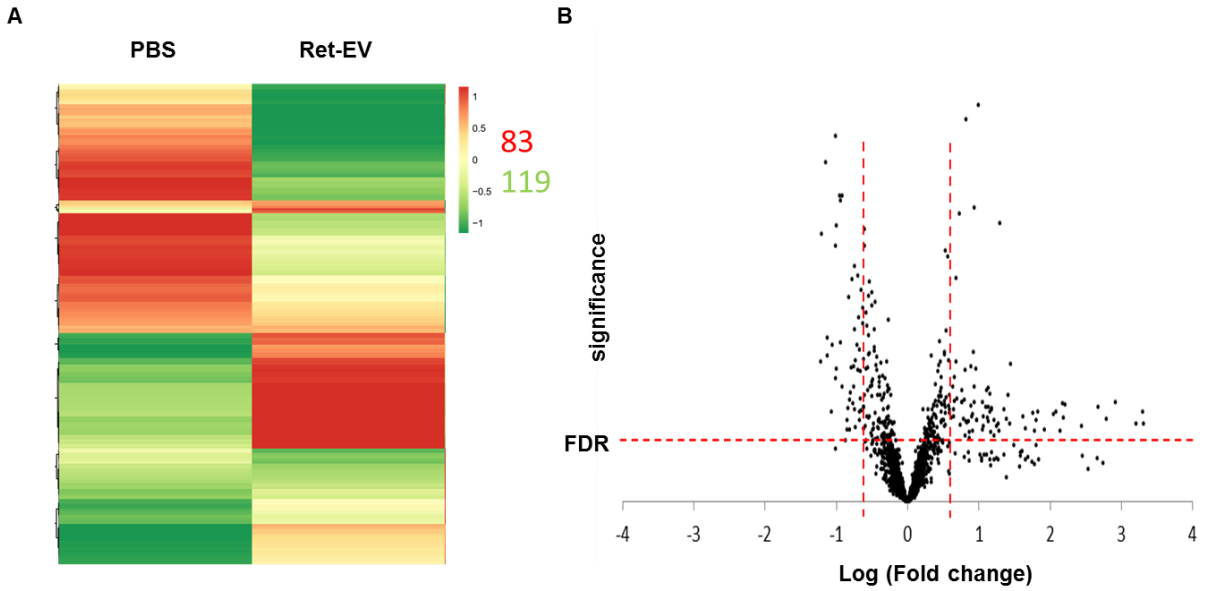

Figure 14: IMC show altered miRNA expression profile after Ret-EV treatment. IMC isolated from the BM of wild type C57BL/6 mice were treated with Ret-EV or PBS for 3 h. After 3 h whole RNA content was isolated and miRNA microarray was performed using Agilent chip. **A)** Heat-map analysis and **B)** Volcano-plot showed different miRNA expression profile of IMC treated with either Ret-EV or PBS.

By clustering these 202 differentially expressed miRNA in a pathways analyzing tool, we found that most of the differentially expressed miRNA are associated with pathways in cancers and especially 34 of those miRNA were correlated with melanoma progression (Table 2).

miRNA Pathways analysis	
Pathways in cancer	>90
PI3K-Akt signaling pathway	46
Regulation of actin cytoskeleton	42
MAPK signaling Pathway	42
TNF Signaling pathway	39
Melanoma	34

Table 4: Pathways analysis (Diana tools V.5) of IMC treated with Ret-EV.

To verify the miRNA microarray data, we examined via RT-PCR the expression of specific miRNA in IMC after Ret-EV treatment. Hereby, we picked miRNA, which were shown to be important for MDSC function and biology. Figure 10A confirms the microarray data. All chosen miRNA were up regulated, and miRNA 125a and miRNA 690 showed the highest upregulation after Ret-EV treatment.

Besides miRNA, we tested the expression of distinct mRNA from cytokines in IMC after Ret-EV treatment, which are known to be produced in high amounts by MDSC. Figure 10B demonstrate the upregulation of several cytokines produced by IMC after Ret-EV treatment. The pro-inflammatory molecules TNF-α and COX-2, as well the anti-inflammatory cytokine IL-10 showed the highest upregulation upon Ret-EV stimulation.

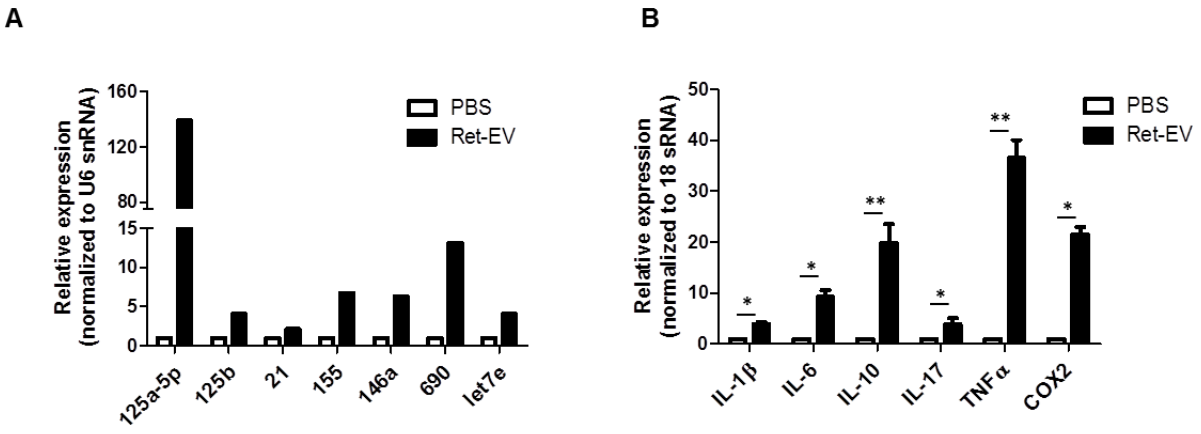

Figure 15: Ret-EV-mediated upregulation of miRNA and cytokines important for MDSC biology. IMC isolated from the BM of wild type C57BL/6 mice were treated for 3 h with Ret-EV. Afterwards whole RNA was isolated and converted into cDNA. RT-PCR analysis of respective **A)** miRNA (n=2) and **B)** cytokines show relative expression level of PBS and Ret-EV-treated IMC (mean ± SEM; n=3). *p < 0.05, **p < 0.01.

4.4 Production of immunosuppressive factors by IMC treated by Ret-EVs

In order to test whether Ret-EV can induce the upregulation of known immunosuppressive mediators, we treated IMC for 16 h with Ret-EV followed by flow cytometry. Interestingly, we could not see a difference in the production of ROS and NO, as well the expression of Arg-1 between Ret-EV-treated IMC and the control group. (Fig. 11A-C). To confirm that Arg-1 expression and activity is unchanged, we measured the activity of Arg-1 to catabolize its substrate arginine into ornithine. Figure 11D demonstrate that Arg-1 activity is unchanged in IMC upon Ret-EV treatment.

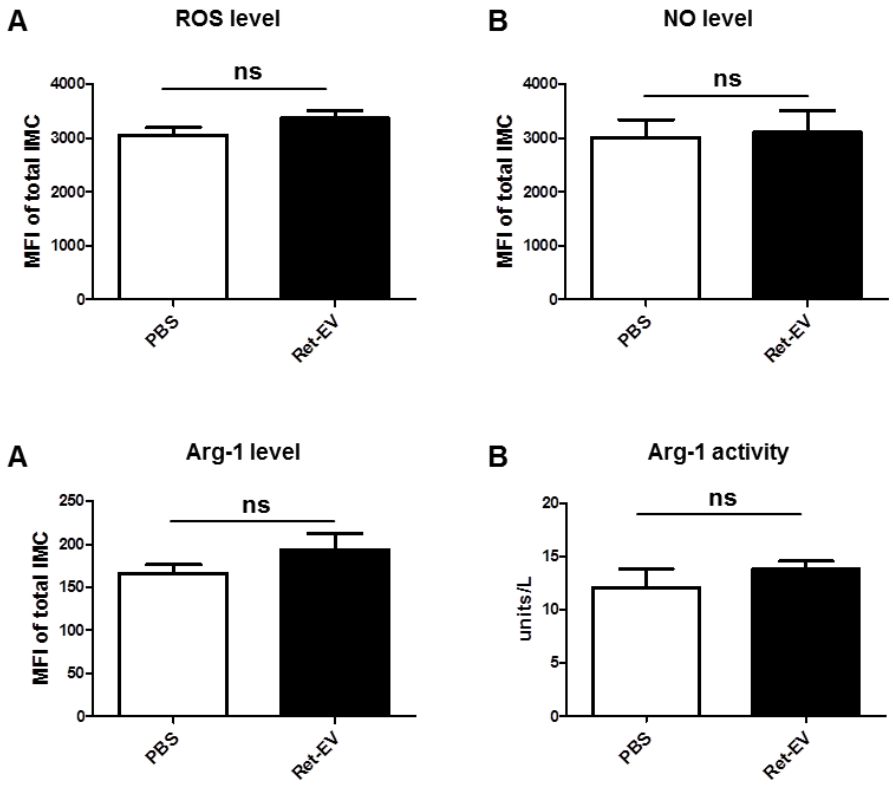

Figure 16: Well-known immunosuppressive mediators are unchanged in IMC upon Ret-EV treatment. IMC isolated from the BM of wild type C57BL/6 mice were treated with Ret-EV for 16 h. Afterwards IMC were stained for flow cytometry **A-C)** MFI of ROS, NO and Arg-1 from whole IMC population is shown. **D)** Represents Arg-1 activity in Units/l measured by photometrical assay to measure Arg-1 activity. (mean ± SEM; n=3)

4.5 PD-L1 expression on IMC is up regulated after Ret-EV treatment

Next, we examine the expression of PD-L1 on IMC after Ret-EV treatment. Figure 12A demonstrates a representative dot plot measured via flow cytometry. After Ret-EV treatment, almost half of the population acquires positivity for PD-L1, whereas the control group (treated with PBS) showed only 2-3 % of the population to be positive. To verify if this PD-L1 upregulation is specific for tumor-derived EV, we isolated treated IMC with EV from cardiac fibroblasts (Fibro-EV) and could not detect significant alterations compared to the PBS control (Fig. 12B). Interestingly, besides the frequency of PD-L1^{+} IMC, also the expression level of PD-L1 (measured by median fluorescence intensity, MFI) was increased upon Ret-EV treatment (Fig. 12C). Western blot analysis confirmed the data of flow cytometry (Fig. 12D).

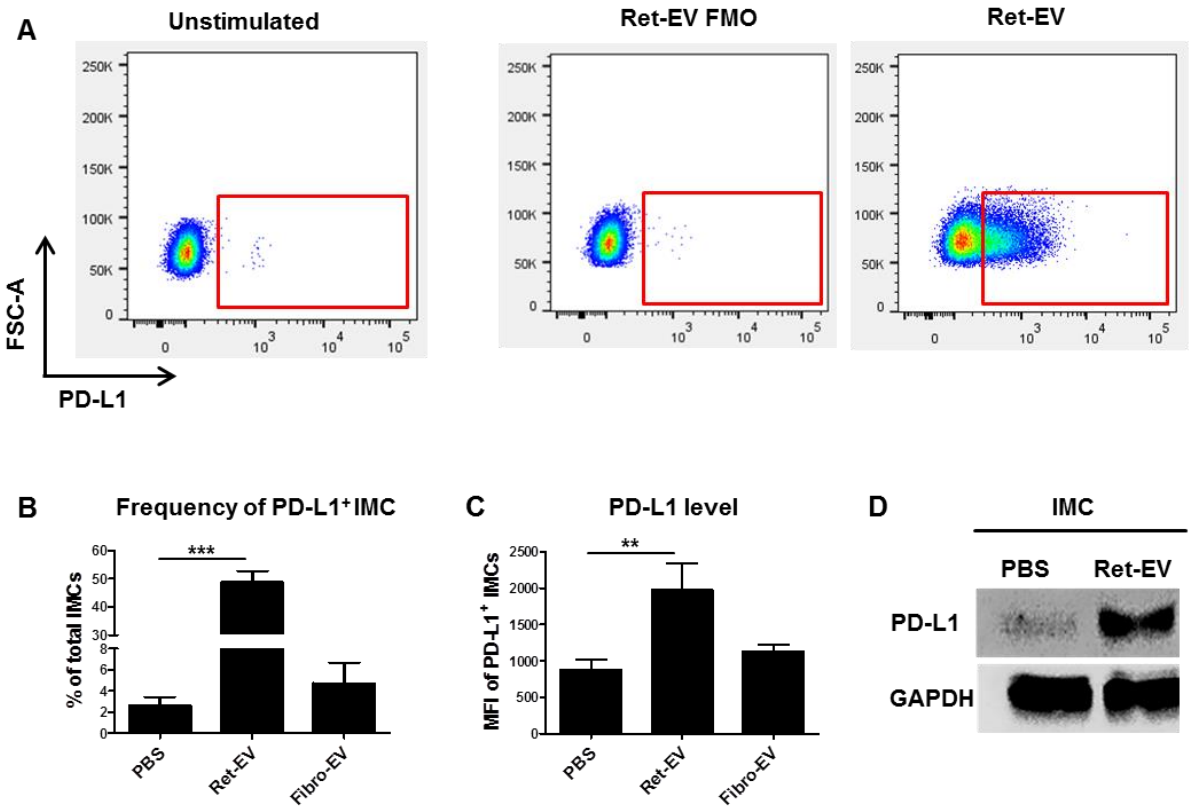

Figure 17: PD-L1 expression is up regulated on IMC after Ret-EV treatment. IMC isolated from the BM of wild type C57BL/6 mice were treated with Ret-EV for 16 h. **A)** Representative dot plots of PD-L1 expression on IMC before and after 16 h Ret-EV treatment (including FMO control of Ret-EV treated IMC). PD-L1 expression on IMC with Ret-EV or EV isolated from cardiac fibroblasts (Fibro-EV) was evaluated by flow cytometry. **B)** represents the percentage of PD-L1$^+$ IMC within total IMC and **C)** the level of PD-L1 expression measured as mean median fluorescence intensity (MFI) **D)** Representative Western blot analysis showing PD-L1 expression in IMC upon Ret-EV treatment. (mean ± SEM; n=3). *p < 0.05, **p < 0.01, ***p < 0.001.

4.6 Co-culture of IMC and Ret cells

To exclude that the Ret-EV-mediated PD-L1 upregulation on IMC is due to endotoxin contamination or side effects of the harsh procedure of ultracentrifugation, we performed co-culturing studies in the trans-well system. Figure 13A shows the outline of the experimental setup. Ret cells or fibroblasts were seeded into wells and above IMC were seeded into trans-wells. The pore size of the trans-wells were 0.4 µm in size, excluding thereby a direct cell to cell contact and allowing only soluble factors and EV to circulate. Figure 13B and C show

that only Ret cells up regulate the expression of PD-L1 on IMC, whereas fibroblasts do not show a significant effect on PD-L1 expression on IMC. To prove if the PD-L1 upregulation is due to EV, we co-cultured Ret cells in media supplemented with dimethyl-amiloride (DMA), an H^+-antiporter inhibitor that was shown to indirectly block the secretion of EV [126]. The addition of DMA into the co-culture system significantly reduced PD-L1 upregulation, suggesting that EV play a major role in the induction of PD-L1 on IMC.

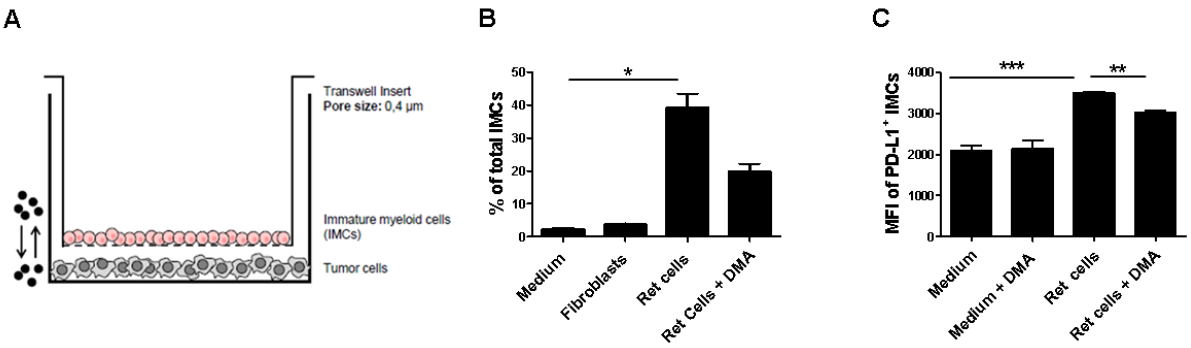

Figure 18: Trans-well studies confirm the Ret-EV-mediated PD-L1 up regulation on IMC. A) Ret cells or fibroblasts were co-incubated with IMC for 24 h using a 0.4 µm trans-well system. The analysis of PD-L1 expression on IMC was performed by flow cytometry. **B)** Data are shown as the percentage of PD-L1$^+$ IMC among total IMC and **C)** the level of PD-L1 expression as MFI (mean ± SEM; n=4) *p < 0.05, **p < 0.01, ***p < 0.001.

4.7 Ret-EV mediated PD-L1 upregulation occurs *in vivo*

Next we address the question if Ret-EV could mediate PD-L1 upregulation also *in vivo*. For this, we genetically modified the Ret cell line by transducing a construct that overexpress GFP-coupled to CD81. This CD81-fusion protein should be included into EV, since CD81 is a predominant protein in EV. The uptake of CD81-GFP$^+$ EV by recipient cells makes it possible to visualize them via flow cytometry and to follow EV uptake *in vivo* (Fig. 14A). We injected subcutaneously the modified Ret cells into C57Bl/6 mice. After 14 days of tumor development, we sacrificed tumor-bearing mice and found CD81-GFP$^+$ MDSC (Fig. 14B). Those MDSC showed a tendency to have higher expression levels of PD-L1 (Fig. 14C). This data highlights the importance of Ret-EV-mediated PD-L1 up regulation *in vivo* and confirms *in vitro* effects.

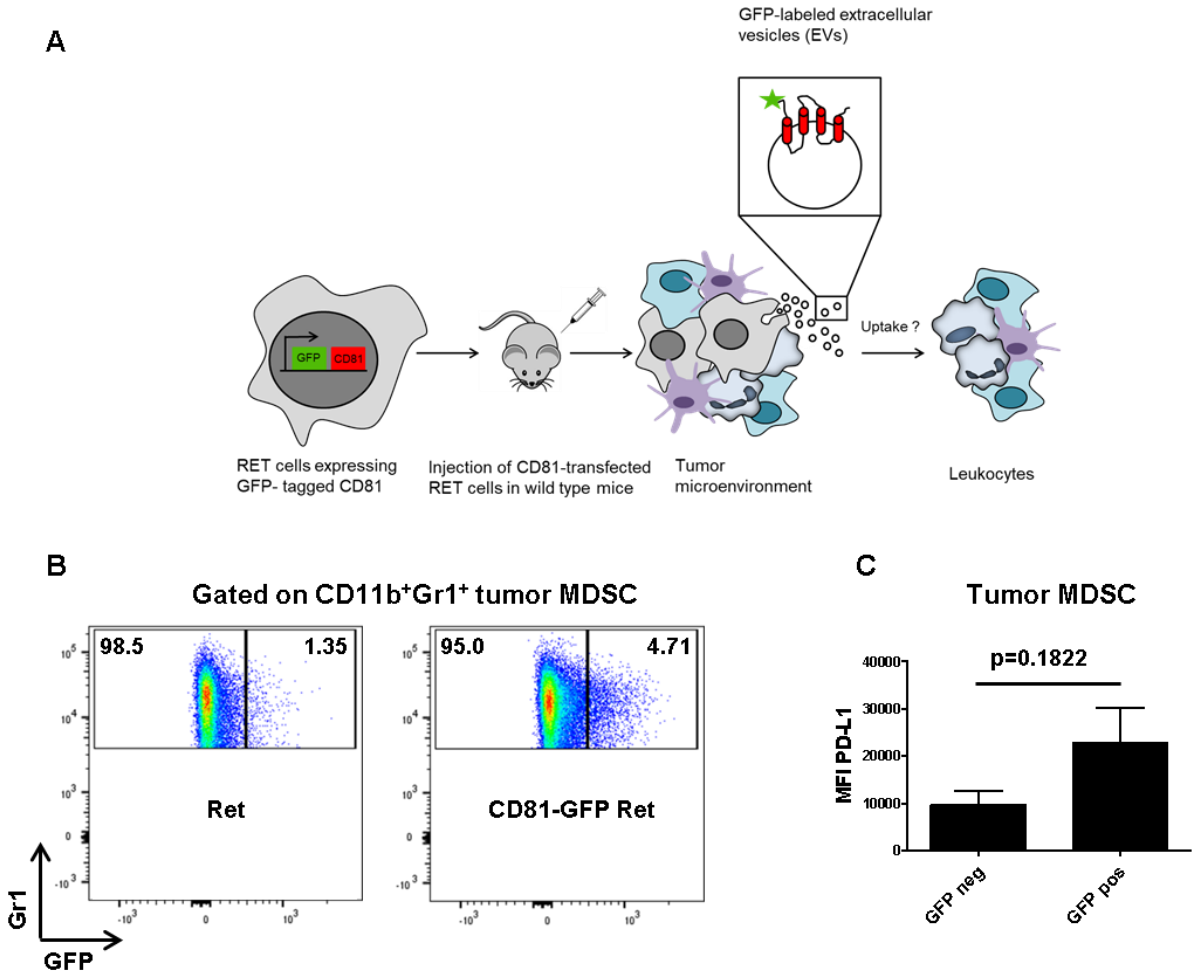

Figure 19: Ret-EV mediated upregulation occurs *in vivo*. A) Demonstrates a schematic overview of the experiment. GFP is linked to CD81 that is incorporated into EV. EV are released by tumor cells and recipient cells take up the GFP-labeled tumor-derived EV. Ret cells were transduced with vector expressing CD81 linked to GFP or control vector. **B-C)** Transduced cells were injected subcutaneously into C57BL/6 mice. Upon 14 days of tumor growth, mice were sacrificed and single cell suspension from tumor tissue was made followed by staining for MDSC. Stained samples were measured by flow cytometry. **B)** Representative dot plots for GFP expression in tumor-infiltrating $CD11b^{+}Gr1^{+}$ are shown. **C)** Expression of PD-L1 on GFP^{+} MDSC was presented as MFI (mean ± SEM; n=3).

4.8 Ret-EV convert IMC into immunosuppressive cells

To test whether Ret-EV convert IMC into immunosuppressive cells, we performed T cell proliferation assays with Ret-EV treated IMC. After 16 h of incubation, we washed out Ret-EV twice and added CFSE-labelled splenic $CD8^+$ T cells to the IMC. After three days, we measured the proliferation rate of the T cells via flow cytometry and found a decreased proliferation rate of $CD8^+$ T cells. The inhibition of proliferation was dependent on the ratio between Ret-EV treated IMC and $CD8^+$ T cells. As expected, we did not observe alterations in proliferation when we cultured PBS-treated IMC with activated $CD8^+$ T cells or $CD8^+$ T cells alone (Fig. 15A). To elucidate if PD-L1 was the major immunosuppressive mediator, we blocked PD-L1 via neutralizing antibody and observed that the proliferation rate was almost completely restored when blocking PD-L1 on IMC treated with Ret-EV (Fig. 15B). Besides the proliferation rate, we measured the secretion of IFN-γ by $CD8^+$ T cells as an indicator for their activity. Similar to the proliferation rate, Ret-EV treated IMC were able to dampen the IFN-γ production, which was restored upon blocking PD-L1 on IMC. Our data indicates that PD-L1 upregulation on Ret-EV-treated IMC is the major driver for their immunosuppressive activity.

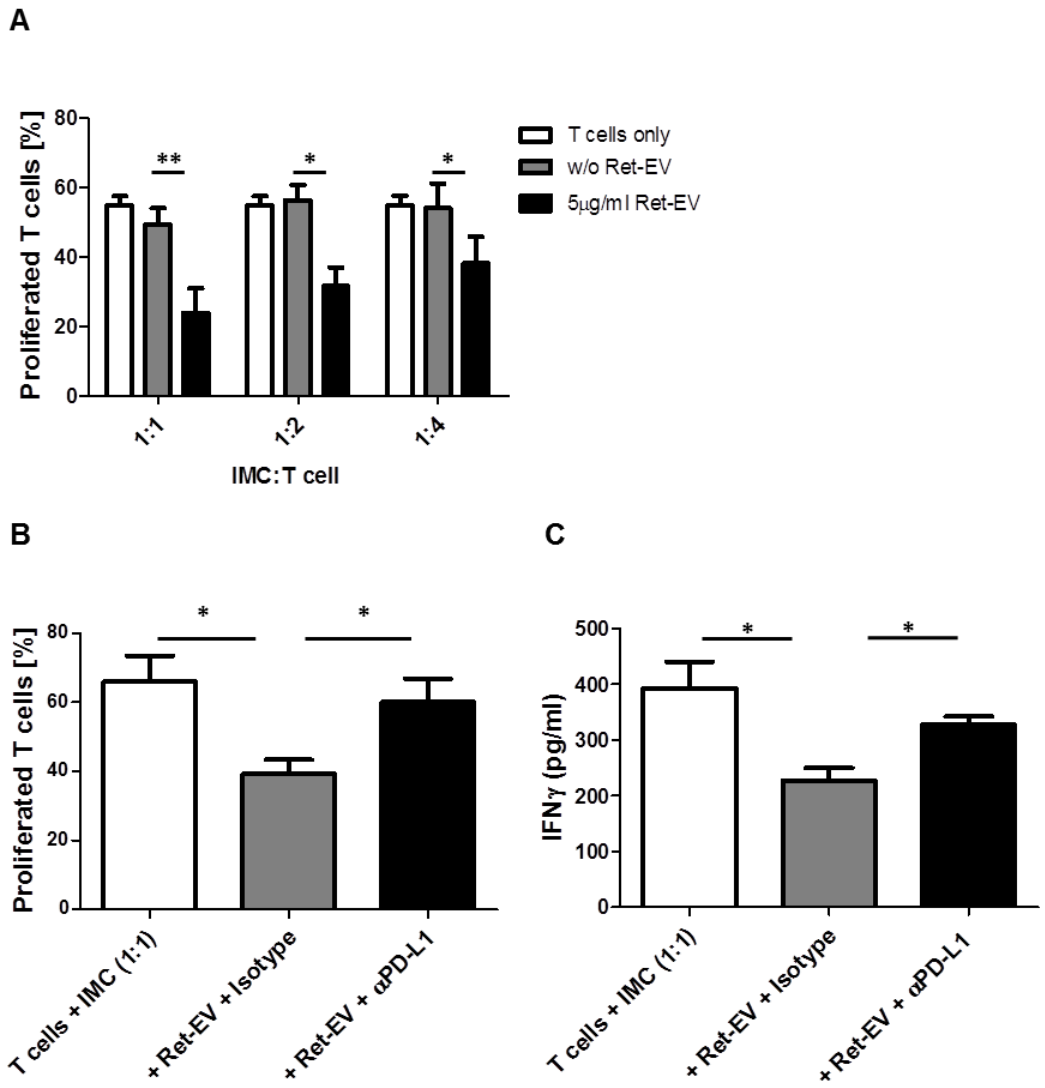

Figure 20: EV-treated IMC show immunosuppressive capacity mediated by PD-L1. IMC isolated from the BM of C57BL/6 mice were incubated with Ret-EV for 16 h. After washing out the rest of EV, cells were treated with PD-L1 neutralizing or isotype control mAbs (Iso) for 15 min followed by the co-incubation with normal spleen $CD8^+$ T cells labeled with CFSE and stimulated with anti-CD3/CD28 Dynabeads for 72 h. T cell proliferation was evaluated by CFSE dilution by flow cytometry. **A)** Inhibition of $CD8^+$ T cell proliferation by EV-treated IMC at indicated IMC:T cell ratio. Data are presented as the percentage of divided T cells (mean ± SEM; n=6). **B)** Proliferation and **C)** IFN-γ secretion of stimulated $CD8^+$ T cells upon blocking PD-L1 expression on IMC (IMC:T cell ratio=1:1; mean ± SEM; n=3). *$p < 0.05$, **$p < 0.01$.

4.9 PD-L1 in Ret-EV is not transferred to recipient cells

Next, we investigate if PD-L1 upregulation is due to the transfer of PD-L1 on Ret-EV to recipient cells or is achieved by new synthesis of PD-L1. As shown by Western blot analysis Ret cells strongly express PD-L1 and moreover, Ret-EV also displayed some expression of PD-L1 (Fig. 16A). To study the mechanisms of Ret-EV-mediated PD-L1 upregulation, we used MSC-1 and MSC-2 cells. The treatment of MSC-2 with Ret-EV induced an upregulation of PD-L1, whereas MSC-1 did not show such effect (Fig. 16B). We could exclude that MSC-1 cells are incapable to take up Ret-EV as we proved it before (Fig. 8A). To test whether PD-L1 upregulation is due to its new synthesis, we treated MSC-2 cells with actinomycin-D (an inhibitor of RNA synthesis) prior Ret-EV treatment. As shown in Figure 16C, MSC-2 cells treated with actinomycin-D did not show an induction of PD-L1, indicating that PD-L1 new synthesis is induced upon Ret-EV treatment, whereas transfer of vesicular PD-L1 plays a minor role.

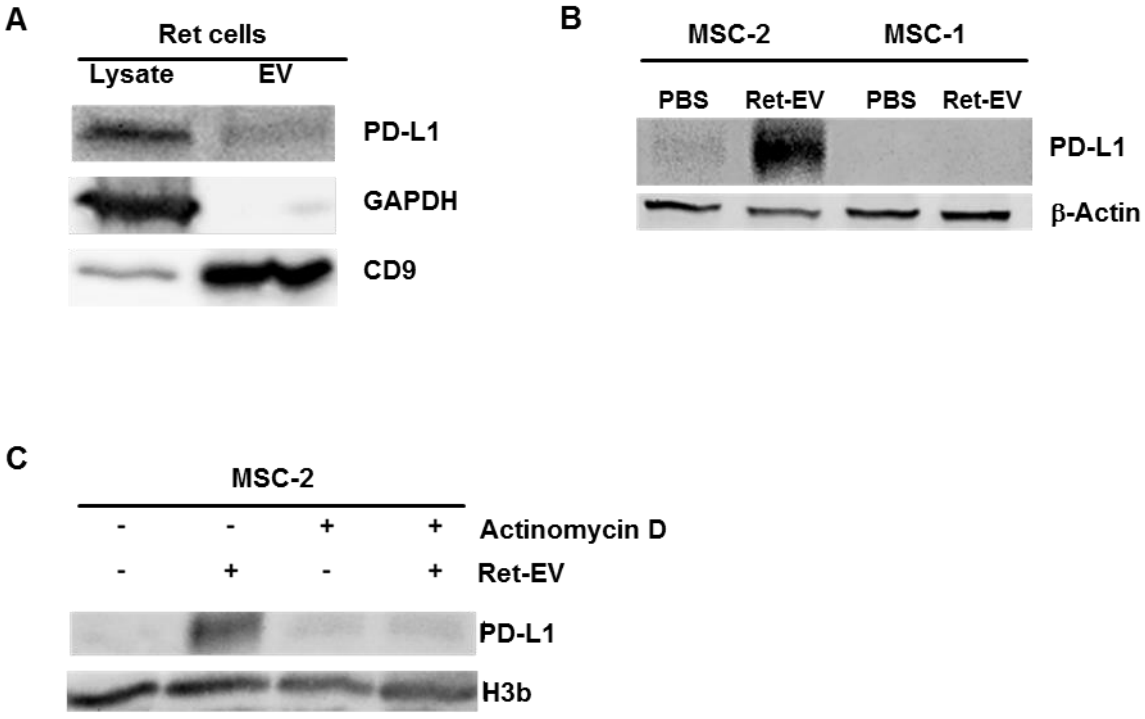

Figure 21: PD-L1 is not transferred via vesicular transport. A) Representative Western blot of PD-L1 in Ret-lysate and Ret-EV. **B)** MSC-2 and MSC-I cells were treated with Ret-EV and PD-L1 expression was determined after 16 h via Western blot. **C)** MSC-2 cells were treated with the RNA synthesis inhibitor actinomycin-D followed by Ret-EV incubation for 16 h. Ret cells were lysed and PD-L1 expression was determined via Western blot analysis.

4.10 PD-L1 upregulation is induced by NF-κB activation

Recent studies showed that tumor-derived EV induce the phophorylation of NF-κB promoting an inflammatory response [127]. Western blot analysis verified that Ret-EV stimulate the phophorylation of NF-κB in a time-dependent manner (Fig. 17A). After 30 min of incubation, MSC-2 cells showed a strong activation of NF-κB with a maximum at 5 h followed by the reduction of NF-κB activation upon 10 h. To find out if NF-κB was crucial for the Ret-EV mediated PD-L1 upregulation, we treated MSC-2 cells with the NF-κB inhibitor BAY11-7082 (Bay) prior the incubation with Ret-EV. PD-L1 expression intensity on MSC-2 cells was found to be decreased (Fig. 17A). To test if IMC also activates NF-κB upon Ret-EV treatment, we performed intracellular staining of phoshporylated NF-κB after 30 min of Ret-EV treatment. Flow cytometry data confirmed the activation of NF-κB in IMC after Ret-EV treatment (Fig. 17C). Importanly this activation was almost as strong as using LPS, a known inducer of NF-κB signaling in myeloid cells.

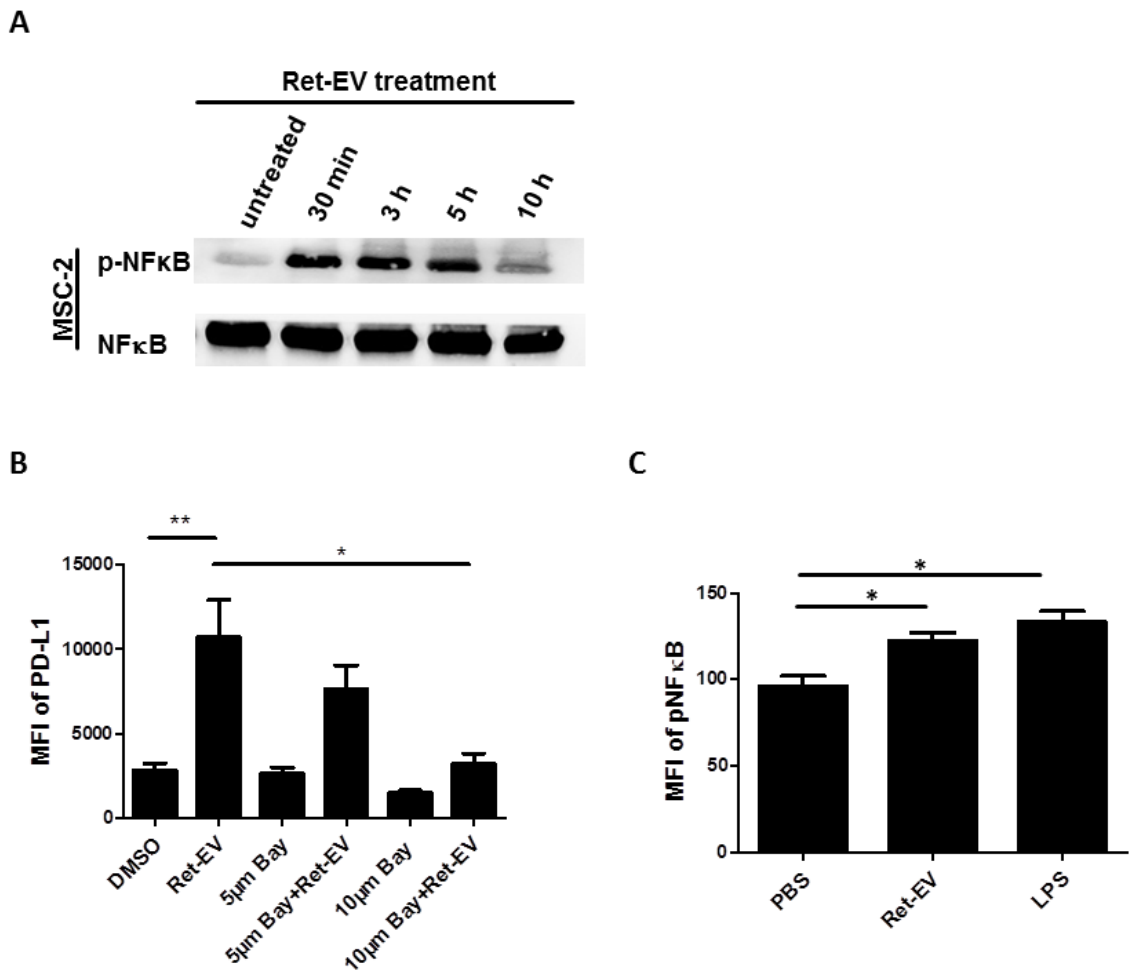

Figure 22: PD-L1 up-regulation induced by Ret-EV is mediated by NF-κB activation. A) Time dependent accumulation of pNF-κB in MSC-2 cells under the treatment with Ret-EV detected by Western blot. **B)** MSC-2 cells were treated with the NF-κB inhibitor Bay followed by Ret-EV incubation followed by flow cytometry. Results are presented as the level of PD-1 expression on MSC-2 measured as MFI (mean ± SEM; n=4). **C)** IMC isolated from the BM of C57BL/6 mice were incubated with Ret-EV for 16 h and pNF-κB was stained and measured by flow cytometry. Results are presented as MFI of whole IMC population. (mean ± SEM; n=4) *$p < 0.05$, **$p < 0.01$.

4.11 TLR agonists induce NF-κB activation in myeloid cells

TLR signaling is a known inducer of the NF-κB pathway [91]. Furthermore, many studies showed that tumor-derived EV stimulated cells via different TLR [126-128]. To test weather MSC-1 and MSC-2 cells are activated upon TLR signaling, we treated them with TLR2, TLR4 and TLR7/8 agonists and measured NF-κB activation via Western blot. All TLR agonists could stimulate NF-κB activation on both MSC cells (Fig 18). The TLR2 agonist Pam3/CSK4 induced a strong NF-κB activation already after 30 min, which was lasting up to 10 h of incubation. Interestingly, LPS the TLR4 agonist induced NF□□B activation similar to TLR 2 agonist in MSC-2 cells but it differs in MSC-1 cells, in which only a weak phosphorylation of NF-κB was observed after 30 min. The activation diminished after 3 h. In contrast, TLR7 agonist R848 did not show an induction of NF-κB in MSC-2 cells, whereas a very slight activation could be observed in MSC-1 cells after 1 h, which diminished after 5 h. Taken together, our results underline the importance of TLR signaling in myeloid cells. TLR agonists are able to induce NF-κB activation in a time-dependent manner, which also shows differences in different types of myeloid cells.

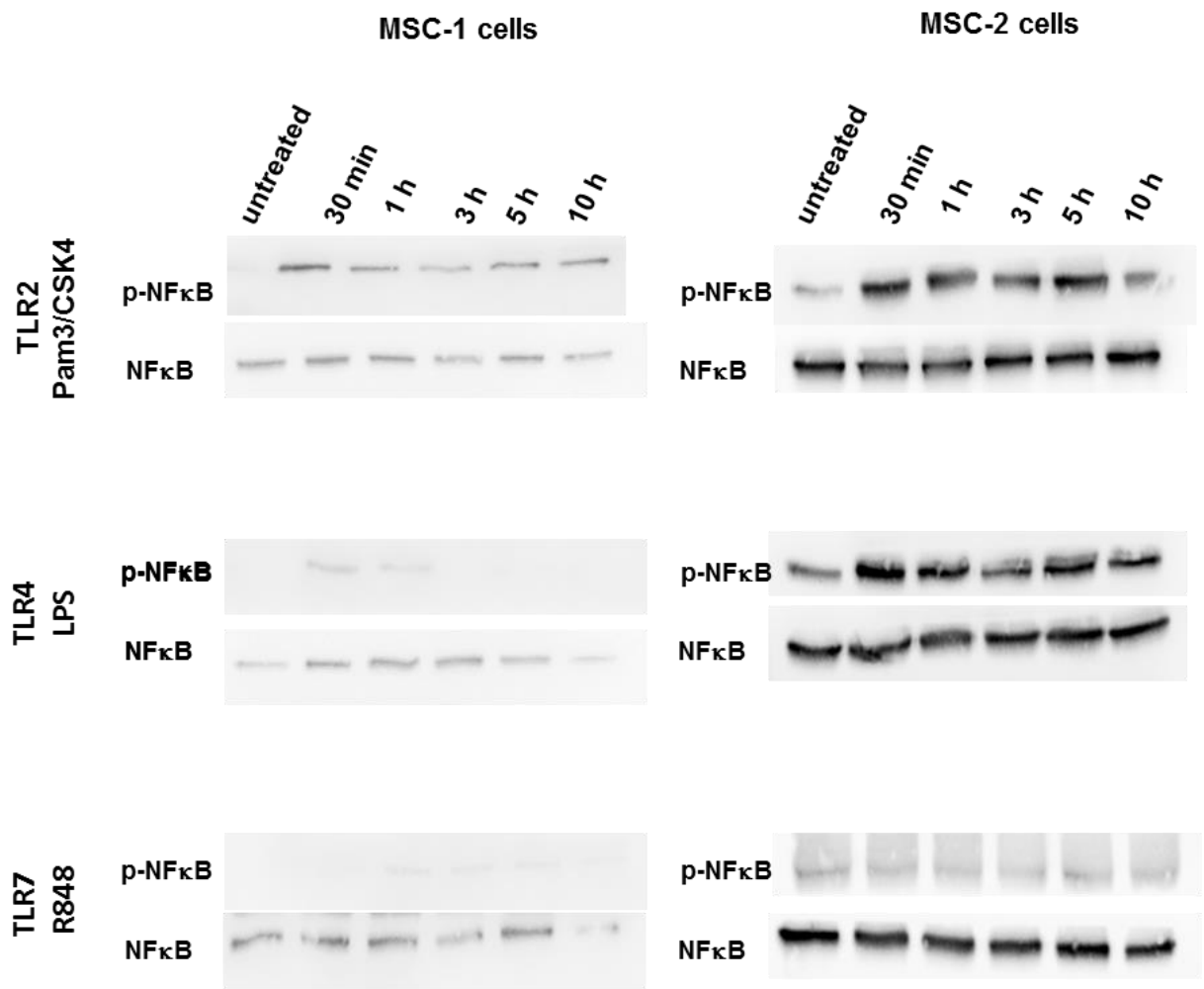

Figure 23: TLR agonist stimulate activation of NF-κB in MSC cell lines. MSC-1 and MSC-2 cells were treated with respective TLR agonist for indicated time. MSC cells were lysed afterwards and pNF-κB was detected by Western blot analysis.

4.12 PD-L1 upregulation is induced by MyD88-dependent TLR signaling

Stimulation with TLR agonist showed a similar NF-κB activation kinetics as Ret-EV did on MSC-2 cells. To test whether Ret-EV dependent PD-L1 upregulation on IMC is dependent on TLR signaling, we investigated *Myd88*$^{-/-}$ and *Myd8*$^{-/-}$*/Trif*$^{-/-}$ mice. We isolated IMC from wild type and both knockout mice and treated them with Ret-EV as described before. Interestingly, we determined that the upregulation of PD-L1 was almost completely dependent on the MyD88 pathway. The frequency of PD-L1^{+} IMC (Fig. 19A) and the expression level of PD-L1 on PD-L1^{+} IMC (Fig. 19B) did not show any significant difference between Ret-EV treated and PBS-treated IMC. The double knock-out mice showed similar results as the *Myd88*$^{-/-}$ mice. Therefore, MyD88-dependent TLR signaling could be the main mechanism of the Ret-EV mediated PD-L1 upregulation on IMC.

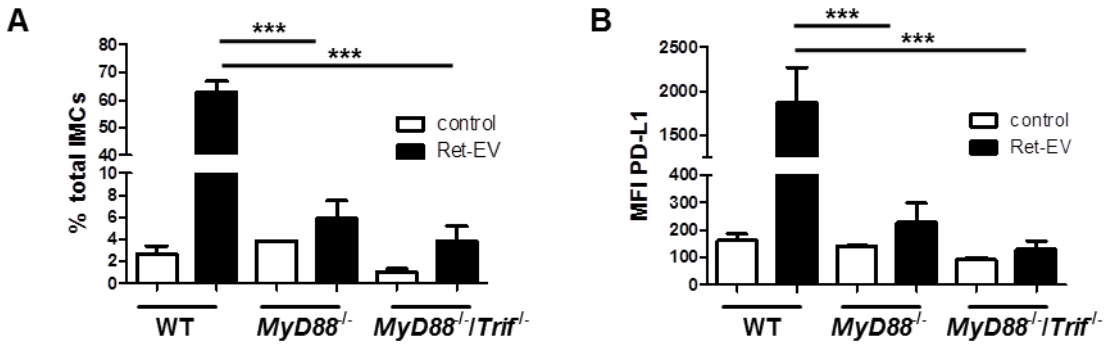

Figure 24: Ret-EV induced PD-L1 upregulation is mediated by the MyD88 dependent TLR pathway. IMC were isolated from the BM of mice deficient for MyD88 or for MyD88 and TRIF followed by incubation for 16 h followed by flow cytometry. **A)** Data are shown as the percentage of PD-L1^{+} IMC within total IMC or **B)** the level of PD-L1 expression as MFI (mean; n=2).

4.13 TLR4 signaling is the main driver for PD-L1 upregulation

To figure out which TLR is responsible for the Ret-EV mediated PD-L1 upregulation, we study the expression of TLR on IMC. We could determine high amounts of TLR7 and as well traceable amounts of TLR2 and TLR4 (Fig. 20A). Next, we investigated if the TLR are also functional. Therefore, we treated IMC with TLR2 (Pam3CSK4), TLR4 (LPS) and TLR7/8 (R848) agonists and found that all TLR agonist induced a strong PD-L1 upregulation on IMC (Fig. 20B). Next, we isolated IMC from *Tlr2*$^{-/-}$, *Tlr4*$^{-/-}$ and *Tlr7*$^{-/-}$mice and treated them with Ret-EV. All TLR deficient IMC showed impaired PD-L1 induction compared to wild type IMC. We compared the percentage of PD-L1^{+} IMC in knock-out IMC compared to wild type IMC (Fig. 20C). The data revealed that TLR4 is mostly responsible for the PD-L1 induction on IMC. This data concludes that TLR signaling is indeed involved in the Ret-EV mediated PD-L1 upregulation. However, it seems that many TLR could play a role with the predominance of TLR4. The frequency of PD-L1^{+} IMC isolated from *Tlr4*$^{-/-}$ mice increased after Ret-EV treatment from 4.37 % up to 14.73 %, whereas IMC from wild type mice increased from 7.03 % to 54.13 %. We could see the same elevation for the intensity level of PD-L1 expression (Fig. 20E). Moreover, we checked if in IMC from *Tlr4*$^{-/-}$ mice, new synthesis of PD-L1 is induced. As seen in Figure 20F, we could not see any differences between stimulated and unstimulated TLR4-deficient IMC, whereas wild type IMC showed higher PD-L1 mRNA transcription. Confirming our hypothesis, performing inhibition of T cell proliferation assays, revealed that IMC from *Tlr4*$^{-/-}$ mice were not able to inhibit T cell proliferation (Fig. 20F). Taken together, TLR signaling, especially TLR4 is essential for the transcription of PD-L1 mRNA in IMC.

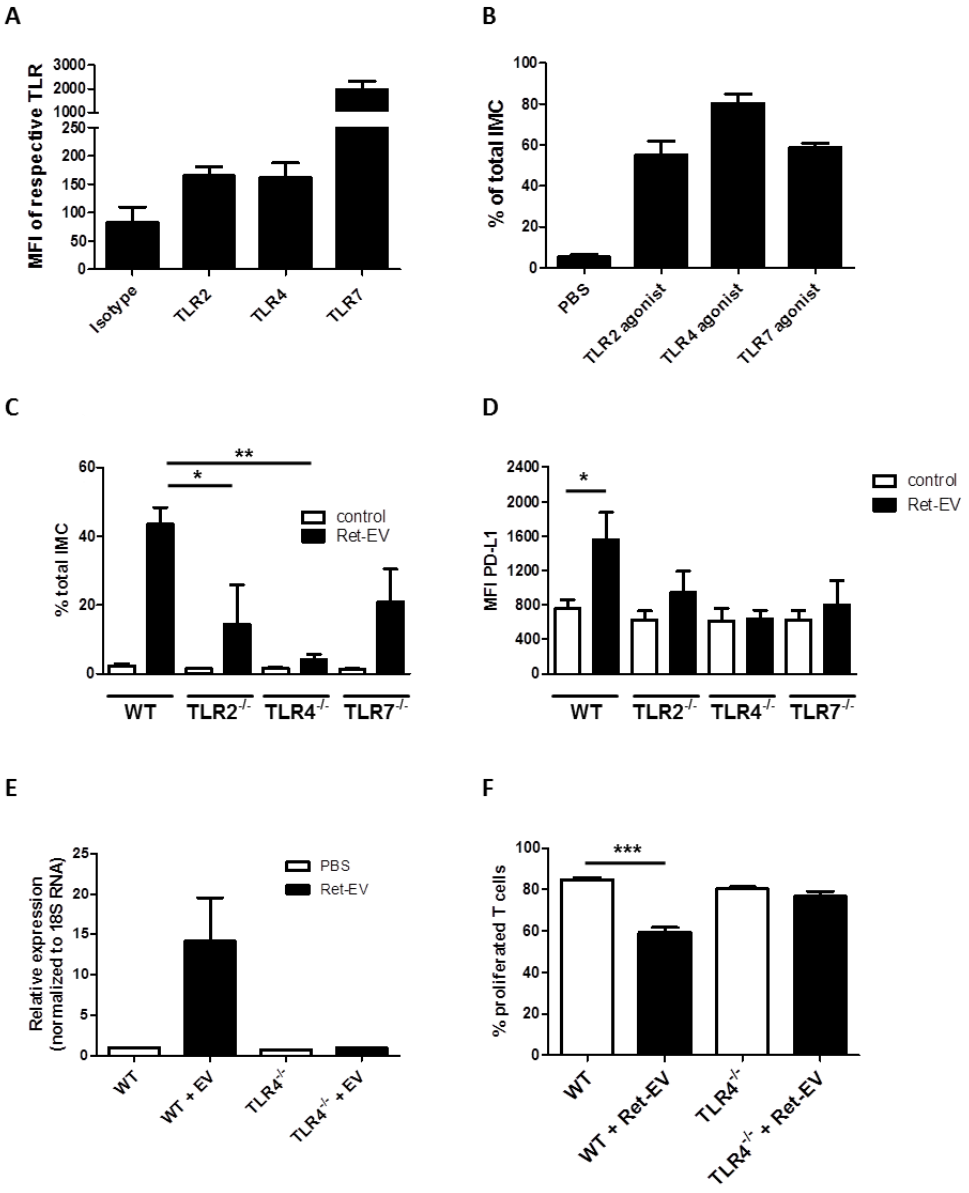

Figure 25: Ret-EV mediated PD-L1 upregulation is triggered mostly by TLR4 signaling. A) IMC were isolated from the BM of wild type and the intensity of indicated TLR was measured via flow cytometry **B)** IMC were treated with respective TLR agonist and PD-L1 upregulation was measured via flow cytometry. PD-L1 expression is presented as the percentage of PD-L1^{+} IMC within total IMC **C)** IMC were isolated from the BM of wild type and TLR-deficient C57BL/6 mice and treated with Ret-EVs for 16 h followed by flow cytometry. **C)** PD-L1 expression is presented as the percentage of PD-L1^{+} IMC within total IMC or **D)** as the level of PD-1 expression on IMC measured as MFI (mean ± SEM; n=4). **E)** Expression of PD-L1 in wild type and *Tlr4*$^{-/-}$ IMC measured by RT-PCR and normalized to 18s RNA **F)** Inhibition of CD8^{+} T cell proliferation by wild type and TLR4$^{-/-}$ IMC treated with Ret-EV (IMC:T cell ratio = 1:1??). Data are presented as the percentage of divided T cells (mean ± SEM; n=6). *p < 0.05, **p < 0.01.

4.14 Ret-EV educated mice develop tumors faster

Several studies showed that mice treated with tumor-derived EV can display accelerated tumor growth [126, 129]. Here, we injected every second day 50 µg of Ret-EV intraperitoneally into C57BL/6 mice. On day 5, we injected Ret cells into the flank and monitored tumor growth for 14 days. Our results demonstrated a Ret-EV mediated acceleration of tumor growth (Fig. 21A). In contrast, when we perform the aforementioned experiments in *Tlr4*$^{-/-}$ mice, Ret-EV pretreatment failed to accelerate the tumor growth (Fig. 21B).

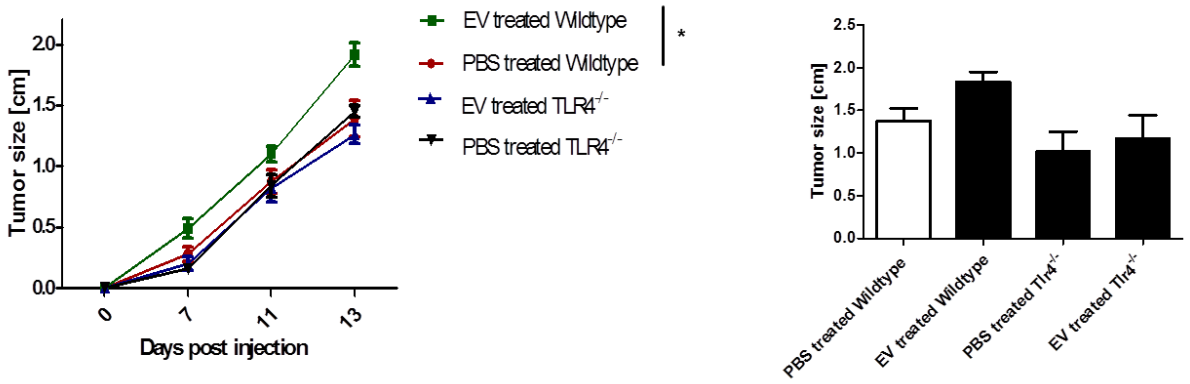

Figure 26: Educating mice with Ret-EV promotes tumor growth in wild type mice but not in TLR4-deficient mice. Ret-EV or PBS were injected each second day into wild type or *Tlr4*$^{-/-}$ mice. On day 5, Ret cells were injected subcutaneously into the flank. **A)** Tumor progression was monitored for 14 day and **B)** tumor was weight on day 14 after mice were sacrificed (mean ± SEM; n=3) *p < 0.05.

4.15 Ret-EV express high amounts of HSP86

Next, we aim to decipher the ligands for the Ret-EV mediated TLR4 signaling. Several ligands on tumor-derived EV were previously shown to induce TLR2 and TLR4 signaling [126, 130]. Figure 22A demonstrates that HSP86 that was previously shown to mediate TLR2/4 signaling [131-133], is strongly expressed in all Ret-EV preparations. We found also small amounts of HSP72 on Ret-EV. HSP72 on tumor-derived EV was previously reported to exert immunosuppressive properties on myeloid cells [126, 130, 134]. HMGB1 and HSP60 were absent on our preparations, whereas cells showed a high expression of both proteins. S100A8 and S100A9 were also described to be a potent inducer of TLR4 signaling, however, we failed to detect these proteins in Ret-EV and Ret cell lysate (data not shown). Next, we investigated the localization of HSP72 and HSP86 on Ret-EV. Therefore, we coupled Ret-EV on latex-beads. By this technique, it is possible to measure EV by flow cytometry. Figure 22B demonstrates that HSP72 and HSP86 are expressed on the surface of Ret-EV, with higher intensity of HSP86, which confirm the results of Western blot.

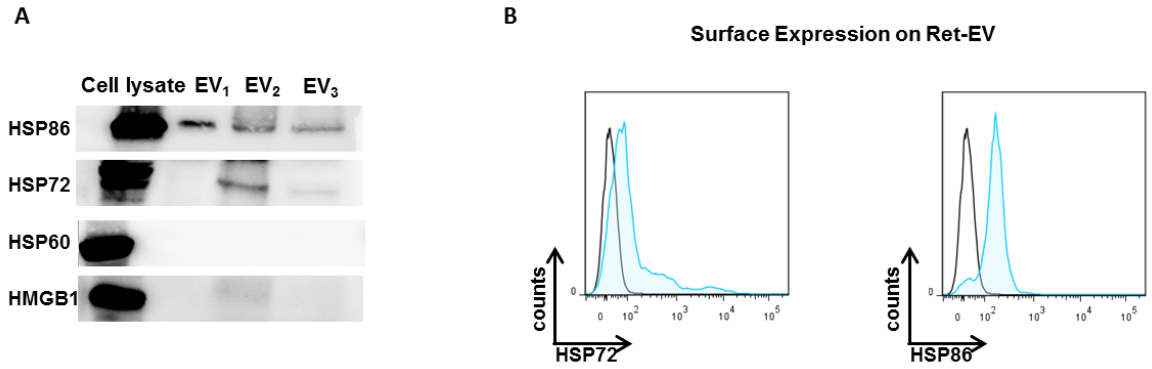

Figure 27: Ret-EV carry high amounts of HSP86 and HSP72. A) Different batches of Ret-EV were lysed and indicated proteins were analyzed by Western blot. **B)** Ret-EV were coupled onto latex beads and stained for indicated HSP. HSP expression level was measured via flow cytometry. Black line indicates the secondary antibody control and blue - the expression of indicated HSP.

4.16 Inhibition of inducible HSP abrogate Ret-EV-mediated PD-L1 induction

Next, we treated Ret cells with KNK-437, a potent inhibitor of the transcription of inducible HSP [135]. Upon the treatment with higher concentration of KNK-437, Ret cells showed a reduced expresssion of HSP72 and HSP86 (Fig. 23A). Then, we isolated EV from Ret cells treated with 500 nM KNK-437 or DMSO and measured the quantity and size distribution of both EV types. KNK-EV or DMSO-EV (Ret-EV) did not show differences in terms of quantity and size distribution (Fig. 23B and C), indicating that KNK-437 does not effect the EV secretion by Ret cells. We found that EV isolated from KNK-437-treated Ret cells were incapable to induce PD-L1 upregulation on murine IMC, whereas EV from control Ret cells could upregulate PD-L1 expression (Fig. 23D and E). Taken together, inhibiting the synthesis of inducible HSP impairs the Ret-EV mediated upregulation of PD-L1 on IMC. Since we could not fully exclude any contamination of KNK-437 in the isolated Ret-EV preparations, additional controls should be included.

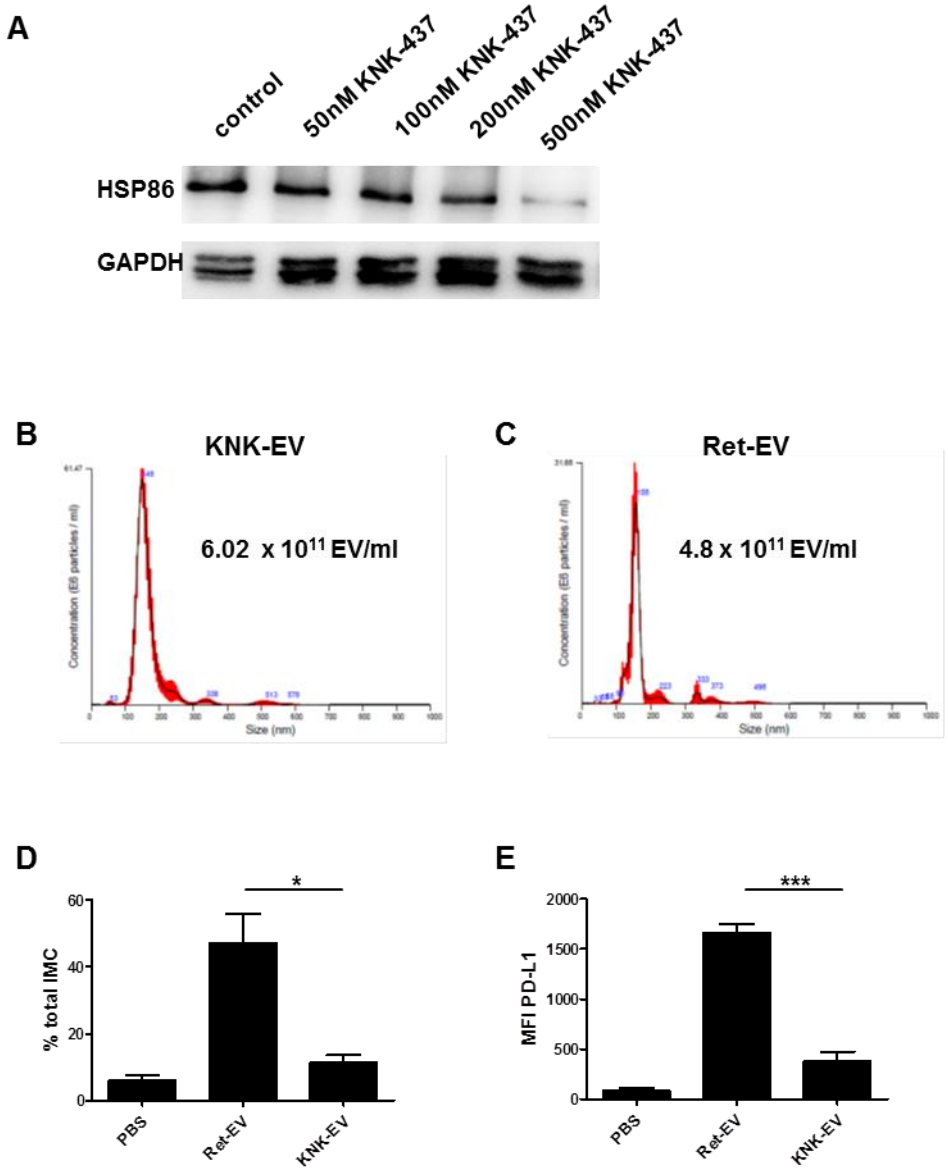

Figure 28: HSP86 is critical for Ret-EV mediated PD-L1 upregulation on IMC. A) Ret cells were treated with the indicated concentrations of KNK-437. After 24 h Ret cells were lysed and proteins were isolated. The expression of HSP86 in cell lysates was analyzed by Western blot. **B-C)** NTA of KNK-EV and Ret-EV showing the size distribution and concentration of EV. **D)** IMC were treated with Ret-EV isolated from KNK437-treated (KNK-EV) or untreated Ret cells (RET-EV). PD-L1 expression was determined by flow cytometry and shown as the percentage of PD-L1$^+$ IMC among total IMC or **E)** as the level of PD-1 expression as MFI. (mean ± SEM; n=3) *p < 0.05, **p < 0.01, ***p < 0.001.

4.17 HSP86-deficient Ret cells are unable to induce PD-L1 on IMC

To evaluate if inducible HSP are responsible for the Ret-EV mediated PD-L1 upregulation on myeloid cells, we stably knocked-down HSP86 in Ret melanoma cells (Fig. 24A). We chose construct #6 for the trans-well experiments, which revealed that HSP86-deficient Ret cells displayed impaired PD-L1 upregulation on IMC upon their co-culture (Fig. 24B). The frequency of PD-L1$^+$ IMC and PD-L1 intensity on PD-L1$^+$ IMC was lower as compared to co-culturing with the scramble shRNA control (Fig.24 C), suggesting a critical role of HSP86 in the observed PD-L1 upregulation on IMC.

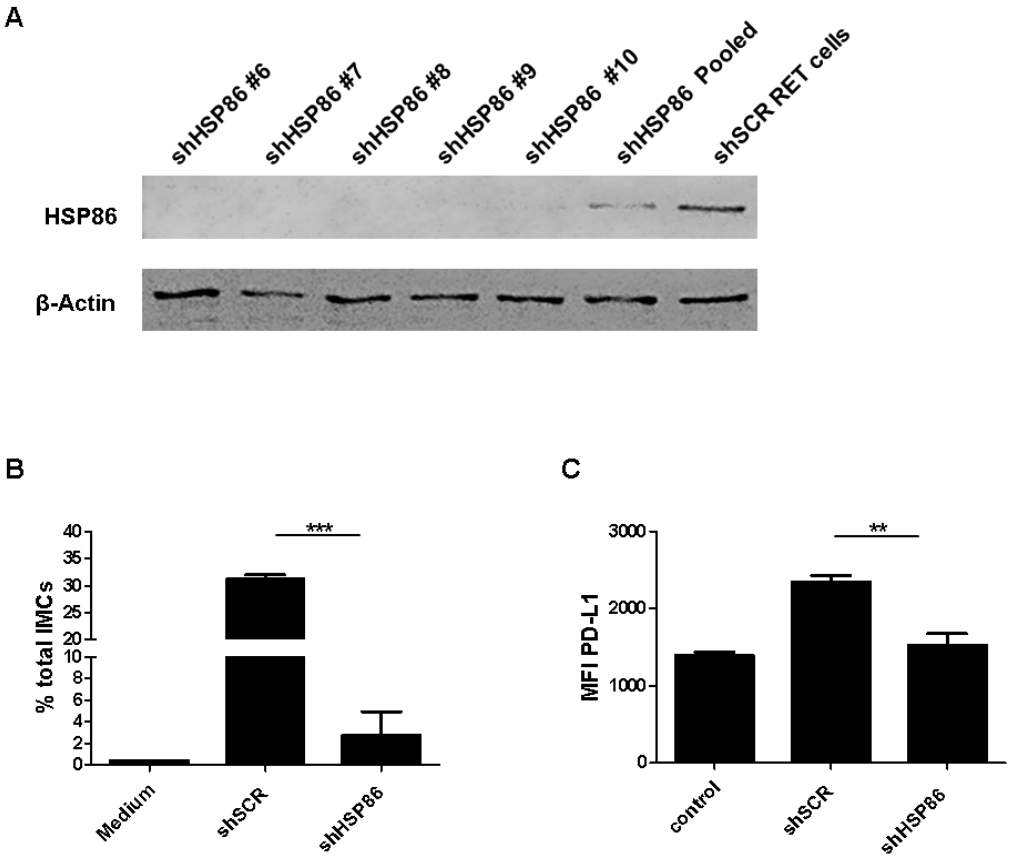

Figure 29: HSP86 is crucial for Ret-EV mediated PD-L1 upregulation. HSP86 on Ret cells were stably knock-down by lentiviral transduction. **A)** Western blot analysis demonstrates the efficiency of HSP86 knock-down and respective scramble control. **B-C)** shSCR or shHSP86 Ret cells were co-cultured with wild type IMC in a trans-well assay for 24 h. Data on are shown as **B)** the percentage of PD-L1$^+$ IMC and **C)** level of PD-L1 expression as MFI. (mean ± SEM; n=3) *p < 0.05, **p < 0.01.

4.18 Depletion of HSP86 in Ret melanoma cells impairs tumor growth and reduces PD-L1 expression on MDSC

To study the impact of HSP86 expression in tumor cells on their growth *in vivo*, we injected HSP86-deficient Ret cells (shHSP86) and their respective scramble control (shSCR) subcutaneously into C57BL/6 mice. We monitored tumor growth for 14 days (Fig. 25A). It was found that HSP86-deficient Ret cells grow slower than shSCR counterpart, which reached the endpoint (tumor size 1.5 cm) already 14 days after their injection. We found also a strong tendency for decreased tumor weight in mice injected with shHSP86 cells (Fig. 25B). To exclude that HSP86-deficient Ret cells have impaired proliferation capacity, we tested it via alamar blue assay and found no difference between shHSP86 and shSCR Ret cells (Fig. 25C).

In addition, shHSP86 tumors showed decreased frequency of MDSC in the TME (Fig. 25D). Furthermore, we found a decreased frequency of PD-L1$^+$ MDSC in tumors of mice injected with shHSP86 Ret cells. In addition, MDSC showed lower expression level of PD-L1 in HSP86 deficient tumors compared to the respective control (Fig. 25F). Analyzing the BM, we observed no changes in the frequency of MDSC between both experimental groups (Fig. 25G). However, we could measure a significant reduction in the frequency of PD-L1$^+$ MDSC (Fig. 25D) and in the intensity of PD-L1 expression (Fig. 25I) in mice injected with HSP86-deficient Ret cells.

Taken together, the absence of HSP86 expression in tumor cells and tumor-derived EV leads to a less immunosuppressive TME due to reduced frequencies of MDSC and PD-L1 expression on these cells.

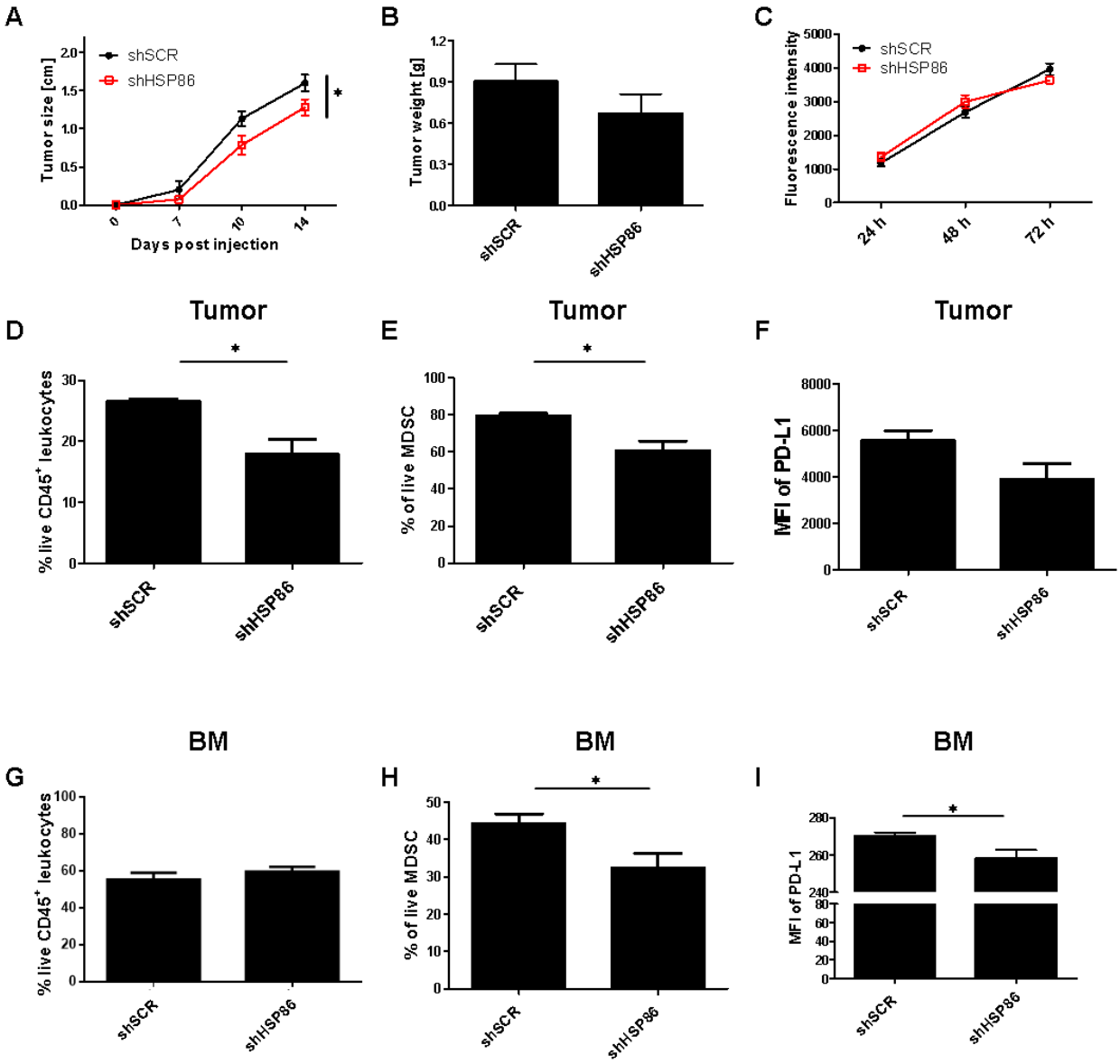

Figure 30: Reduced growth of HSP86-deficient Ret cells *in vivo*. HSP86-deficient Ret cells (shHSP86) or scramble control (shSCR cells) were injected subcutaneously into C57BL/6 mice. Tumor growth was monitored for 14 days in both tumor bearing mice. **A)** Kinetics of tumor growth is shown. **B)** Tumor weight was measured on day 14 after mice were sacrificed. **C)** shHSP86 Ret cells and shSCR Ret cells were incubated with alamar blue, and their metabolic activity was measured via spectrometry. **D-I)** At day 14, tumor and BM single cell suspensions were analyzed by flow cytometry. D-F) Data on tumor infiltrating MDSC are shown as the percentage among total leukocytes **(D)**. PD-L1 expression is presented as **E)** the percentage of PD-L1$^+$ MDSC in tumors and **F)** level of PD-1 expression as MFI. **G-I)** Data on BM MDSC are shown as the percentage of these cells among total leukocytes **(G)**. PD-L1 expression is presented as **F)** the percentage of PD-L1$^+$ MDSC in BM and **I)** level of PD-1 expression as MFI (mean ± SEM; n=4). *p < 0.05.

5 Discussion

Malignant melanoma is a therapy-resistant and very aggressive type of cancer [1]. One major reason for this is the accumulation of highly immunosuppressive myeloid cells, mainly MDSC, in the TME. The hallmark of MDSC biology is the suppression and inactivation of effector T cells through numerous mechanisms [46]. One of these is the upregulation of PD-L1 expression on MDSC. To date, many pathways were described to be important for PD-L1 upregulation [66]. However, most pathways are linked with the induction by soluble factors and only little is known about EV-mediated upregulation of PD-L1 on myeloid cells and how tumor-derived EV can reprogram IMC into immunosuppressive cells. Unveiling the mechanisms of the conversion of myeloid cells into immunosuppressive cells by tumor-derived EV could help finding new targets for cancer immunotherapy.

5.1 Quality and characteristics of Ret-EV

Proliferating tumor cells secrete high amounts of EV, which are distributed systematically through the body [136]. Those EV are taken up by many cell types, which in turn influence their activity and metabolism [75, 76, 78, 137, 138]. During the last years, accumulating data highlighted that tumor-derived EV reprogram the host cells into a more tumor-supporting phenotype [139]. Ridder et al. (139) showed that tumor-derived EV were taken up *in vivo* preferentially by myeloid cells in the TME. Those myeloid cells showed a more immunosuppressive phenotype due to their uptake of tumor-derived EV *in vivo*. To study the underlying mechanism of this reprogramming, it is essential to isolate pure and functional tumor-derived EV that are free from organelles and cell debris.

Using our modified protocol, adopted from Lobb and Möller [121], we could demonstrate that Ret-EV preparations fulfill all the minimal requirements to define them as pure EV [122]. First of all, NTA analysis visualized the size distribution of our Ret-EV that was approximately 100 nm in diameter and correlated with the size attributed to small EV, mainly exosomes. This size-distribution was confirmed by immunogold labeling of CD81 on the Ret-EV. In addition, we showed that the EV-surface marker CD81 and CD9 as well the intraluminal marker ALIX

was present in Ret-EV preparations, whereas Ret-EV were negative for the endoplasmatic reticulum marker calreticulin.

5.2 Expression of PD-L1 on Ret-EV

Interestingly, we found that Ret-EV were positive for PD-L1. This indicates that Ret-EV could act directly suppressive on activated T cells, when encountering them. Indeed, previous studies demonstrated the suppressive potential of PD-L1 expressing EV [140]. In melanoma patients, the level of circulating-PD-L1 positive EV correlated with IFN-γ in the plasma [141]. Those circulating melanoma-derived PD-L1-positive EV were shown to suppress T cells and to mediate immune evasion. Furthermore, PD-L1-positive EV were associated with the response of anti-PD-1 therapy. In a similar fashion, Ricklefs et al. [140] showed that patients suffering from glioblastoma produced high amounts of PD-L1 positive EV that suppress antitumor immunity and led to immune evasion of glioblastomas.

Next to PD-L1 also Fas ligand (FasL) was found on tumor-derived exosomes [142]. It has been shown that EV isolated from the body fluids of acute myelogenous leukaemia patients induced apoptosis in T cells that was mediated by Fas/FasL signaling [142]. In addition, studies described that EV isolated from LNCaP, a human prostate cancer cell line, induced Fas/FasL driven apoptosis in T cells [143]. FasL on EV was also found to promote tumor growth in an apoptosis independent fashion [144]. In this study, EV-derived from activated T cells were isolated from tumor-bearing mice. Those EV expressed FasL but had little effect on the apoptosis of tumor cells. Instead, FasL promoted the ERK and NF-κB pathway, which subsequently increased the expression of MMP9 in the TME. This led to a more aggressive invasion of tumor cells. Using blocking antibodies against FasL, the migration capacity of tumor cells was significantly reduced.

We did not study here the direct immunosuppressive effect of Ret-EV on effector $CD8^+$ T cells but focused on the Ret-EV educated immunosuppression of myeloid cells, in particular MDSC. However, it is important to keep in mind that PD-$L1^+$ EV could also exhibit direct immunosuppressive properties on effector $CD8^+$ T cells.

5.3 Ret-EV promote tumor progression by inducing PD-L1 expression on myeloid cell

Initial studies reported that tumor-derived EV could be a source of tumor-associated antigens and therefore, they could activate the immune system and stimulate a T cell-mediated anti-tumor response [145]. However, pioneering work by Taylor and Black in 1985 indicated that vesicles shed by melanoma cells could also have immunosuppressive properties [146]. In their study, they showed that melanoma-derived vesicles inhibit the upregulation of co-stimulatory molecules on murine macrophages. However, the conversion of myeloid cells into immunosuppressive cells was still under discussion. Only 21 years later Valenti et al. (146) demonstrated that melanoma-derived EV converted monocytes into TGF-β secreting myeloid suppressive cells, which was accompanied by the loss of human leukocyte antigen (HLA) class II expression. Furthermore, they showed that EV-educated monocytes were able to reduce the lytic activity of effector $CD8^+$ T cells. Since then, the interest to the immunosuppressive properties of tumor-derived EV increased dramatically. In the last 10 years, many studies reported a tumor-promoting effect of tumor-derived EV rather than an anti-tumorigenic effect. Thus tumor-derived EV were reported to drive the formation of pre-metastatic niches [52, 80], immunosuppressive microenvironment [139] and as well promoting migratory and invasiveness of tumor cells [147-149].

In this study, we could prove that Ret-EV convert IMC from the BM into immunosuppressive MDSC by upregulating inflammatory cytokines and PD-L1 expression. This immunosuppression was systemic as we found a strong PD-L1 upregulation in the TME and in the BM of tumor-bearing mice. Such upregulation of PD-L1 was reduced when we injected tumor cells deficient in HSP86, which was found to be a predominant mediator of PD-L1 upregulation in this study. Similarly, Haderk et al. (128) reported that EV isolated from the plasma of chronic lymphocytic leukemia patients induced a strong upregulation of PD-L1 in circulating $CD14^+$ monocytes. This upregulation was due to the loading of the non-coding Y RNA hY4 into patients' EV, whereas EV isolated from healthy donor showed less amounts of

this non-coding RNA. Further studies investigated the role of EV isolated from hepatocellular carcinoma cells, showing that tumor-derived EV upregulated PD-L1 on human monocytic cell line THP-1 and murine macrophages [150]. The authors did not describe the mediator of this induction. However, since they found the reduction of PD-L1 stimulation by treating tumor cells with melatonin that was earlier reported to decrease the induction of several HSP after oxidative stress [151], we believe that HSP86 on tumor-derived EV might trigger PD-L1 expression also in their system.

Recently, it was reported that EV isolated from glioblastoma stem cells could reprogram monocytes into immunosuppressive M2 macrophages [123]. This conversion was associated with PD-L1 upregulation. Using mass spectrometry the group identified components in the tumor-derived EV that induce the STAT3 pathway in treated monocytes. In our study, we found also EV-dependent STAT3 activation. It seems that EV from different tumor types use similar mechanisms to induce an immunosuppressive microenvironment. Studying the effect of tumor-derived EV on DC, Ning et al. (152) could show that tumor-derived EV blocked the differentiation of progenitor DC into fully matured DC and furthermore, those DC showed immunosuppressive capacities as priming of T cells led to decreased amounts of IFN-γ production. Interestingly, when the authors blocked PD-L1 on EV-treated DC, the immunosuppressive properties were strongly decreased. This data highlights the important role of EV-mediated PD-L1 upregulation also on other myeloid cell subsets.

5.4 Ret-EV promote tumor progression by inducing MDSC

Besides, upregulating PD-L1 on myeloid cells, tumor-derived EV use further mechanism to convert normal myeloid cells into pro-tumorigenic cells. We could demonstrate that tumor-derived EV stimulated the production of miRNA and cytokines associated with MDSC biology and function. We have observed a strong upregulation of IL-6, Cox-2 and TGF-β. In line with our data, Xiang et al. [152] showed that treating myeloid cells with tumor-derived EV enhanced the secretion of IL-6, Cox-2, VEGF and TGF-β *in vitro*. By blocking vesicular TGF-β and PGE2, the differentiation of BM myeloid cells into MDSC was inhibited.

Furthermore, they could show that educating naïve mice with tumor-derived EV led to expansion of MDSC that correlated with the growth of TS/A tumor cells. Peinado et al. (129) demonstrated that melanoma-derived EV educated BM progenitor cells towards a pro-metastatic phenotype promoted by the MET receptor. Highly metastatic melanoma cells sort the c-MET oncogene into EV. Those melanoma-derived EV are taken up by BM cells that lead to BM cells with a pro-vasculogenic and pro-metastatic phenotype. Using EV from non-metastatic melanoma cells or directly reducing MET expression in EV, resulted in reduced pro-metastatic behavior of BM cells. Chalmin et al. (126) also observed the differentiation of BM cells into MDSC. They described that EV-mediated expansion of MDSC was due to HSP72 on tumor-derived EV. HSP72 was shown to trigger TLR2/MyD88 and STAT3 signaling in BM cells, leading to increased production of IL-6. EV-treated IMC acquired immunosuppressive functions upon EV-treatment proved by T cell proliferation assays similar to our studies. Interestingly, by blocking EV secretion *in vivo* by DMA or omeprazole, they observed less MDSC was observed in the TME and tumor growth was significantly slowed down. Similar studies were performed in models for multiple myeloma [152, 153]. EV isolated from multiple myeloma cell lines stimulated the expansion of MDSC *in vitro* and converted IMC into MDSC in the BM. The conversion and expansion were found to activate STAT3 signaling. By testing their immunosuppressive potential, the authors could prove the immunosuppressive properties of MDSC by inhibition of T cell proliferation. Contrary to our studies, they associated the increased immunosuppressive capacity with increased levels of iNOS. Upon the treatment with tumor-derived EV a more resistant to apoptosis phenotype was observed. This was linked to increased STAT1 and STAT3 activation that in turn activated the anti-apoptotic proteins B-cell lymphoma-extra-large (Bcl-xL) and induced myeloid leukemia cell differentiation protein (Mcl)-1. Further studies reported that EV isolated from pancreatic ductal adenocarcinoma (PDAC) cell lines induced MDSC expansion in the TME [154]. This expansion was dependent on mothers against decapentaplegic homolog (SMAD)-4 signaling which increased calcium influx and glycolysis in myeloid cells [155-157]. SMAD-4 signaling was found to be induced by miRNA-494 and miRNA-1260 transferred by

PDAC-derived EV. Furthermore, tumor-derived EV were shown to stimulate an immunosuppressive TME due to their mutation in p53 [124]. P53-mutated tumors selectively produced EV enriched with miRNA-1246 that induced polarization of macrophages into a M2 phenotype. Those reprogrammed macrophages were shown to be more pro-tumorigenic and anti-inflammatory after EV treatment from p53 mutated tumor cells.

The potential to induce immunosuppressive DC by EV were also intensively studied. Samilu et al. (159) could show that tumor cells deficient in exosomes secretion produced enhanced T cell responses *in vitro* compared to the control counterpart [158]. They found that tumor-derived EV induced immunosuppressive DC. This was due to abundant amounts of PGE2 in tumor-derived EV. PGE2 induced CD73 expression in DC accompanied with a higher activity of CD39. Both proteins led to increased hydrolysis of AMP into adenosine that inhibits T cells activity and supports tumor immune evasion.

5.5 Myeloid cell predominantly take up tumor-derived EV

We demonstrated in *in vivo* studies that Ret-EV were taken up by MDSC. Here, we coupled GFP to the EV marker CD81. The CD81-GFP fusion protein was incorporated into EV during their biogenesis and released into the extracellular space. By the uptake of EV and this fusion GFP-CD81 protein respectively, the recipient cells became positive for GFP, allowing to analyze the recipient cells via flow cytometry. Confirming the *in vitro* results, we observed that GFP-positive MDSC in the TME showed a strong tendency to express more PD-L1 on their surface.

Similar findings were reported by Ridder et al. [159] who used a sophisticated Cre-Lox system to track tumor-derived EV *in vivo*. The group demonstrated that functional Cre-mRNA is sorted into EV. After the release of those EV from the tumor cells, they are predominantly taken up by myeloid cells, preferentially by MDSC. Upon the uptake, the MDSC translated the Cre-mRNA into functional Cre-recombinase. The Cre-recombinase cut offs the Lox-sites on the DNA that allowed the reported gene to become transcribed. MDSC positive for the reported gene were analyzed via flow cytometry and they showed higher PD-L1 and

TGF-β expression. Zomer et al. (160) demonstrated by using the same technique that EV interacted with different tumor cells *in vivo* [160]. The uptake of EV in this study led to more aggressive tumors by enhancing their migratory behavior and metastatic capacity. However, most studies did not track *in vivo* generated EV but rather *in vitro* isolated EV from various cell lines and injected those into wild type mice. It was shown that the administration of fluorescently labeled EV from metastatic cancer cell lines *in vivo* revealed that they were engulfed mainly by $CD45^+$ immune cells in the BM [161]. Repeated injections of those EV increased the frequency of MDSC within the lung and liver. To prove that those effects were EV mediated, they administrated liposomes into naïve mice. Interestingly, liposomes were also taken up by the same type of cells that showed no immunosuppressive properties. Only EV-treated myeloid cells could inhibit T cell proliferation and reduce NK cell cytotoxicity. This comprehensive study clearly demonstrated a specific effect of tumor-derived EV in the conversion of IMC and expansion of MDSC.

Plebanek et al. [162] observed that exogenously administrated fluorescently labeled EVs were also predominantly taken up by $Ly6C^+$ myeloid cells in the BM. Depending on the origin of the EV, the $Ly6C^+$ myeloid cells showed a different phenotype. EV from poorly metastatic cancer cells converted the myeloid cells into anti-tumorigenic patrolling monocytes, which assisted in the clearance of cancer cells at the pre-metastatic niche via the recruitment of NK cells. However, using EV from highly metastatic cancer cell lines led to larger tumor burden and increased formation of metastasis. However, in this study, the monocytes were not characterized when treated with EV from metastatic cell lines. Similar data were obtained with EV isolated from PDAC cell lines [163]. These EV carried macrophage migration inhibitory factor (MIF). By the uptake of MIF-containing EV, myeloid cells started to produce abundant amounts of TGF-β, which in turn promoted an immunosuppressive microenvironment. Interestingly, the uptake of those EV by Kupffer cells in the liver also resulted in the secretion of TGF-β, which induced the recruitment of BM-derived macrophages and neutrophils into the liver, which primed the formation of pre-metastatic niches in the liver (163). Knock-down of exosomal MIF resulted in a decrease of numbers of

macrophages and neutrophils in the liver and subsequently less formation of pre-metastatic niches. Further studies indicated that tumor cells reprogrammed BM microenvironment during tumor progression by releasing EV, which promoted the expansion of immunosuppressive cells in the BM.

5.6 Tumor-derived EV induce inflammatory pathways in myeloid cells

Immune cells developed various mechanisms to sense efficiently pathogens. TLR signaling, working through the NF-κB pathway, allows immune cells to react quickly on invaders and to eliminate them [91]. However, incomplete clearance of the pathogens often results in chronic inflammation. Rudolf Virchow proposed already in 1863 that chronic irritation and inflammation causes cancer [164, 165]. In 1915, first experiments proved the hypothesis of Rudolf Virchow [165, 166]. Katsusaburo Yamagiwa, a student of Virchows, used coal tar on rabbit's ears to induce chemical carcinogenesis. He observed atypical epithelial growth on the rabbit ears and announced:" Cancer is identified! Proudly I walk a few steps" [166]. Yamagiwa's findings proved inflammation as a hallmark of cancer progression. In this work, we found that tumor-derived EV induced a chronic inflammatory environment. Ret-EV constantly activated the NF-κB pathway in IMC. This activation was triggered by several TLR, with TLR4 as the predominant signaling pathway, leading to the expansion of immunosuppressive MDSC.

Although TLR4 signaling in myeloid cells activates strong immune responses by inducing pro-inflammatory myeloid cells, mainly macrophages, it also causes collateral tissue damage if it is not properly regulated [167]. Therefore, feedback mechanisms were developed to regulate excessive immune activation [168]. One mechanisms is the decoyed activation of MDSC, which tempers the immune cells [167]. Arora et al. (169) demonstrated that LPS, a ligand of TLR4, can induce the expansion of MDSC in the lung [169]. They performed linage-tracing experiments of BM progenitor cells in naïve mice. Upon LPS airway administration, the progenitors accumulated in the lung and showed an immunosuppressive phenotype. Blocking T cell effector function proved that those cells were MDSC. Further studies by Poe

et al. (170) demonstrated that MDSC accumulated in the lung upon LPS administration [170]. This accumulation was delayed compared to other myeloid cell subsets, but after three days, MDSC were the predominant myeloid population within the lung. The enriched lung MDSC suppressed DC ability to promote Th2 responses. Furthermore, these MDSC engulfed apoptotic neutrophils to restore lung homeostasis.

Besides LPS, further TLR4 ligands were found to induce MDSC function and expansion. S100A9 was found to act through the NF-κB pathway by triggering TLR4 [101]. Later on, Cheng et al. (171) found that S100A9 was a potent inducer of MDSC expansion [171]. S100A9 expression was up regulated through the STAT3 pathways in myeloid cells and acted as an inflammatory cytokine, blocking the differentiation of DC and promoting the differentiation and expansion of MDSC. Furthermore, it was shown that S100A9 and its dimerization partner S100A8 induced the expression of iNOS in macrophages in a NF-κB/TLR4 dependent pathway [172]. In addition to S100A9, high mobility group box 1 (HMGB1) was found to be a ligand for TLR4 [173]. It binds to TLR4 via the A-box domain with high affinity, which was proved by surface plasmon resonance [173]. In general, HMGB1 is secreted by macrophages and also by necrotic cells [104]. This results in elevated HMGB1 level in plasma of cancer patients. HMGB1 was described to induce MDSC via the TLR4 signaling pathway (104). Here, IMC were cultured *in vitro* with either GM-CSF or GM-CSF together with HMGB1. After 4 days of culture, IMC become more immunosuppressive when cultured with both stimuli. Further studies proved the importance of HMGB1 on MDSC biology and tumor growth [174-176]. The correlation of tumor growth, HMGB1 and MDSC were proved by using a mouse model for renal cell carcinoma [177]. Here, tumor-bearing mice were treated with neutralizing antibodies against HMGB1 that resulted in tumor growth inhibition. Interestingly, when MDSC were depleted in the same experimental set up, the HMGB1 blocking showed no effect any more on tumor growth, proving the importance of HMGB1 in MDSC biology.

Although the TLR4 signal cascade was evolved to protect the host against gram-negative bacteria, many tumor cells use this particular receptor for immune evasion. There is a growing body of evidence that tumors induce chronic inflammation through TLR4 signaling. Lee et al. (178) performed tumor growth experiments in wild type and TLR4-deficient mice that proved this hypothesis [178]. TLR4-deficient mice showed a reduced growth of several tumor cell lines studied due to TLR4 signaling in TAM. TAM produced pro-inflammatory cytokines upon TLR4 signaling, which resulted in chronic inflammation. By adoptive transfer of wild type TAMs into TLR4 deficient mice, the beneficial effects could be abrogated, indicating that TAMs are the main reason for the TLR4-dependent tumor growth [178]. Interestingly, the TLR4 was shown to be triggered by HSP70 and HSP90. By blocking both HSP with neutralizing antibodies in tumor-bearing mice, the production of inflammatory mediators, especially VEGF and TNF-α was decreased.

5.7 Tumor-derived EV induce inflammatory pathways in myeloid cells

In this work, we found that TLR4 was a predominant inducer of MDSC after Ret-EV treatment. However, we could also identify that TLR2 and TLR7 promoted immunosuppressive properties. It seems that tumor cells use a broad spectrum of TLR to induce immunosuppression. Haderk et al. [128] found that TLR7 was the dominant signaling pathway to induce PD-L1 on monocytes. In addition, Chalmin et al. [126] found that tumor-derived EV promoted MDSC expansion by the TLR2 signaling cascade. Although many studies used TLR agonist to promote anti-tumor responses, the promotion of immunosuppression was often ignored.

Preclinical studies, using the TLR2 agonist Pam2/CSK4, could demonstrate that tumor growth was accelerated in mice due to the increase of monocytic MDSC with enhanced immunosuppressive properties [179]. Similar studies were performed by using lipopeptides to induce TLR2/6 signaling in skin-bacteria infected mice [180]. The authors showed that the immune response was decreased due to the expansion of MDSC, which was induced by TLR2/6 stimulated secretion of IL-6 by skin resident cells. However, other studies described

beneficial effects of TLR agonist as adjuvants for immunotherapy by inhibiting MDSC expansion. Wang et al. (181) used TLR7/8 agonist to convert human monocytic MDSC into tumoricidal M1-like macrophages [181]. Another study applied Poly (I:C) as an adjuvant for immunotherapy of tumor-bearing mice and showed a reduction of tumor growth [182]. The reason for this was the modulation of the immunosuppressive properties of MDSC and their reduced frequency. It seems that TLR agonist acts as a two-sided sword. On one hand, they can induce immune responses by activating myeloid cells, and on the other hand they stimulate a time-delayed immunosuppression to prevent excessive immune responses.

5.8 HSP are drivers of immunosuppression

In the last years, many studies described that subtypes of HSP60, HSP70, HSP90 and HSP110 acted in a TLR dependent manner, [126, 130-133, 183, 184]. Recently, Hong et al. (185) have proved that gp96, an isoform of HSP90, interacted with TLR2 and TLR4 [185]. They used a comprehensive interactome study to map all ligands for gp96, where they found 511 clients, including TLR2 and TLR4. Besides stimulating TLR signaling HSP were associated with MDSC biology. *In vitro* studies by Janssen et al. (186) demonstrated the capacity of HSP70 and HSP90 to convert human monocytes into immunosuppressive MDSC [186]. They treated several melanoma cell lines with blocking antibodies against HSP70 and HSP90 followed by their co-culture with monocytes. Interestingly, HSP70 and HSP90 treated melanoma cells were less effective in converting monocytes into MDSC compared to isotype treated control. The efficacy of reprogramming was measured by T cell suppression. *In vivo* experiments by Roa et al. (187) showed a therapeutic potential of HSP90 [187]. 17-Dimethylaminoethylamino-17-demethoxygeldanamycin (17-DMAG), an inhibitor of HSP90 was used to treat mice with MCA205 sarcoma. Upon administration of 17-DMAG treated MCA205 sarcoma cells into mice, tumor growth was significantly reduced compared to untreated control that was accompanied by enhanced recognition of tumors by $CD8^+$ T cells and reduced frequencies of MDSC in the TME. Furthermore, using 17-DMAG as an immune adjuvant together with adoptive T cell transfer into tumor-bearing mice resulted in better immunotherapeutic effects compared to adoptive T cell transfer alone. Combined treatment

led to the destruction. HSP were also shown to block the differentiation of BM cells into fully matured DCs [134, 188]. Motta et al. used recombinant HSP70 to block the differentiation of BM precursors into mature DC [188]. The treated cells showed a regulatory phenotype due to a secretion high IL-10 levels Moreover, theses DC became suppressive, which was shown by T cell proliferation assays *in vitro*. Another group that performed similar experiments confirmed these findings [134]. Taken together, these data indicates the immunosuppressive properties of HSP that block the differentiation of naïve BM precursor cells into mature immune cells and direct them to immunosuppressive cells.

5.9 Conclusion

The generation and activation of MDSC is a limiting step for successful immunotherapeutic approaches. Therefore, it is crucial to find targets, helping to reduce MDSC activity and improve immunotherapies.

In this study, we unveil a new mechanism of MDSC induction by tumor cells. Our data highlight the molecular mechanism of the conversion of murine IMC into MDSC by melanoma-derived EV. We could prove that melanoma cells secrete EV with HSP86 on their surface. The melanoma-derived EV were taken up by myeloid cells and induced PD-L1 expression on their surface. The PD-L1 expression is triggered by the HSP86-TLR4 axis, resulting in NF-κB signaling. Furthermore, we could demonstrate that EV-treated IMC acquired immunosuppressive features showed by the inhibition of T cell proliferation and IFN-γ secretion. Blocking PD-L1 on IMC resulted in the abrogation of immunosuppressive capacity of EV-educated cells, suggesting a critical role of this pathway in the acquisition of immunosuppressive properties. This study delivers a new target for future immunotherapies. Besides using checkpoint inhibitors or adoptive T cell transfer, we suggest to use inhibitors of vesicular HSP86 to enhance the efficiency of tumor immunotherapy.

6 References

1. Eggermont, A.M., A. Spatz, and C. Robert, *Cutaneous melanoma.* Lancet, 2014. **383**(9919): p. 816-27.
2. Restifo, N.P., M.J. Smyth, and A. Snyder, *Acquired resistance to immunotherapy and future challenges.* Nat Rev Cancer, 2016. **16**(2): p. 121-6.
3. Gray-Schopfer, V., C. Wellbrock, and R. Marais, *Melanoma biology and new targeted therapy.* Nature, 2007. **445**(7130): p. 851-7.
4. Domingues, B., et al., *Melanoma treatment in review.* ImmunoTargets and Therapy, 2018. **7**: p. 35-49.
5. Cust, A.E., K. Mishra, and M. Berwick, *Melanoma - role of the environment and genetics.* Photochem Photobiol Sci, 2018.
6. Roskoski, R., Jr., *Targeting oncogenic Raf protein-serine/threonine kinases in human cancers.* Pharmacol Res, 2018.
7. Johnson, D.B. and I. Puzanov, *Treatment of NRAS-mutant melanoma.* Curr Treat Options Oncol, 2015. **16**(4): p. 15.
8. Whiteman, D.C., A.C. Green, and C.M. Olsen, *The Growing Burden of Invasive Melanoma: Projections of Incidence Rates and Numbers of New Cases in Six Susceptible Populations through 2031.* J Invest Dermatol, 2016. **136**(6): p. 1161-71.
9. Schmid-Wendtner, M.H., et al., *Disease progression in patients with thin cutaneous melanomas (tumour thickness < or = 0.75 mm): clinical and epidemiological data from the Tumour Center Munich 1977-98.* Br J Dermatol, 2003. **149**(4): p. 788-93.
10. Brunet, J.F., et al., *A new member of the immunoglobulin superfamily--CTLA-4.* Nature, 1987. **328**(6127): p. 267-70.
11. Araujo, P.B., et al., *Ipilimumab-induced hypophysitis: review of the literature.* J Endocrinol Invest, 2015. **38**(11): p. 1159-66.
12. Hodi, F.S., et al., *Improved survival with ipilimumab in patients with metastatic melanoma.* N Engl J Med, 2010. **363**(8): p. 711-23.

13. Chinai, J.M., et al., *New immunotherapies targeting the PD-1 pathway.* Trends Pharmacol Sci, 2015. **36**(9): p. 587-95.

14. Raedler, L.A., *Opdivo (Nivolumab): Second PD-1 Inhibitor Receives FDA Approval for Unresectable or Metastatic Melanoma.* Am Health Drug Benefits, 2015. **8**(Spec Feature): p. 180-3.

15. Scott, L.J., *Nivolumab: A Review in Advanced Melanoma.* Drugs, 2015. **75**(12): p. 1413-24.

16. Schachter, J., et al., *Pembrolizumab versus ipilimumab for advanced melanoma: final overall survival results of a multicentre, randomised, open-label phase 3 study (KEYNOTE-006).* Lancet, 2017. **390**(10105): p. 1853-1862.

17. Weide, B., et al., *Combined treatment with ipilimumab and intratumoral interleukin-2 in pretreated patients with stage IV melanoma-safety and efficacy in a phase II study.* Cancer Immunol Immunother, 2017. **66**(4): p. 441-449.

18. Young, K., A. Minchom, and J. Larkin, *BRIM-1, -2 and -3 trials: improved survival with vemurafenib in metastatic melanoma patients with a BRAF(V600E) mutation.* Future Oncol, 2012. **8**(5): p. 499-507.

19. Kuske, M., et al., *Immunomodulatory effects of BRAF and MEK Inhibitors: Implications for Melanoma therapy.* Pharmacol Res, 2018.

20. Robert, C., et al., *Improved overall survival in melanoma with combined dabrafenib and trametinib.* N Engl J Med, 2015. **372**(1): p. 30-9.

21. Pol, J., G. Kroemer, and L. Galluzzi, *First oncolytic virus approved for melanoma immunotherapy.* Oncoimmunology, 2016. **5**(1): p. e1115641.

22. Malissen, N. and J.J. Grob, *Metastatic Melanoma: Recent Therapeutic Progress and Future Perspectives.* Drugs, 2018.

23. Hersey, P. and S. Gallagher, *Intralesional immunotherapy for melanoma.* J Surg Oncol, 2014. **109**(4): p. 320-6.

24. Maru, G.B., et al., *The role of inflammation in skin cancer.* Adv Exp Med Biol, 2014. **816**: p. 437-69.

25. Hanahan, D. and R.A. Weinberg, *Hallmarks of cancer: the next generation.* Cell, 2011. **144**(5): p. 646-74.

26. Grivennikov, S.I., F.R. Greten, and M. Karin, *Immunity, inflammation, and cancer.* Cell, 2010. **140**(6): p. 883-99.

27. Klein, G., *Tumor resistance.* Oncoimmunology, 2012. **1**(8): p. 1355-1359.

28. Burnet, F.M., *Immunological surveillance in neoplasia.* Transplant Rev, 1971. **7**: p. 3-25.

29. Dunn, G.P., et al., *Cancer immunoediting: from immunosurveillance to tumor escape.* Nat Immunol, 2002. **3**(11): p. 991-8.

30. Smyth, M.J., et al., *Differential tumor surveillance by natural killer (NK) and NKT cells.* J Exp Med, 2000. **191**(4): p. 661-8.

31. Swann, J.B. and M.J. Smyth, *Immune surveillance of tumors.* J Clin Invest, 2007. **117**(5): p. 1137-46.

32. Ribatti, D., *The concept of immune surveillance against tumors. The first theories.* Oncotarget, 2017. **8**(4): p. 7175-7180.

33. Finn, O.J., *A Believer's Overview of Cancer Immunosurveillance and Immunotherapy.* J Immunol, 2018. **200**(2): p. 385-391.

34. Khong, H.T. and N.P. Restifo, *Natural selection of tumor variants in the generation of "tumor escape" phenotypes.* Nat Immunol, 2002. **3**(11): p. 999-1005.

35. Wang, D. and R.N. DuBois, *Immunosuppression associated with chronic inflammation in the tumor microenvironment.* Carcinogenesis, 2015. **36**(10): p. 1085-93.

36. Umansky, V. and A. Sevko, *Tumor microenvironment and myeloid-derived suppressor cells.* Cancer Microenviron, 2013. **6**(2): p. 169-77.

37. Gabrilovich, D.I., *Myeloid-Derived Suppressor Cells.* Cancer Immunol Res, 2017. **5**(1): p. 3-8.

38. Kalbasi, A., et al., *Radiation and immunotherapy: a synergistic combination.* J Clin Invest, 2013. **123**(7): p. 2756-63.

39. Gabrilovich, D.I. and S. Nagaraj, *Myeloid-derived suppressor cells as regulators of the immune system.* Nat Rev Immunol, 2009. **9**(3): p. 162-74.

40. Umansky, V., et al., *Myeloid-derived suppressor cells and tumor escape from immune surveillance.* Semin Immunopathol, 2017. **39**(3): p. 295-305.

41. Baniyash, M., *Myeloid-derived suppressor cells as intruders and targets: clinical implications in cancer therapy.* Cancer Immunol Immunother, 2016. **65**(7): p. 857-67.

42. Diaz-Montero, C.M., et al., *Increased circulating myeloid-derived suppressor cells correlate with clinical cancer stage, metastatic tumor burden, and doxorubicin-cyclophosphamide chemotherapy.* Cancer Immunol Immunother, 2009. **58**(1): p. 49-59.

43. Jiang, H., et al., *Elevated chronic inflammatory factors and myeloid-derived suppressor cells indicate poor prognosis in advanced melanoma patients.* Int J Cancer, 2015. **136**(10): p. 2352-60.

44. Gebhardt, C., et al., *Myeloid Cells and Related Chronic Inflammatory Factors as Novel Predictive Markers in Melanoma Treatment with Ipilimumab.* Clin Cancer Res, 2015. **21**(24): p. 5453-9.

45. Santegoets, S.J., et al., *Myeloid derived suppressor and dendritic cell subsets are related to clinical outcome in prostate cancer patients treated with prostate GVAX and ipilimumab.* J Immunother Cancer, 2014. **2**: p. 31.

46. Fleming, V., et al., *Targeting Myeloid-Derived Suppressor Cells to Bypass Tumor-Induced Immunosuppression.* Front Immunol, 2018. **9**: p. 398.

47. Veglia, F., M. Perego, and D. Gabrilovich, *Myeloid-derived suppressor cells coming of age.* Nat Immunol, 2018. **19**(2): p. 108-119.

48. Blattner, C., et al., *CCR5(+) Myeloid-Derived Suppressor Cells Are Enriched and Activated in Melanoma Lesions.* Cancer Res, 2018. **78**(1): p. 157-167.

49. Umansky, V., et al., *CCR5 in recruitment and activation of myeloid-derived suppressor cells in melanoma.* Cancer Immunol Immunother, 2017. **66**(8): p. 1015-1023.

50. Jacob, A. and R. Prekeris, *The regulation of MMP targeting to invadopodia during cancer metastasis.* Front Cell Dev Biol, 2015. **3**: p. 4.

51. Kitamura, T., B.Z. Qian, and J.W. Pollard, *Immune cell promotion of metastasis.* Nat Rev Immunol, 2015. **15**(2): p. 73-86.

52. Peinado, H., S. Lavotshkin, and D. Lyden, *The secreted factors responsible for pre-metastatic niche formation: old sayings and new thoughts.* Semin Cancer Biol, 2011. **21**(2): p. 139-46.

53. Safarzadeh, E., et al., *Myeloid-derived suppressor cells: Important contributors to tumor progression and metastasis.* J Cell Physiol, 2018. **233**(4): p. 3024-3036.

54. Bronte, V. and P. Zanovello, *Regulation of immune responses by L-arginine metabolism.* Nat Rev Immunol, 2005. **5**(8): p. 641-54.

55. Fletcher, M., et al., *l-Arginine depletion blunts antitumor T-cell responses by inducing myeloid-derived suppressor cells.* Cancer Res, 2015. **75**(2): p. 275-83.

56. Rodriguez, P.C., D.G. Quiceno, and A.C. Ochoa, *L-arginine availability regulates T-lymphocyte cell-cycle progression.* Blood, 2007. **109**(4): p. 1568-73.

57. Baniyash, M., *TCR zeta-chain downregulation: curtailing an excessive inflammatory immune response.* Nat Rev Immunol, 2004. **4**(9): p. 675-87.

58. Mazzoni, A., et al., *Myeloid suppressor lines inhibit T cell responses by an NO-dependent mechanism.* J Immunol, 2002. **168**(2): p. 689-95.

59. Platten, M., W. Wick, and B.J. Van den Eynde, *Tryptophan catabolism in cancer: beyond IDO and tryptophan depletion.* Cancer Res, 2012. **72**(21): p. 5435-40.

60. Frumento, G., et al., *Tryptophan-derived catabolites are responsible for inhibition of T and natural killer cell proliferation induced by indoleamine 2,3-dioxygenase.* J Exp Med, 2002. **196**(4): p. 459-68.

61. Munn, D.H., et al., *GCN2 kinase in T cells mediates proliferative arrest and anergy induction in response to indoleamine 2,3-dioxygenase.* Immunity, 2005. **22**(5): p. 633-42.

62. Kumar, V., et al., *The Nature of Myeloid-Derived Suppressor Cells in the Tumor Microenvironment.* Trends Immunol, 2016. **37**(3): p. 208-220.

63. Berger, K.N. and J.J. Pu, *PD-1 pathway and its clinical application: A 20year journey after discovery of the complete human PD-1 gene.* Gene, 2018. **638**: p. 20-25.

64. Cheng, X., et al., *Structure and interactions of the human programmed cell death 1 receptor.* J Biol Chem, 2013. **288**(17): p. 11771-85.

65. Dai, S., et al., *The PD-1/PD-Ls pathway and autoimmune diseases.* Cell Immunol, 2014. **290**(1): p. 72-9.

66. Shi, Y., *Regulatory mechanisms of PD-L1 expression in cancer cells.* Cancer Immunol Immunother, 2018.

67. Abiko, K., et al., *IFN-gamma from lymphocytes induces PD-L1 expression and promotes progression of ovarian cancer.* Br J Cancer, 2015. **112**(9): p. 1501-9.

68. Noguchi, T., et al., *Temporally Distinct PD-L1 Expression by Tumor and Host Cells Contributes to Immune Escape.* Cancer Immunol Res, 2017. **5**(2): p. 106-117.

69. Sun, C., R. Mezzadra, and T.N. Schumacher, *Regulation and Function of the PD-L1 Checkpoint.* Immunity, 2018. **48**(3): p. 434-452.

70. Wang, Y., et al., *Regulation of PD-L1: Emerging Routes for Targeting Tumor Immune Evasion.* Front Pharmacol, 2018. **9**: p. 536.

71. Zerdes, I., et al., *Genetic, transcriptional and post-translational regulation of the programmed death protein ligand 1 in cancer: biology and clinical correlations.* Oncogene, 2018.

72. Dang, C.V., *MYC on the path to cancer.* Cell, 2012. **149**(1): p. 22-35.

73. Noman, M.Z., et al., *PD-L1 is a novel direct target of HIF-1alpha, and its blockade under hypoxia enhanced MDSC-mediated T cell activation.* J Exp Med, 2014. **211**(5): p. 781-90.

74. Yang, Q., et al., *Regulation of cancer immune escape: The roles of miRNAs in immune checkpoint proteins.* Cancer Lett, 2018. **431**: p. 73-84.

75. Tkach, M. and C. Thery, *Communication by Extracellular Vesicles: Where We Are and Where We Need to Go.* Cell, 2016. **164**(6): p. 1226-1232.

76. Colombo, M., G. Raposo, and C. Théry, *Biogenesis, Secretion, and Intercellular Interactions of Exosomes and Other Extracellular Vesicles.* Annual Review of Cell and Developmental Biology, 2014. **30**(1): p. 255-289.

77. György, B., et al., *Membrane vesicles, current state-of-the-art: emerging role of extracellular vesicles.* Cellular and Molecular Life Sciences, 2011. **68**(16): p. 2667-2688.

78. Valadi, H., et al., *Exosome-mediated transfer of mRNAs and microRNAs is a novel mechanism of genetic exchange between cells.* Nat Cell Biol, 2007. **9**(6): p. 654-9.

79. Raposo, G., et al., *B lymphocytes secrete antigen-presenting vesicles.* J Exp Med, 1996. **183**(3): p. 1161-72.

80. Hoshino, A., et al., *Tumour exosome integrins determine organotropic metastasis.* Nature, 2015. **527**(7578): p. 329-35.

81. Umezu, T., et al., *Leukemia cell to endothelial cell communication via exosomal miRNAs.* Oncogene, 2013. **32**(22): p. 2747-55.

82. Baroni, S., et al., *Exosome-mediated delivery of miR-9 induces cancer-associated fibroblast-like properties in human breast fibroblasts.* Cell Death Dis, 2016. **7**(7): p. e2312.

83. Wei, F., et al., *Exosomes derived from gemcitabine-resistant cells transfer malignant phenotypic traits via delivery of miRNA-222-3p.* Mol Cancer, 2017. **16**(1): p. 132.

84. Ying, X., et al., *Epithelial ovarian cancer-secreted exosomal miR-222-3p induces polarization of tumor-associated macrophages.* Oncotarget, 2016. **7**(28): p. 43076-43087.

85. Li, C., et al., *CD97 promotes gastric cancer cell proliferation and invasion through exosome-mediated MAPK signaling pathway.* World J Gastroenterol, 2015. **21**(20): p. 6215-28.

86. Skog, J., et al., *Glioblastoma microvesicles transport RNA and proteins that promote tumour growth and provide diagnostic biomarkers.* Nat Cell Biol, 2008. **10**(12): p. 1470-6.

87. Al-Nedawi, K., et al., *Intercellular transfer of the oncogenic receptor EGFRvIII by microvesicles derived from tumour cells.* Nat Cell Biol, 2008. **10**(5): p. 619-24.

88. Jena, M.K. and J. Janjanam, *Role of extracellular matrix in breast cancer development: a brief update.* F1000Res, 2018. **7**: p. 274.

89. Ge, R., et al., *Exosomes in Cancer Microenvironment and Beyond: have we Overlooked these Extracellular Messengers?* Cancer Microenviron, 2012. **5**(3): p. 323-32.

90. Zheng, N.X., et al., *The role of pattern recognition receptors in the innate recognition of Candida albicans.* Virulence, 2015. **6**(4): p. 347-61.

91. Takeda, K. and S. Akira, *Toll-like receptors.* Curr Protoc Immunol, 2015. **109**: p. 14 12 1-10.

92. Netea, M.G., et al., *An integrated model of the recognition of Candida albicans by the innate immune system.* Nat Rev Microbiol, 2008. **6**(1): p. 67-78.

93. Wang, L. and S. Ning, *"Toll-free" pathways for production of type I interferons.* AIMS Allergy Immunol, 2017. **1**(3): p. 143-163.

94. Brown, G.D., J.A. Willment, and L. Whitehead, *C-type lectins in immunity and homeostasis.* Nat Rev Immunol, 2018. **18**(6): p. 374-389.

95. Yoneyama, M., et al., *Viral RNA detection by RIG-I-like receptors.* Curr Opin Immunol, 2015. **32**: p. 48-53.

96. Sellge, G. and T.A. Kufer, *PRR-signaling pathways: Learning from microbial tactics.* Semin Immunol, 2015. **27**(2): p. 75-84.

97. Motta, V., et al., *NOD-like receptors: versatile cytosolic sentinels.* Physiol Rev, 2015. **95**(1): p. 149-78.

98. Szatmary, Z., *Molecular biology of toll-like receptors.* Gen Physiol Biophys, 2012. **31**(4): p. 357-66.

99. Vidya, M.K., et al., *Toll-like receptors: Significance, ligands, signaling pathways, and functions in mammals.* Int Rev Immunol, 2018. **37**(1): p. 20-36.

100. Oosting, M., et al., *Human TLR10 is an anti-inflammatory pattern-recognition receptor.* Proc Natl Acad Sci U S A, 2014. **111**(42): p. E4478-84.

101. Vogl, T., et al., *Mrp8 and Mrp14 are endogenous activators of Toll-like receptor 4, promoting lethal, endotoxin-induced shock.* Nat Med, 2007. **13**(9): p. 1042-9.

102. Chakraborty, D., et al., *Alarmin S100A8 Activates Alveolar Epithelial Cells in the Context of Acute Lung Injury in a TLR4-Dependent Manner.* Front Immunol, 2017. **8**: p. 1493.

103. Al-Ofi, E.A. and B.S. Al-Ghamdi, *High-Mobility Group Box 1 (HMGB1), an Endogenous Ligand of Toll-Like Receptors 2 and 4, Induces Astroglial Inflammation via NF-beta Pathway.* Folia Morphol (Warsz), 2018.

104. Tachibana, M., *[The Immunosuppressive Function of Myeloid-derived Suppressor Cells Is Regulated by the HMGB1-TLR4 Axis].* Yakugaku Zasshi, 2018. **138**(2): p. 143-148.

105. Narayanan, K.B. and H.H. Park, *Toll/interleukin-1 receptor (TIR) domain-mediated cellular signaling pathways.* Apoptosis, 2015. **20**(2): p. 196-209.

106. Feng, Y. and W. Chao, *Toll-like receptors and myocardial inflammation.* Int J Inflam, 2011. **2011**: p. 170352.

107. Vinaiphat, A. and V. Thongboonkerd, *Chaperonomics in leptospirosis.* Expert Rev Proteomics, 2018. **15**(7): p. 569-579.

108. Garbuz, D.G., *[Regulation of heat shock gene expression in response to stress].* Mol Biol (Mosk), 2017. **51**(3): p. 400-417.

109. Zhang, L., J.H. Fok, and F.E. Davies, *Heat shock proteins in multiple myeloma.* Oncotarget, 2014. **5**(5): p. 1132-48.

110. Wu, J., et al., *Heat Shock Proteins and Cancer.* Trends Pharmacol Sci, 2017. **38**(3): p. 226-256.

111. Radli, M. and S.G.D. Rudiger, *Dancing with the Diva: Hsp90-Client Interactions.* J Mol Biol, 2018.

112. Zabinsky, R.A., et al., *It's not magic - Hsp90 and its effects on genetic and epigenetic variation.* Semin Cell Dev Biol, 2018.

113. Hoter, A., M.E. El-Sabban, and H.Y. Naim, *The HSP90 Family: Structure, Regulation, Function, and Implications in Health and Disease.* Int J Mol Sci, 2018. **19**(9).

114. Zuehlke, A.D., M.A. Moses, and L. Neckers, *Heat shock protein 90: its inhibition and function.* Philos Trans R Soc Lond B Biol Sci, 2018. **373**(1738).

115. Graner, M.W., *HSP90 and Immune Modulation in Cancer.* Adv Cancer Res, 2016. **129**: p. 191-224.

116. Mellatyar, H., et al., *Targeted cancer therapy through 17-DMAG as an Hsp90 inhibitor: Overview and current state of the art.* Biomed Pharmacother, 2018. **102**: p. 608-617.

117. De Mattos-Arruda, L. and J. Cortes, *Breast cancer and HSP90 inhibitors: is there a role beyond the HER2-positive subtype?* Breast, 2012. **21**(4): p. 604-7.

118. Kato, M., et al., *Transgenic mouse model for skin malignant melanoma.* Oncogene, 1998. **17**(14): p. 1885-8.

119. Zhao, F., et al., *Activation of p38 mitogen-activated protein kinase drives dendritic cells to become tolerogenic in ret transgenic mice spontaneously developing melanoma.* Clin Cancer Res, 2009. **15**(13): p. 4382-90.

120. Apolloni, E., et al., *Immortalized myeloid suppressor cells trigger apoptosis in antigen-activated T lymphocytes.* J Immunol, 2000. **165**(12): p. 6723-30.

121. Lobb, R.J., et al., *Optimized exosome isolation protocol for cell culture supernatant and human plasma.* J Extracell Vesicles, 2015. **4**: p. 27031.

122. Lotvall, J., et al., *Minimal experimental requirements for definition of extracellular vesicles and their functions: a position statement from the International Society for Extracellular Vesicles.* J Extracell Vesicles, 2014. **3**: p. 26913.

123. Gabrusiewicz, K., et al., *Glioblastoma stem cell-derived exosomes induce M2 macrophages and PD-L1 expression on human monocytes.* Oncoimmunology, 2018. **7**(4): p. e1412909.

124. Cooks, T., et al., *Mutant p53 cancers reprogram macrophages to tumor supporting macrophages via exosomal miR-1246.* Nat Commun, 2018. **9**(1): p. 771.

125. Cereghetti, D.M. and P.P. Lee, *Tumor-Derived Exosomes Contain microRNAs with Immunological Function: Implications for a Novel Immunosuppression Mechanism.* Microrna, 2014. **2**(3): p. 194-204.

126. Chalmin, F., et al., *Membrane-associated Hsp72 from tumor-derived exosomes mediates STAT3-dependent immunosuppressive function of mouse and human myeloid-derived suppressor cells.* J Clin Invest, 2010. **120**(2): p. 457-71.

127. Bretz, N.P., et al., *Body fluid exosomes promote secretion of inflammatory cytokines in monocytic cells via Toll-like receptor signaling.* J Biol Chem, 2013. **288**(51): p. 36691-702.

128. Haderk, F., et al., *Tumor-derived exosomes modulate PD-L1 expression in monocytes.* Sci Immunol, 2017. **2**(13).

129. Peinado, H., et al., *Melanoma exosomes educate bone marrow progenitor cells toward a pro-metastatic phenotype through MET.* Nat Med, 2012. **18**(6): p. 883-91.

130. Shen, Y., et al., *Tumor-derived exosomes educate dendritic cells to promote tumor metastasis via HSP72/HSP105-TLR2/TLR4 pathway.* Oncoimmunology, 2017. **6**(12): p. e1362527.

131. Hutchinson, M.R., et al., *Evidence for a role of heat shock protein-90 in toll like receptor 4 mediated pain enhancement in rats.* Neuroscience, 2009. **164**(4): p. 1821-32.

132. O'Neill, S., et al., *Heat shock protein 90 inhibition abrogates TLR4-mediated NF-kappaB activity and reduces renal ischemia-reperfusion injury.* Sci Rep, 2015. **5**: p. 12958.

133. Segreto, F., et al., *HSP90 and TLR4 Interplay in Keloids.* Plast Reconstr Surg, 2016. **137**(2): p. 480e-481e.

134. Stocki, P., X.N. Wang, and A.M. Dickinson, *Inducible heat shock protein 70 reduces T cell responses and stimulatory capacity of monocyte-derived dendritic cells.* J Biol Chem, 2012. **287**(15): p. 12387-94.

135. Yokota, S., M. Kitahara, and K. Nagata, *Benzylidene lactam compound, KNK437, a novel inhibitor of acquisition of thermotolerance and heat shock protein induction in human colon carcinoma cells.* Cancer Res, 2000. **60**(11): p. 2942-8.

136. Keller, S., et al., *Exosomes: from biogenesis and secretion to biological function.* Immunol Lett, 2006. **107**(2): p. 102-8.

137. Qadir, F., et al., *Transcriptome reprogramming by cancer exosomes: identification of novel molecular targets in matrix and immune modulation.* Mol Cancer, 2018. **17**(1): p. 97.

138. Shah, N., et al., *Extracellular vesicle-mediated long-range communication in stressed retinal pigment epithelial cell monolayers.* Biochim Biophys Acta, 2018. **1864**(8): p. 2610-2622.

139. Barros, F.M., et al., *Exosomes and Immune Response in Cancer: Friends or Foes?* Front Immunol, 2018. **9**: p. 730.

140. Ricklefs, F.L., et al., *Immune evasion mediated by PD-L1 on glioblastoma-derived extracellular vesicles.* Sci Adv, 2018. **4**(3): p. eaar2766.

141. Chen, G., et al., *Exosomal PD-L1 contributes to immunosuppression and is associated with anti-PD-1 response.* Nature, 2018. **560**(7718): p. 382-386.

142. Whiteside, T.L., *Immune modulation of T-cell and NK (natural killer) cell activities by TEXs (tumour-derived exosomes).* Biochem Soc Trans, 2013. **41**(1): p. 245-51.

143. Abusamra, A.J., et al., *Tumor exosomes expressing Fas ligand mediate CD8+ T-cell apoptosis.* Blood Cells Mol Dis, 2005. **35**(2): p. 169-73.

144. Cai, Z., et al., *Activated T cell exosomes promote tumor invasion via Fas signaling pathway.* J Immunol, 2012. **188**(12): p. 5954-61.

145. Jeanteur, P., *[From dendritic cells to the exosomes that they secrete: a decisive advance for anticancer vaccine therapy?].* Bull Cancer, 1998. **85**(6): p. 521.

146. Taylor, D.D. and P.H. Black, *Inhibition of macrophage Ia antigen expression by shed plasma membrane vesicles from metastatic murine melanoma lines.* J Natl Cancer Inst, 1985. **74**(4): p. 859-67.

147. Li, M., et al., *Horizontal transfer of exosomal CXCR4 promotes murine hepatocarcinoma cell migration, invasion and lymphangiogenesis.* Gene, 2018. **676**: p. 101-109.

148. Liu, H., et al., *Tumor-derived exosomes promote tumor self-seeding in hepatocellular carcinoma by transferring miRNA-25-5p to enhance cell motility.* Oncogene, 2018. **37**(36): p. 4964-4978.

149. Blackwell, R.H., K.E. Foreman, and G.N. Gupta, *The Role of Cancer-Derived Exosomes in Tumorigenicity & Epithelial-to-Mesenchymal Transition.* Cancers (Basel), 2017. **9**(8).

150. Cheng, L., et al., *Exosomes from Melatonin Treated Hepatocellularcarcinoma Cells Alter the Immunosupression Status through STAT3 Pathway in Macrophages.* Int J Biol Sci, 2017. **13**(6): p. 723-734.

151. Rezzani, R., et al., *Protective role of melatonin in cyclosporine A-induced oxidative stress in rat liver.* Int Immunopharmacol, 2005. **5**(9): p. 1397-405.

152. Xiang, X., et al., *Induction of myeloid-derived suppressor cells by tumor exosomes.* Int J Cancer, 2009. **124**(11): p. 2621-33.

153. Wang, J., et al., *The bone marrow microenvironment enhances multiple myeloma progression by exosome-mediated activation of myeloid-derived suppressor cells.* Oncotarget, 2015. **6**(41): p. 43992-4004.

154. Basso, D., et al., *PDAC-derived exosomes enrich the microenvironment in MDSCs in a SMAD4-dependent manner through a new calcium related axis.* Oncotarget, 2017. **8**(49): p. 84928-84944.

155. El Kasmi, K.C. and K.R. Stenmark, *Contribution of metabolic reprogramming to macrophage plasticity and function.* Semin Immunol, 2015. **27**(4): p. 267-75.

156. Kelly, B. and L.A. O'Neill, *Metabolic reprogramming in macrophages and dendritic cells in innate immunity.* Cell Res, 2015. **25**(7): p. 771-84.

157. Wegiel, B., et al., *Metabolic Switch in the Tumor Microenvironment Determines Immune Responses to Anti-cancer Therapy.* Front Oncol, 2018. **8**: p. 284.

158. Salimu, J., et al., *Dominant immunosuppression of dendritic cell function by prostate-cancer-derived exosomes.* J Extracell Vesicles, 2017. **6**(1): p. 1368823.

159. Ridder, K., et al., *Extracellular vesicle-mediated transfer of functional RNA in the tumor microenvironment.* Oncoimmunology, 2015. **4**(6): p. e1008371.

160. Zomer, A., et al., *In Vivo imaging reveals extracellular vesicle-mediated phenocopying of metastatic behavior.* Cell, 2015. **161**(5): p. 1046-1057.

161. Wen, S.W., et al., *The Biodistribution and Immune Suppressive Effects of Breast Cancer-Derived Exosomes.* Cancer Res, 2016. **76**(23): p. 6816-6827.

162. Plebanek, M.P., et al., *Pre-metastatic cancer exosomes induce immune surveillance by patrolling monocytes at the metastatic niche.* Nat Commun, 2017. **8**(1): p. 1319.

163. Costa-Silva, B., et al., *Pancreatic cancer exosomes initiate pre-metastatic niche formation in the liver.* Nat Cell Biol, 2015. **17**(6): p. 816-26.

164. Balkwill, F. and A. Mantovani, *Inflammation and cancer: back to Virchow?* Lancet, 2001. **357**(9255): p. 539-45.

165. Karin, M., et al., *NF-kappaB in cancer: from innocent bystander to major culprit.* Nat Rev Cancer, 2002. **2**(4): p. 301-10.

166. Fujiki, H., *Gist of Dr. Katsusaburo Yamagiwa's papers entitled "Experimental study on the pathogenesis of epithelial tumors" (I to VI reports).* Cancer Sci, 2014. **105**(2): p. 143-9.

167. Ray, A., K. Chakraborty, and P. Ray, *Immunosuppressive MDSCs induced by TLR signaling during infection and role in resolution of inflammation.* Front Cell Infect Microbiol, 2013. **3**: p. 52.

168. Liew, F.Y., et al., *Negative regulation of toll-like receptor-mediated immune responses.* Nat Rev Immunol, 2005. **5**(6): p. 446-58.

169. Arora, M., et al., *TLR4/MyD88-induced CD11b+Gr-1 int F4/80+ non-migratory myeloid cells suppress Th2 effector function in the lung.* Mucosal Immunol, 2010. **3**(6): p. 578-93.

170. Poe, S.L., et al., *STAT1-regulated lung MDSC-like cells produce IL-10 and efferocytose apoptotic neutrophils with relevance in resolution of bacterial pneumonia.* Mucosal Immunol, 2013. **6**(1): p. 189-99.

171. Cheng, P., et al., *Inhibition of dendritic cell differentiation and accumulation of myeloid-derived suppressor cells in cancer is regulated by S100A9 protein.* J Exp Med, 2008. **205**(10): p. 2235-49.

172. Pouliot, P., et al., *Myeloid-related proteins rapidly modulate macrophage nitric oxide production during innate immune response.* J Immunol, 2008. **181**(5): p. 3595-601.

173. He, M., et al., *Exploring the biological functional mechanism of the HMGB1/TLR4/MD-2 complex by surface plasmon resonance.* Mol Med, 2018. **24**(1): p. 21.

174. Parker, K.H., L.A. Horn, and S. Ostrand-Rosenberg, *High-mobility group box protein 1 promotes the survival of myeloid-derived suppressor cells by inducing autophagy.* J Leukoc Biol, 2016. **100**(3): p. 463-70.

175. Su, Z., et al., *Bio-HMGB1 from breast cancer contributes to M-MDSC differentiation from bone marrow progenitor cells and facilitates conversion of monocytes into MDSC-like cells.* Cancer Immunol Immunother, 2017. **66**(3): p. 391-401.

176. Su, Z., et al., *[Recombinant HMGB1 induces the differentiation of mouse myeloid cells into myeloid-derived suppressor cells in vitro].* Xi Bao Yu Fen Zi Mian Yi Xue Za Zhi, 2016. **32**(10): p. 1362-1365.

177. Li, J., et al., *HMGB1 promotes myeloid-derived suppressor cells and renal cell carcinoma immune escape.* Oncotarget, 2017. **8**(38): p. 63290-63298.

178. Lee, C.H., C.L. Wu, and A.L. Shiau, *Toll-like receptor 4 signaling promotes tumor growth.* J Immunother, 2010. **33**(1): p. 73-82.

179. Shime, H., et al., *Toll-like receptor 2 ligand and interferon-gamma suppress anti-tumor T cell responses by enhancing the immunosuppressive activity of monocytic myeloid-derived suppressor cells.* Oncoimmunology, 2017. **7**(1): p. e1373231.

180. Skabytska, Y., et al., *Cutaneous innate immune sensing of Toll-like receptor 2-6 ligands suppresses T cell immunity by inducing myeloid-derived suppressor cells.* Immunity, 2014. **41**(5): p. 762-75.

181. Wang, J., et al., *Effect of TLR agonists on the differentiation and function of human monocytic myeloid-derived suppressor cells.* J Immunol, 2015. **194**(9): p. 4215-21.

182. Forghani, P. and E.K. Waller, *Poly (I: C) modulates the immunosuppressive activity of myeloid-derived suppressor cells in a murine model of breast cancer.* Breast Cancer Res Treat, 2015. **153**(1): p. 21-30.

183. Ding, F., et al., *Oxymatrine inhibits microglia activation via HSP60-TLR4 signaling.* Biomed Rep, 2016. **5**(5): p. 623-628.

184. Zhang, G., et al., *Tumor induces muscle wasting in mice through releasing extracellular Hsp70 and Hsp90.* Nat Commun, 2017. **8**(1): p. 589.

185. Hong, F., et al., *Mapping the Interactome of a Major Mammalian Endoplasmic Reticulum Heat Shock Protein 90.* PLoS One, 2017. **12**(1): p. e0169260.

186. Janssen, N., et al., *Inhibiting HSP90 prevents the induction of myeloid-derived suppressor cells by melanoma cells.* Cell Immunol, 2018. **327**: p. 68-76.

187. Rao, A., et al., *Combination therapy with HSP90 inhibitor 17-DMAG reconditions the tumor microenvironment to improve recruitment of therapeutic T cells.* Cancer Res, 2012. **72**(13): p. 3196-206.

188. Motta, A., et al., *Mycobacterium tuberculosis heat-shock protein 70 impairs maturation of dendritic cells from bone marrow precursors, induces interleukin-10 production and inhibits T-cell proliferation in vitro.* Immunology, 2007. **121**(4): p. 462-72.

Abbreviations

A	
Alix	ALG-2-interacting protein X
APC	Antigen-presenting cells
ARG-1	Arginase-1
B	
BCA	Bicinchoninic acid assay
Bcl-xL	B-cell lymphoma-extra-large
bFGF	Basic fibroblast growth factor
BM	Bone marrow
B-RAF	B-Rapidly accelerated fibrosarcoma
BSA	Bovine serum albumin
C	
CCL	Chemokine (C-C motif) ligands
CCR	C-C chemokine receptor
CD	Cluster of differentiation
CLR	C-type lectine receptors
CTLA-4	Cytotoxic T lymphocyte-associated antigen 4
CXCL	C-X-C motif chemokine
Cy	Cyanin
D	
DAMP	Damage-associated molecular patterns
DC	Dendritic cells
DMA	dimethyl-amiloride
DMAG	Dimethylaminoethylamino-17-demethoxygeldanamycin
DMSO	Dimethyl sulfoxide
DNA	Deoxyribonucleic acid
E	
EDTA	Ethylene diamine-tetra-acetic acid
EGFR	Epidermal growth factor receptor
EGFRvIII	Epidermal growth factor receptor variant III
EMT	Epithelial to mesenchymal transition
Et al.	Et alteri
EV	Extracellular vesicles

F	
FACS	Fluorescence activated cell sorting
FasL	Fas ligand
FBS	Fetal bovine serum
FITC	Fluorescein-isothiocyanat
FMO	Fluorescent minus one
FSC	Forward scatter
G	
g	G-force
GM-CSF	Granulocyte-macrophage colony-stimulating factor
H	
HER-2	Human epidermal growth factor receptor 2
HIF	Hypoxia-inducible factor
HLA-DR	Human leucocyte antigen-DR
HMGB-1	high mobility group box 1
HRE	Hypoxia response element
HSP	Heat-shock proteins
I	
IDO	indoleamine 2 3-dioxygenase
IFN	Interferon
IKK	IκB kinase
IL	Interleukin
IL-1R	IL-1 receptor
IMC	Immature myeloid cells
iNOS	inducible nitric oxide synthase
IRAK	IL-1R associated kinase
IRF	Interferon response factor
ITIM	immunoreceptor tyrosine based inhibitory motif
ITSM	immunoreceptor tyrosine based switch motif
K	
kDa	Kilo Dalton
L	
LN	Lymph nodes
LPS	Lipopolysaccharides
M	
MACS	Magnetic-activated cell sorting

MAPK	Mitogen-activated protein kinase
Mcl	Myeloid leukemia cell differentiation protein
MDSC	Myeloid-derived suppressor
MFI	Median fluorescence intensity
MHC	Major histocompatibility complex
MIF	Migration inhibitory factor
min	Minutes
miRNA	Micro RNA
MM	Malignant Melanoma
MMP	Matrix metalloproteinases
MSC	Myeloid suppressor cell line
MVB	Multivesicular bodies
MyD88	Myeloid differentiation primary response 88
N	
NFκB	Nuclear factor 'κ-light-chain-enhancer' of activated B-cells
NK	Natural killer
NO	Nitric oxide
NOD	Nucleotide-binding oligomerization domain
NTA	Nanoparticle tracking analysis
P	
PAMP	Pathogen-associated molecular patterns
PBS	Phosphate buffer saline
PD-1	Programmed cell death protein I
PDAC	Pancreatic ductal adenocarcinoma
PD-L1	PD-ligand 1
PE	Phycoerythrin
PFS	Progression-free survival
PMN	Polymorphonuclear
PRR	Pathogen Recognition Receptors
R	
Ras	Rat sarcoma
RIG-I	Retinoic-acid-inducible gene I
RLR	Retinoic-acid-inducible gene I (RIG-I)-like receptors
ROS	Reactive oxygen species
rpm	Rounds per minute
RPMI	Roswell Park Memorial Institute medium

RT	Room temperature
S	
s	Seconds
SHP	Src homology region 2 domain-containing phosphatase
SMAD	Mothers against decapentaplegic homolog
SSC	Side scatter
T	
TBK1	Tank-binding kinase 1
TGF	Transforming growth factor
TIR	Toll/interleukin-1 receptor
TLR	Toll-like receptors
TME	Tumor microenvironment
TNF	Tumor necrosis factor
TRAF	TNF receptor associated factor
Treg	Regulator $CD4^+$ T cells
TRIF	TIR-domain-containing adapter-inducing interferon-β
T-VEC	Talimogen laherparepvec
V	
VEGF	Vascular endothelial growth factor
Z	
ZAP70	Zeta-chain-associated protein kinase 70

List of Figures

Acknowledgements

This Ph.D. thesis would not exist without the help of many colleagues and friends. Therefore, I want to thank all of them.

First of all, I want to thank **Prof. Dr. Viktor Umansky** for supporting me throughout the whole Ph.D. time. Due to extensive and informative discussions with him, he gave me lots of ideas and encouraged me to think more critically. His scientific guidance and supervision also motivated me to successfully perform this project.

A great thanks goes to **Prof. Dr. Hans-Peter Altevogt** who introduced me to the world of exosomes. I benefited from his extensive experience in exosomal research and biochemistry, which accelerated the progress of this project.

I want to thank **Prof. Dr. Rienk Offringa** and **Dr. Stefan Momma** for being members of my thesis advisory committee. Their knowledge and criticism in meetings helped me to design better and more sophisticated experiments. Moreover, I want to thank **Prof. Dr. Ana Martin-Villalba** and **Prof. Dr. Stefan Wiemann** for being examiners in the Ph.D. defense.

I want to thank **Prof. Dr. Jochen Utikal** to be part of his group and his scientific input in our group seminars.

Céline Weller, Beatriz Gomez, Eva-Maria Storck and **Elisabeth Fuhry** were great Master and Bachelor students. Their great performance and amazing results were crucial for the progress of this thesis.

I want to thank my former lab members **Dr. Carolin Blattner** and **Dr. Mareike Grees**. Both helped me to have a successful start and showed me many techniques. But most important, we had great coffee breaks ☺

I want also to thank my current lab **members Xiaoying Hu (YingYing), Rebekka Weber, Christopher Groth, Sonja Simon** and **Zeno Riester** for being such great lab members and colleagues. I am looking forward for the next social evening with them.

A thousand thanks are addressed to my **parents** and my both **brothers**. They are always willing to help, no matter what happens and how far they are away. They motivated me throughout the whole Ph.D. period and made me proud to be a scientist. I am really lucky to have such an amazing and wonderful family.

At the end, I want to thank **Sarah Kolleth**. She makes my life so much easier and more enjoyable. Sarah always calmed me down in stressful times and consoled me when experiments failed. She was always considerate when I had to work on weekends and public holidays. By being such a great person, Sarah makes me overjoyed whenever I think about her.

Thank you all!